

# Radiative Heat Transfer and Applications for Glass Production Processes

Martin Frank and Axel Klar

## 1 Introduction

In glass manufacturing, a hot melt of glass is cooled down to room temperature. The annealing has to be monitored carefully in order to avoid excessive temperature differences which may affect the quality of the product or even lead to cracks in the material. In order to control this process it is, therefore, of interest to have a mathematical model that accurately predicts the temperature evolution. The model will involve the direction-dependent thermal radiation field because a significant part of the energy is transported by photons. Unfortunately, this fact makes the numerical solution of the radiative transfer equations much more complex, especially in higher dimensions, since, besides position and time variables, the directional variables also have to be accounted for. Therefore, approximations of the full model that are computationally less time consuming but yet sufficiently accurate have to be sought. It is our purpose to present several recent approaches to this problem that have been co-developed by the authors.

This manuscript is organized as follows. In Sect. 2, we derive the underlying kinetic equation model for radiative transfer in glass. This model is supplemented by initial and boundary conditions. In addition, several versions of this model, that are later used, are introduced. For later reference and for the reader who wants to skip the derivation, the basic model is summarized in Sect. 2.6. Section 3 deals with direct numerical methods for the solution of the radiative transfer equations. These methods will later be used to compute benchmark results. Thus, we present convergence and robustness results. The rest of the discussion focuses on two approximation methods that have been co-developed by the authors, namely

---

M. Frank (✉)

University of Kaiserslautern, Erwin-Schrödinger-Strasse, 67663 Kaiserslautern, Germany  
e-mail: [frank@mathematik.uni-kl.de](mailto:frank@mathematik.uni-kl.de)

A. Klar

University of Kaiserslautern, Erwin-Schrödinger-Strasse, 67663 Kaiserslautern, Germany and  
Fraunhofer ITWM, Fraunhofer Platz 1, 67663 Kaiserslautern, Germany  
e-mail: [klar@itwm.fhg.de](mailto:klar@itwm.fhg.de)

higher-order diffusion (Sect. 4) and moment methods (Sects. 5 and 6). These models are compared numerically in Sect. 7, where we also present results specifically related to glass cooling. Parts of this work have been taken from the articles [18, 23–25, 27, 47, 48, 76, 85].

## 2 Radiative Heat Transfer Equations for Glass

Radiative transfer has to compete with the two other modes of energy transfer, namely heat conduction and convection. In everyday life, these three effects can be seen at a cup of hot coffee. The cup itself gets warmer because of heat conduction between the coffee and the cup material. The warmth felt near the outside walls of the cup is due to radiation and the vapor emerging from the top of the cup carries energy by convection. The distinguishing features of the three modes are given in Table 1.

Radiation consists of electromagnetic waves, which have the same nature as visible light. The elementary particle of the radiation field is the photon. Heat is conducted in solids and fluids by free electrons and phonon–phonon interactions, whereas convection is energy transport by material transport.

While radiation can also be transported through the vacuum, conduction and convection need a medium. The conductive and convective heat flux is directly proportional to temperature differences. On the other hand, the celebrated Stefan–Boltzmann law states that the radiative heat flux is proportional to the difference of the fourth powers of the temperature. Because of this, radiation becomes the dominant effect at large temperatures.

Conduction and convection are local phenomena, which occur at the atomic length scale of approximately  $10^{-9}$  m. Radiation on the other hand is a non-local phenomenon. The average distance a photon travels between two collisions can vary between the atomic length scale of  $10^{-9}$  m up to  $10^{10}$  m (distance earth-sun) and even more. As a consequence, the commonly used mathematical descriptions of radiative heat transfer and conduction/convection are different.

Table 1 Modes of energy transfer			
	Radiation	Conduction	Convection
Energy transport by	photons	free electrons, Phonon interaction	material transport
Medium required	no	yes	yes
Temperature dependence	$q \sim T^4 - T_\infty^4$	$q \sim \nabla T$	$q \sim T - T_\infty$
Mean free path	$10^{-9} \sim 10^{10} m$	$\sim 10^{-9} m$	$\sim 10^{-9} m$
Depends on	$x, t, \Omega, \nu$	$x, t$	$x, t$

Furthermore, the physical quantities describing the radiation field depend on space, time, direction and frequency, while those used to describe conduction and convection depend only on space and time.

## 2.1 Fundamental Quantities

In this section we want to define the fundamental physical quantities describing the radiation field.

### 2.1.1 Intensity

The basic variable is the *spectral intensity*

$$\psi(t, x, \Omega, \nu), \quad (1)$$

the radiative energy flow per time, per area normal to the rays, per solid angle and per frequency. This means that  $\psi dt dA d\Omega d\nu$  has the dimension of energy flux and is proportional to the number of photons. The spectral intensity depends on position  $x \in \mathbf{R}^3$ , time  $t \in \mathbf{R}$ , direction  $\Omega \in S^2 = \{x \in \mathbf{R}^3 : \|x\| = 1\}$ , and frequency  $\nu \in \mathbf{R}^+$ .

The *total intensity*

$$\psi(t, x, \Omega) = \int_0^\infty \psi(t, x, \Omega, \nu) d\nu \quad (2)$$

is the spectral intensity integrated over the whole spectrum.

### 2.1.2 Energy Flux

The *total energy flux* is defined as

$$E(t, x) = \varphi(t, x) = \int_{S^2} \psi(t, x, \Omega) d\Omega = \int_{S^2} \int_0^\infty \psi(t, x, \Omega, \nu) d\nu d\Omega. \quad (3)$$

In the context of moment models, this quantity is denoted by  $E$ , in the context of diffusion models it is traditionally denoted by  $\varphi$  or  $\phi$ . The radiative energy is the zeroth order moment of the total intensity with respect to the direction  $\Omega$ . Several other moments will play an important role in the following.

### 2.1.3 Heat Flux

Consider an infinitesimal surface element with outward normal  $n$ . The ingoing and outgoing spectral heat fluxes are

$$\begin{aligned}
|F| &= \left| -|F^{\text{in}}| + |F^b| \right| \\
&= \int_{n \cdot \Omega < 0} (n \cdot \Omega) \psi d\Omega + \int_{n \cdot \Omega > 0} (n \cdot \Omega) \psi d\Omega \\
&= \int_{S^2} (n \cdot \Omega) \psi d\Omega.
\end{aligned} \tag{4}$$

Thus the *spectral heat flux* is

$$F(t, x, \nu) = \int_{S^2} \Omega \psi(t, x, \Omega, \nu) d\Omega. \tag{5}$$

To obtain the *total heat flux*, we integrate over the spectrum,

$$F(t, x) = \int_{S^2} \int_0^\infty \Omega \psi(t, x, \Omega, \nu) d\nu d\Omega. \tag{6}$$

#### 2.1.4 Radiation Pressure

The heat flux into a surface element  $dA$  is, as above,

$$(n \cdot \Omega) \psi dA d\Omega. \tag{7}$$

Thus the beam carries momentum at a rate

$$\frac{1}{c} (n \cdot \Omega) \psi n dA d\Omega. \tag{8}$$

The fraction of momentum falling onto  $dA$  is  $|n \cdot \Omega|$ . Therefore, the flow of momentum into  $dA$  in the normal direction is

$$\frac{1}{c} \psi |n \cdot \Omega|^2 dA d\Omega. \tag{9}$$

This must be counteracted by a pressure force  $p dA$  leading to the *spectral radiation pressure*

$$p = \frac{1}{c} \int_{S^2} \psi |n \cdot \Omega|^2 d\Omega. \tag{10}$$

The *spectral radiative pressure tensor*  $P_\nu$  is defined by

$$n^T P n = p, \tag{11}$$

thus

$$P(t, x, \nu) = \frac{1}{c} \int_{S^2} (\Omega \otimes \Omega) \psi(t, x, \Omega, \nu) d\Omega. \tag{12}$$

Here,  $\Omega \otimes \Omega$  is the outer product (tensor product). The *total radiative pressure tensor* is

$$P(t, x) = \frac{1}{c} \int_0^\infty \int_{S^2} (\Omega \otimes \Omega) \psi(t, x, \Omega, \nu) d\Omega d\nu. \quad (13)$$

Not quite correctly, we will also call the second order moment of  $\psi$ , without the factor  $\frac{1}{c}$ , radiative pressure.

## 2.2 Blackbody Radiation

In this section we want to define a perfect absorber, also called blackbody, and derive the Planck equilibrium distribution. The Planckian plays a crucial role in the following.

Consider an electromagnetic wave that hits the surface of a medium. The wave can either be reflected at the surface or penetrate the medium. If the wave passes through the medium without attenuation, the medium is called *transparent*. If no radiation reemerges it is called *opaque*. Otherwise, in the case of partial attenuation, it is called *semitransparent*.

A *blackbody* or perfect absorber is defined to have an opaque surface that does not reflect any radiation. A blackbody is thus a maximal absorber. A simple thermodynamical argument [66] shows that it is also a perfect emitter at every frequency and into any direction.

The blackbody emissive power spectrum has first been derived by Max Planck in his famous work on Quantum Statistics [65]. In standard textbooks on Quantum Mechanics nowadays it is usually derived in the context of second quantization of the electromagnetic field. Here, we want to give a different derivation by entropy minimization/maximization which fits into the context of this work.

If  $N(x, p)$  is the average number of photons with position  $x$  and momentum  $p$  in a phase space element of volume  $h^3$ , where  $h$  is Planck's constant, then

$$\int \int N(x, p) \frac{dx dp}{h^3} \quad (14)$$

is the number of photons in the phase space volume under consideration. Photons are integer-spin particles and obey Bose–Einstein statistics. According to a standard result [32] from statistical physics, the entropy of an ensemble of bosons is

$$S = -2k \int \int (N \log N - (N + 1) \log(N + 1)) \frac{dx dp}{h^3}. \quad (15)$$

Another standard result [32] relates the spectral intensity  $\psi$  and the number density  $N$ ,

$$N = \frac{c^2}{2h\nu^3} \psi. \quad (16)$$

The momentum can be written in terms of frequency and direction (“spherical coordinates”) as

$$p = \frac{h\nu}{c}\Omega, \quad (17)$$

thus

$$dp = \left(\frac{h}{c}\right)^3 \nu^2 d\nu d\Omega. \quad (18)$$

Consequently, the entropy density of the radiation field is

$$H = - \int \int \frac{2k\nu^2}{c^3} (N \log N - (N+1) \log(N+1)) d\nu d\Omega. \quad (19)$$

We want to define the mathematical entropy as

$$H_R = -S. \quad (20)$$

According to the Second Law of Thermodynamics, the entropy is a non-decreasing function of time. Thus, the equilibrium distribution for a given temperature has to maximize  $S$ , or equivalently minimize  $H_R$ . This principle yields the Planck equilibrium distribution

$$B(\nu, T) = \frac{2h\nu^3}{c^2} \frac{1}{\exp(\frac{h\nu}{kT}) - 1}, \quad (21)$$

which describes the emissive spectrum of a blackbody. Blackbody emissive power spectrum in nondimensional coordinates. In this derivation we made use of the Stefan–Boltzmann law,

$$B(T) = \int_0^\infty B(\nu, T) d\nu = \sigma_{\text{SB}} T^4, \quad (22)$$

with the Stefan–Boltzmann constant  $\sigma_{\text{SB}} = 5.670 \cdot 10^{-8} \frac{\text{W}}{\text{m}^2 \text{K}^4}$ , which gives the celebrated dependence of the total emissive power of a blackbody on the fourth power of its temperature.

### 2.3 The Transfer Equation

If the medium through which radiative energy travels is participating, then any incident beam will be affected by absorption and scattering while it travels through the medium. In the following, we want to consider a medium at rest (compared to the speed of light) and with constant refractive index. Furthermore, it is assumed that the medium is nonpolarizing and that it is in local thermodynamical equilibrium. For a very thorough discussion of these limitations see [88].

First we want to derive a discrete transfer equation and then, by passing to the limit, obtain the integro-differential equation describing radiative transfer.

Let us assume that there is only a finite set of directions ( $\Omega_j$ ) into which the photons can travel. Consider a beam into direction  $\Omega_i$  which travels a distance  $\Delta s$  through the medium. Several effects can lead to the augmentation and reduction of the beam.

### 2.3.1 Absorption

When a photon hits an atom or molecule inside the medium with the right amount of energy it can be absorbed, thus leading to an excited state of the atom/molecule. The amount of absorbed photons is directly proportional to the distance traveled and to the number of photons itself. Thus the change in the spectral intensity due to absorption is

$$(\Delta \psi)_{\text{abs}} = -\kappa \psi \Delta s. \quad (23)$$

### 2.3.2 Scattering

The photons can hit atoms or molecules in the medium and change their direction. We assume that the energy (or frequency) of the photons does not change (elastic scattering). We denote the fraction of photons that change their direction from  $\Omega_j$  to  $\Omega_i$  by  $S_{ij}$ . Note that the normalization condition

$$\sum_i S_{ij} = 1 \quad (24)$$

has to hold. The win/loss balance reads

$$(\Delta \psi(\Omega_i))_{\text{scat}} = \sigma \left( -\psi(\Omega_i) + \sum_j S_{ij} \psi(\Omega_j) \right) \Delta s. \quad (25)$$

### 2.3.3 Emission

If the medium has a finite temperature then it also emits thermal radiation which is distributed as blackbody radiation. The emitted intensity along a path is again proportional to the length of the path. If the spectral intensity of the photons  $\psi$  were a Planckian itself there should be no net absorption/emission. Hence the proportionality constant must be  $\kappa$ . Thus the intensity change caused by emission is

$$(\Delta \psi)_{\text{em}} = \kappa B \Delta s. \quad (26)$$

### 2.3.4 Overall Balance

Drawing a balance of the different effects, we obtain the discrete transfer equation

$$\begin{aligned} \psi(s + \Delta s, \Omega_i) = & \psi(s, \Omega_i) \\ & + \Delta s \left( \kappa(B(T) - \psi(\Omega_i)) + \sigma \left( \sum_j S_{ij} \psi(\Omega_j) - \psi(\Omega_i) \right) \right). \end{aligned} \quad (27)$$

The sum on the right hand side can be interpreted as a numerical quadrature rule. The matrix  $S_{ij}$  can be interpreted as the evaluation of a function,

$$S_{ij} = s(\Omega_i, \Omega_j). \quad (28)$$

If we assume that the set of directions is continuous, then the summation over all directions becomes an integration over the unit sphere. We obtain for all  $\Omega \in S^2$ ,

$$\begin{aligned} \psi(s + \Delta s, \Omega) = & \psi(s, \Omega) \\ & + \Delta s \left( \kappa(B(T) - \psi(\Omega)) + \sigma \left( \int_{S^2} s(\Omega, \Omega') \psi(\Omega') d\Omega' - \psi(\Omega) \right) \right). \end{aligned} \quad (29)$$

The normalization property (24) becomes

$$\int_{S^2} s(\Omega, \Omega') d\Omega' = 1. \quad (30)$$

A beam travels a distance  $\Delta x$  in a time  $\frac{\Delta x}{c}$ , where  $c$  is the speed of light. Thus we have

$$\begin{aligned} \psi(t + \Delta x/c, x + \Omega \Delta x, \Omega) = & \psi(t, x, \Omega) \\ & + \Delta x \left( \kappa(B(T) - \psi(t, x, \Omega)) + \sigma \left( \int_{S^2} s(\Omega, \Omega') \psi(t, x, \Omega') d\Omega' - \psi(t, x, \Omega) \right) \right). \end{aligned} \quad (31)$$

Taking the limit  $\Delta x \rightarrow 0$  we arrive at the *radiative transfer equation*. The frequency  $\nu$  can be incorporated as an additional parameter. At a position  $x$  and a time  $t$ , for all directions  $\Omega \in S^2$ , for all frequencies  $\nu \in [0, \infty]$  it holds

$$\begin{aligned} \frac{1}{c} \partial_t \psi(t, x, \Omega, \nu) + \Omega \nabla \psi(t, x, \Omega, \nu) \\ = \kappa(B(\nu, T) - \psi(t, x, \Omega, \nu)) + \sigma \left( \int_{S^2} s(\Omega, \Omega') \psi(t, x, \Omega', \nu) d\Omega' - \psi(t, x, \Omega, \nu) \right). \end{aligned} \quad (32)$$



We will also consider the special case of a one-dimensional *slab geometry*. We consider a plate which is finite in one dimension and infinite in the other dimensions. Thus, the intensity depends only on one space variable and is axially symmetric. Hence the equation simplifies to

$$\begin{aligned} \frac{1}{c} \partial_t \psi(t, x, \mu, \nu) + \mu \partial_x \psi(t, x, \mu, \nu) \\ = \kappa(2\pi B(\nu, T) - \psi(t, x, \mu, \nu)) + \sigma \left( \frac{1}{2} \int_{-1}^1 \psi(t, x, \mu', \nu) d\mu' - \psi(t, x, \mu, \nu) \right). \end{aligned} \quad (33)$$

Here,  $\mu$  is the cosine of the angle between direction and  $x$ -axis.

There are several other versions of the transfer equation, that we will consider in the following. First of all, in most applications, the time scale is much larger than the time the radiation needs to propagate into the medium. Thus we neglect the time-derivative and thus obtain the *steady* transfer equation. The absorption coefficient  $\kappa$  and the scattering coefficient  $\sigma$  can in general also depend on position and time. In the following, we want to assume *isotropic scattering*. This means that the scattering kernel is actually a constant,  $s = \frac{1}{4\pi}$ . For the purpose of glass, it often suffices to consider only absorption.

If frequency-dependence is not important, the so-called *grey* approximation can be used, meaning that all quantities are frequency-dependent. For glass manufacturing, however, frequency-dependence is important. Table 2 shows typical absorption coefficients for glass, depending on frequency. For smaller frequencies, absorption becomes very large. For all practical purposes, glass is perfectly opaque for frequencies smaller than a limit  $\nu_1$ .

## 2.4 Overall Energy Conservation

The radiation field, by emission, strongly depends on the temperature of the medium. On the other hand, by absorption, it also affects the temperature of the medium. For an overall energy balance we have to take into account this connection.

**Table 2** Eight frequency bands for glass

Band $i$	$\nu_i$	$\nu_{i+1}$	$\kappa_i$
1	$\infty$	5	0.40
2	5	0.3333	0.50
3	0.3333	0.2857	7.70
4	0.2857	0.2500	15.45
5	0.2500	0.2222	27.98
6	0.2222	0.1818	267.98
7	0.1818	0.1666	567.32
8	0.1666	0.1428	7136.06
	0.1428	0	Opaque

Also, we have to consider the two other modes of energy transfer, heat conduction and convection.

The general energy conservation equation for a moving compressible fluid may be stated as [66]

$$\rho_m \frac{Du}{Dt} = \rho(\partial_t u + v \nabla u) = -\nabla q - p \nabla v + \mu \Phi + \dot{Q}''', \quad (34)$$

where  $u$  is the internal energy,  $v$  is the velocity vector,  $q$  is the total heat flux vector,  $\Phi$  is the dissipation function, and  $\dot{Q}'''$  is the heat generated within the medium.

If the medium interacts with the radiation field through emission, absorption and scattering, then the heat flux term  $q$  in (34) contains the radiative heat flux. The radiative contributions to the internal energy and the pressure tensor can be neglected [66].

If we assume that  $du = c_m dT$  and furthermore that Fourier's law of heat conductivity holds,

$$q = q_{\text{con}} + F = -k \nabla T + F, \quad (35)$$

then (34) becomes

$$\rho_m c_m (\partial_t T + v \nabla T) = \nabla k \nabla T - p \nabla v + \mu \Phi + \dot{Q}''' - \nabla F. \quad (36)$$

In the following we want to restrict ourselves to a fluid at rest or a solid, i.e.  $v = 0$ . Furthermore we want to assume  $\Phi = 0$  and  $\dot{Q}''' = 0$ . Thus we consider

$$\rho_m c_m \partial_t T = \nabla k \nabla T - \nabla F. \quad (37)$$

By integrating the transfer equation with respect to  $\Omega$  and  $v$ , we see that this can be written as

$$\rho_m c_m \partial_t T = \nabla k \nabla T - \int_0^\infty \int_{S^2} \kappa(\psi - B) d\Omega dv. \quad (38)$$

## 2.5 Boundary Conditions

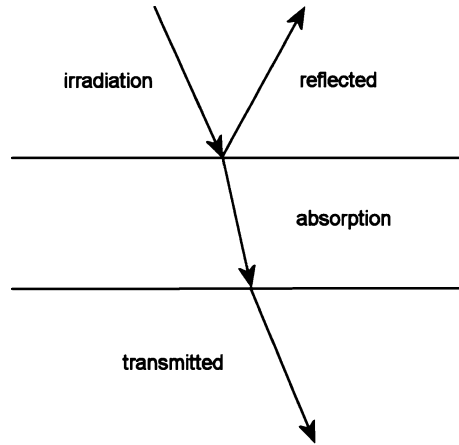
Consider a beam of photons hitting a slab, as shown in Fig. 1. Some of the irradiation will be reflected at the surface. A fraction of the radiation which penetrates the medium will be absorbed, the remaining will be transmitted. Thus we define the quantities

$$\text{Reflectivity} \quad \rho = \frac{\text{reflected part of radiation}}{\text{incoming radiation}}$$

$$\text{Absorptivity} \quad \alpha = \frac{\text{absorbed part of radiation}}{\text{incoming radiation}}$$

$$\text{Transmittivity} \quad \tau = \frac{\text{transmitted part of radiation}}{\text{incoming radiation}}.$$

**Fig. 1** Reflection, absorption, and transmission



By definition,  $\rho + \alpha + \tau = 1$ . A medium is called opaque if  $\tau = 0$ , i.e. no radiation is transmitted. For a black body,  $\alpha = 1$  and  $\rho = \tau = 0$ .

Radiative energy can also be emitted inside a medium and can be released through the surface. Since a blackbody is a perfect emitter, we define

$$\text{emissivity } \varepsilon = \frac{\text{energy emitted from surface}}{\text{energy emitted from a blackbody at the same temperature}}.$$

Radiative transfer is a long-range phenomenon. In principle, if we want to know the amount of radiation at one point  $x$ , we have to take into account radiation arriving from any direction and any point in space. Thus, an energy balance must be performed either over the whole space or over an enclosure bounded by opaque walls. When speaking of a wall or surface we actually mean a small layer (compared to the size of the enclosure) where radiation is reflected, absorbed and emitted.

Consider a domain bounded by an opaque surface and let  $n$  denote the outward normal vector. For a point on the boundary we have the following energy balance for all incoming directions, i.e. all  $\Omega$  with  $n \cdot \Omega < 0$ ,

$$\psi(x, t, \Omega) = \rho(\Omega') \psi(x, t, \Omega') + (1 - \rho(\Omega)) \psi_b. \quad (39)$$

Here,  $\Omega' = \Omega - 2(\Omega \cdot n)n$  is the outgoing direction that is reflected into  $\Omega$ . Furthermore,  $I_{v,b}$  is the amount of radiation emitted from the surface, cf. Fig. 2.

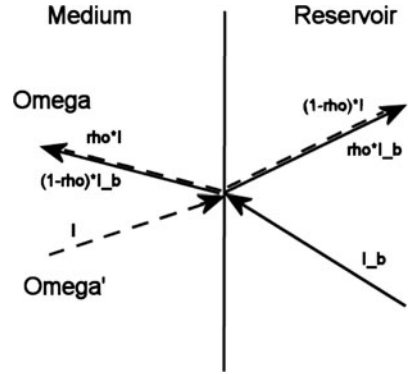
Mostly, we will assume that the incoming radiation is a Planckian at some temperature,

$$\psi_b = B(T_b). \quad (40)$$

The reflectivity  $\rho$  generally depends on the direction  $\Omega$ . It can be computed using Snell's law. On the interface between two media with refraction indexes  $n_1$  and  $n_2$ , the refraction angle (with respect to the normal)  $\theta_2$  of the transmitted ray and the incident angle  $\theta_1$  are related by

$$n_1 \sin \theta_1 = n_2 \sin \theta_2. \quad (41)$$

Fig. 2 Boundary condition



The reflectivity is then given by Fresnel's equation

$$\rho = \frac{1}{2} \left[ \frac{\tan^2(\theta_1 - \theta_2)}{\tan^2(\theta_1 + \theta_2)} + \frac{\sin^2(\theta_1 - \theta_2)}{\sin^2(\theta_1 + \theta_2)} \right]. \quad (42)$$

In the case of total refraction,  $\rho = 1$ .

The heat equation (38) can for example be supplemented with the following boundary conditions. Assuming that the opaque body surrounding the medium under consideration is a gas in a large reservoir, we can consider the heat flux through the boundary due to advection

$$k \frac{\partial T}{\partial n} = h(T_b - T). \quad (43)$$

Here,  $T_b$  is the outside temperature. We want to note that the value of the parameter  $h$  has to be determined by experiment. Also, we have to emphasize that the modeling of heat exchange by advection is actually quite sophisticated and still a subject of research. However, we will assume in the following the simple boundary conditions stated above.

## 2.6 Summary

In order to model glass cooling we consider the following radiative transfer problem. For a point  $x$  in the domain  $V \subset \mathbf{R}^3$

$$c_m \rho_m \frac{\partial T}{\partial t} = \nabla \cdot k \nabla T - \int_{v_1}^{\infty} \int_{S^2} \kappa(B - I) d\Omega dv, \quad (44a)$$

$$\forall v > v_1 : \Omega \cdot \nabla \psi = \kappa(B - \psi) + \sigma(\phi - \psi), \quad (44b)$$

where

$$\phi(x, \Omega, \nu) = \frac{1}{4\pi} \int_{S^2} s(\Omega, \Omega') \psi(x, \Omega', \nu) d\Omega'$$

is the scattered intensity. Here, we have explicitly included the opaque band for frequencies in the interval  $[0, \nu_1]$ , where absorption is infinitely high and thus  $\psi \equiv B$ .

On the boundary, for  $x \in \partial V$ , the ingoing radiation is prescribed by semi-transparent boundary conditions

$$I(\Omega) = \rho(n \cdot \Omega) I(\Omega') + (1 - \rho(n \cdot \Omega)) I_b(\Omega), \quad \forall n \cdot \Omega < 0, \quad (44c)$$

while the temperature is assumed to obey

$$k n \cdot \nabla T = h(T_b - T) + \alpha \pi \left( \frac{n_2}{n_1} \right)^2 \int_0^{\nu_1} B(\nu, T_b) - B(\nu, T) d\nu. \quad (44d)$$

The additional term comes from the fact that in the opaque band  $0 < \nu < \nu_1$  the medium behaves like a perfect black body.

At initial time  $t = 0$ , the temperature shall be given by

$$T(x, 0) = T_0(x). \quad (44e)$$

In these equations,  $\psi(t, x, \Omega, \nu)$  denotes the specific radiation intensity at point  $x \in V$  traveling in direction  $\Omega \in S^2$  with frequency  $\nu > 0$  at time  $t \geq 0$ . The outside radiation  $I_b$  is assumed to be known for the ingoing directions (i.e.  $n \cdot \Omega < 0$ ) on the boundary. We denote the outward normal on  $\partial V$  by  $n$ . Furthermore,  $T(t, x)$  denotes the material temperature and  $T_b$  is the exterior temperature on the boundary. The equations contain as parameters the opacity  $\kappa$ , the scattering coefficient  $\sigma$ , the heat conductivity  $k$  and the convective heat transfer coefficient  $h$ . Moreover,  $B$  denotes Planck's function

$$B(\nu, T) = n_1^2 \frac{2h\nu^3}{c^2} \left( e^{\frac{h\nu}{k_B T}} - 1 \right)^{-1}$$

for black body radiation in glass which involves Planck's constant  $h_P$ , Boltzmann's constant  $k_B$  and the speed of light in vacuum  $c$ . The integration in the second term of the temperature boundary condition (44d) is done on the opaque interval of the spectrum  $[0, \nu_1]$ , where radiation is completely absorbed. At the interface between glass and surrounding air with refractive indices  $n_1 > n_2$ , respectively, light rays are reflected and refracted. This is modeled by the so-called semi-transparent boundary conditions (44c). The reflectivity  $\rho \in [0, 1]$  is the proportion of radiation that is reflected. It is equal to 1 if total reflection occurs i.e. if  $\theta_1 > \theta_c$  where  $\theta_c$  is the critical angle given by  $\sin \theta_c = n_2/n_1$ . Otherwise  $\rho$  is calculated according to Fresnel's equation

$$\rho(\mu) = \frac{1}{2} \left( \frac{\tan^2(\theta_1 - \theta_2)}{\tan^2(\theta_1 + \theta_2)} + \frac{\sin^2(\theta_1 - \theta_2)}{\sin^2(\theta_1 + \theta_2)} \right),$$

where the refraction angles  $\theta_1$  and  $\theta_2$  are given by  $\cos \theta_1 = |n \cdot \Omega| = \mu$  and Snell's law of refraction

$$n_1 \sin \theta_1 = n_2 \sin \theta_2.$$

The solid angles of the reflected ray in (44c) is

$$\Omega' = \Omega - 2(n \cdot \Omega)n.$$

Finally, the hemispheric emissivity  $\alpha$  of the boundary surface in (44d) is related to the reflectivity  $\rho$  by

$$\alpha = 2n_1 \int_0^1 1 - \rho(\mu) d\mu.$$

For these equations and other applications in glass manufacturing problems we refer, for example, to [39, 40, 46, 87], and the monographs [31] and [60].

Analytical results concerning the existence and uniqueness of solutions to the transfer equation itself and to the radiative heat transfer equations, where also energy conservation and additionally heat conduction are considered, have been obtained by many authors. A rather recent review on methods for transport equations can be found in [6], cf. also [5]. The transfer equation together with energy conservation is considered in [28, 58]. The issue of heat conduction is addressed in [37, 43, 44]. Convection, conduction and radiation is treated in [53, 69].

### 3 Direct Numerical Methods

The main difficulties in solving numerically the integro-differential equation (44) are the large set of unknowns and the coupling between the transport and the integral operators. For instance,  $\psi$  is a function of time variable  $t$ , space variable  $x$ , frequency variable  $\nu$ , and direction variable  $\Omega$ . Solving the large linear system of algebraic equations induced by discretizing these variables is computationally very demanding.

Here, we focus on the solution of steady-state, mono-energetic, frequency decoupled, isotropic radiative transfer problems in three space dimensions. However, all the methods presented in this paper can be straightforwardly extended to the more general problem (44). Hence the radiative transfer equation we consider reads

$$\Omega \cdot \nabla \psi + (\sigma + \kappa) \psi = \sigma \phi + \kappa B \quad (45)$$

with boundary values  $\psi = g$ . The (45) models the changes of an intensity  $\psi(x, \Omega)$  as particles are passing through the domain  $V$  at position point  $x = (x, y, z)^T$  in the direction  $\Omega = (\mu, \eta, \xi)^T$  and are subject to losses due to absorption  $\kappa$  and scattering  $\sigma$ , while their number grows due to the source  $B$  inside the domain  $V$ . We assume that  $\sigma$  and  $\kappa$  are nonnegative functions and we introduce the mean intensity  $\phi$  as

$$\phi(x) = \frac{1}{4\pi} \int_{S^2} \psi(x, \Omega') d\Omega'. \quad (46)$$

We also define the scattering ratio  $\gamma$  and the opacity coefficient  $\vartheta$  as

$$\gamma = \max_{x \in V} \left( \frac{\sigma(x)}{\sigma(x) + \kappa(x)} \right) \quad \text{and} \quad \vartheta = \min_{x \in V} (\sigma(x) + \kappa(x)) \text{diam}(V). \quad (47)$$

Here  $\text{diam}(V)$  is the diameter of the space domain  $V$ . In applications,  $\gamma$  and  $\vartheta$  are used to characterize the convergence rates of the iterative methods and the diffusion limits in the optically thick medium.

Many numerical methods have been used to solve the (45). For a review on some of these methods see [52, 75]. It is well known [1] that the standard Source Iteration (SI) becomes extremely costly when the scattering ratio  $\gamma \approx 1$ . The standard Diffusion Synthetic Acceleration (DSA) has been widely used to accelerate the source iteration [4, 10]. The SI and DSA methods can be seen respectively, as Richardson iteration and preconditioned Richardson iteration with the diffusion approach as preconditioner.

We implement SI, DSA and a Krylov subspace method to solve the (45). We also propose a fast multilevel algorithm [36] which uses the approximate inverse operator as a preconditioner and solves the linear system only in the coarse meshes. Numerical results show this algorithm to be faster than DSA in many regimes. The robustness, efficiency and convergence rates of these methods are illustrated by several numerical test examples in both one and two space dimensions. Comparison of the results obtained by different methods is also included in this section. The material in this section is taken from [76].

### 3.1 Ordinates and Space Discretizations

We start with a discrete ordinates discretization in angle. This corresponds to expanding the integrals on the unit sphere  $S^2$  in terms of  $N$  weighted quadrature rules,

$$\int_{S^2} \psi(x, \Omega) d\Omega \simeq \sum_{l=1}^N w_l \psi(x, \Omega_l), \quad (48)$$

where  $\Omega_l = (\mu_l, \eta_l, \xi_l)^T$ , for all  $l = 1, \dots, N$ , with  $N = n(n+2)$ , and  $n$  is the number of direction cosines. Since  $\Omega_l \in S^2$ , we have

$$\mu_l^2 + \eta_l^2 + \xi_l^2 = 1, \quad \text{for all } l = 1, 2, \dots, N.$$

We assume  $n$  an even number of quadrature points so that the points  $(\mu_l, \eta_l, \xi_l)$  are nonzero, symmetric with respect to the  $x$ -,  $y$ - and  $z$ -axis and they are invariant under  $90^\circ$  rotations. Furthermore they satisfy the relation

$$\xi_i^2 = \xi_1^2 + 2 \frac{i-1}{n-2} (1 - 3\xi_1^2),$$

for  $i = 1, 2, \dots, n/2$  and  $0 < \xi_1 < 1/3$ .

In (48)  $w_l$  are the corresponding weights chosen to be positive and satisfy

$$\sum_{l=1}^N \Omega_l = 4\pi, \quad \sum_{l=1}^N \Omega_l \mu_l = 0, \quad \sum_{l=1}^N \Omega_l \eta_l = 0 \quad \text{and} \quad \sum_{l=1}^N \Omega_l \xi_l = 0.$$

In practice we choose  $w_l = 4\pi/N$  and  $(\mu_l, \eta_l, \xi_l)$  are set in such a way the above conditions are guaranteed. Let  $S_N$  be a given set of  $N$  discrete directions in  $S^2$ , then a semi-discrete formulation of (45) is

$$\mu_l \frac{\partial \psi_l}{\partial x} + \eta_l \frac{\partial \psi_l}{\partial y} + \xi_l \frac{\partial \psi_l}{\partial z} + (\sigma + \kappa) \psi_l = \sigma \phi(x) + \kappa q(x), \quad (49)$$

$\psi_l(x)$  denotes approximation to  $\psi(x, \mu_l, \eta_l, \xi_l)$  and  $\phi$  is given by

$$\phi(x) = \frac{1}{4\pi} \sum_{l=1}^N w_l \psi_l(x).$$

To discretize the (49) in space we suppose for simplicity, that the spatial domain is a box,  $V = [a_x, b_x] \times [a_y, b_y] \times [a_z, b_z]$ . Then we cover the domain  $V$  with a uniform numerical mesh defined by

$$V_h = \left\{ x_{ijk} = (x_i, y_j, z_k)^T, \quad x_i = i\Delta x, \quad y_j = j\Delta y, \quad z_k = k\Delta z, \right. \\ \left. i = 0, 1, \dots, I, \quad j = 0, 1, \dots, J, \quad k = 0, 1, \dots, K \right\},$$

where  $x_0 = a_x$ ,  $x_I = b_x$ ;  $y_0 = a_y$ ,  $y_J = b_y$ ;  $z_0 = a_z$ ,  $z_K = b_z$ ; and  $h$  denotes the maximum cell size. We define the averaged grid points

$$\Delta x = x_i - x_{i-1}, \quad \Delta y = y_j - y_{j-1}, \quad \Delta z = z_k - z_{k-1}, \\ x_{i-\frac{1}{2}} = \frac{x_{i-1} + x_i}{2}, \quad y_{j-\frac{1}{2}} = \frac{y_{j-1} + y_j}{2}, \quad z_{k-\frac{1}{2}} = \frac{z_{k-1} + z_k}{2},$$

for  $i = 1, \dots, I$ ,  $j = 1, \dots, J$  and  $k = 1, \dots, K$ . By using the notation  $f_{ijk}$  to denote the approximation value of the function  $f$  at the grid point  $(x_i, y_j, z_k)$ , the fully discrete approximation for the (45) can be written as

$$\mu_l \frac{\psi_{l,ijk} - \psi_{l,i-1,j,k}}{\Delta x} + \eta_l \frac{\psi_{l,ijk} - \psi_{l,i,j-1,k}}{\Delta y} + \xi_l \frac{\psi_{l,ijk} - \psi_{l,i,j,k-1}}{\Delta z} \\ + \left( \sigma_{i-\frac{1}{2},j-\frac{1}{2},k-\frac{1}{2}} + \kappa_{i-\frac{1}{2},j-\frac{1}{2},k-\frac{1}{2}} \right) \psi_{l,i-\frac{1}{2},j-\frac{1}{2},k-\frac{1}{2}} \\ = \sigma_{i-\frac{1}{2},j-\frac{1}{2},k-\frac{1}{2}} \phi_{i-\frac{1}{2},j-\frac{1}{2},k-\frac{1}{2}} + \kappa_{i-\frac{1}{2},j-\frac{1}{2},k-\frac{1}{2}} q_{i-\frac{1}{2},j-\frac{1}{2},k-\frac{1}{2}}, \quad (50)$$

where the cell averages values of  $\psi$  are given by



$$\begin{aligned}
\psi_{l,i-1jk} &= \frac{1}{\Delta x} \int_{y_{j-1}}^{y_j} \int_{z_{k-1}}^{z_k} \psi_l(x_i, y, z) dy dz, \\
\psi_{l,ij-1k} &= \frac{1}{\Delta y} \int_{x_{i-1}}^{x_i} \int_{z_{k-1}}^{z_k} \psi_l(x, y_j, z) dx dz, \\
\psi_{l,ijk-1} &= \frac{1}{\Delta z} \int_{x_{i-1}}^{x_i} \int_{y_{j-1}}^{y_j} \psi_l(x, y, z_k) dx dy, \\
\psi_{l,ijk} &= \frac{1}{\Delta x \Delta y \Delta z} \int_{x_{i-1}}^{x_i} \int_{y_{j-1}}^{y_j} \int_{z_{k-1}}^{z_k} \psi_l(x, y, z) dx dy dz,
\end{aligned} \tag{51}$$

In this paper we use the Diamond difference method to approximate the fluxes in (51). The method consists on centred differences and approximating the function values at the cell centres  $f_{l,i-\frac{1}{2}j-\frac{1}{2}k-\frac{1}{2}}$  by the average of their values at the eight neighbouring nodes as

$$\begin{aligned}
f_{l,i-\frac{1}{2}j-\frac{1}{2}k-\frac{1}{2}} &= \frac{1}{8} \left[ f_{l,i-1j-1k-1} + f_{l,i-1jk-1} + f_{l,i-1j-1k} + f_{l,i-1jk} \right. \\
&\quad \left. + f_{l,ij-1k-1} + f_{l,ijk-1} + f_{l,ij-1k} + f_{l,ijk} \right].
\end{aligned} \tag{52}$$

Hence the discrete mean intensity  $\phi_{i-\frac{1}{2}j-\frac{1}{2}k-\frac{1}{2}}$  in (50) is given by

$$\phi_{i-\frac{1}{2}j-\frac{1}{2}k-\frac{1}{2}} = \sum_{l=1}^N w_l \psi_{l,i-\frac{1}{2}j-\frac{1}{2}k-\frac{1}{2}}.$$

Other discretizations using Legendre polynomial collocation in ordinates and finite element or Petrov–Galerkin methods in space can be used in the same manner, we refer to [10, 52, 81, 82] for details. For the discretization of the boundary conditions in (49) we can proceed as follows:

when  $\hat{x} = a_x$ , the normal  $n(\hat{x}_{0jk}) = (-1, 0, 0)^T$ , then  $n(\hat{x}_{0jk}) \cdot \Omega_l = -\mu_l$ , and for  $\mu_l > 0$  we have  $\psi_{l,0jk} = g_{0jk}$

when  $\hat{y} = a_y$ , the normal  $n(\hat{x}_{i0k}) = (0, -1, 0)^T$ , then  $n(\hat{x}_{i0k}) \cdot \Omega_l = -\eta_l$ , and for  $\eta_l > 0$  we have  $\psi_{l,i0k} = g_{i0k}$

when  $\hat{z} = a_z$ , the normal  $n(\hat{x}_{ij0}) = (0, 0, -1)^T$ , then  $n(\hat{x}_{ij0}) \cdot \Omega_l = -\xi_l$ , and for  $\xi_l > 0$  we have  $\psi_{l,ij0} = g_{ij0}$

The other three cases can be discretized in a similar way. Needless to say that for a given  $l = 1, 2, \dots, N$  no component of  $\Omega_l$  is ever zero and only three of the above six cases can hold. Furthermore, in the discretization (50) there are  $(I+1)(J+1)(K+1)$  unknowns  $\psi_{l,ijk}$  and  $IK + JI + JK + I + J + K + 1$  boundary equations.

### 3.2 Linear System Formulation

In order to simplify the notations and to get closer to a compact linear algebra formulation of (50), we first define the matrix entries

$$\begin{aligned}
d_{l,i-\frac{1}{2}j-\frac{1}{2}k-\frac{1}{2}} &= \frac{|\mu_l|}{\Delta x} + \frac{|\eta_l|}{\Delta y} + \frac{|\xi_l|}{\Delta z} + \frac{\sigma_{i-\frac{1}{2}j-\frac{1}{2}k-\frac{1}{2}} + \kappa_{i-\frac{1}{2}j-\frac{1}{2}k-\frac{1}{2}}}{8}, \\
e_{l,i-\frac{1}{2}j-\frac{1}{2}k-\frac{1}{2}} &= \frac{-|\mu_l|}{\Delta x} + \frac{-|\eta_l|}{\Delta y} + \frac{-|\xi_l|}{\Delta z} + \frac{\sigma_{i-\frac{1}{2}j-\frac{1}{2}k-\frac{1}{2}} + \kappa_{i-\frac{1}{2}j-\frac{1}{2}k-\frac{1}{2}}}{8}.
\end{aligned}$$

and

$$\begin{aligned}
u_{l,i-\frac{1}{2}j-\frac{1}{2}k-\frac{1}{2}} &= \frac{|\mu_l|}{\Delta x} + \frac{|\eta_l|}{\Delta y} + \frac{-|\xi_l|}{\Delta z} + \frac{\sigma_{i-\frac{1}{2}j-\frac{1}{2}k-\frac{1}{2}} + \kappa_{i-\frac{1}{2}j-\frac{1}{2}k-\frac{1}{2}}}{8}, \\
\bar{u}_{l,i-\frac{1}{2}j-\frac{1}{2}k-\frac{1}{2}} &= \frac{|\mu_l|}{\Delta x} + \frac{-|\eta_l|}{\Delta y} + \frac{|\xi_l|}{\Delta z} + \frac{\sigma_{i-\frac{1}{2}j-\frac{1}{2}k-\frac{1}{2}} + \kappa_{i-\frac{1}{2}j-\frac{1}{2}k-\frac{1}{2}}}{8}, \\
\underline{u}_{l,i-\frac{1}{2}j-\frac{1}{2}k-\frac{1}{2}} &= \frac{|\mu_l|}{\Delta x} + \frac{-|\eta_l|}{\Delta y} + \frac{-|\xi_l|}{\Delta z} + \frac{\sigma_{i-\frac{1}{2}j-\frac{1}{2}k-\frac{1}{2}} + \kappa_{i-\frac{1}{2}j-\frac{1}{2}k-\frac{1}{2}}}{8}, \\
v_{l,i-\frac{1}{2}j-\frac{1}{2}k-\frac{1}{2}} &= \frac{-|\mu_l|}{\Delta x} + \frac{|\eta_l|}{\Delta y} + \frac{|\xi_l|}{\Delta z} + \frac{\sigma_{i-\frac{1}{2}j-\frac{1}{2}k-\frac{1}{2}} + \kappa_{i-\frac{1}{2}j-\frac{1}{2}k-\frac{1}{2}}}{8}, \\
\bar{v}_{l,i-\frac{1}{2}j-\frac{1}{2}k-\frac{1}{2}} &= \frac{-|\mu_l|}{\Delta x} + \frac{|\eta_l|}{\Delta y} + \frac{-|\xi_l|}{\Delta z} + \frac{\sigma_{i-\frac{1}{2}j-\frac{1}{2}k-\frac{1}{2}} + \kappa_{i-\frac{1}{2}j-\frac{1}{2}k-\frac{1}{2}}}{8}, \\
\underline{v}_{l,i-\frac{1}{2}j-\frac{1}{2}k-\frac{1}{2}} &= \frac{-|\mu_l|}{\Delta x} + \frac{-|\eta_l|}{\Delta y} + \frac{|\xi_l|}{\Delta z} + \frac{\sigma_{i-\frac{1}{2}j-\frac{1}{2}k-\frac{1}{2}} + \kappa_{i-\frac{1}{2}j-\frac{1}{2}k-\frac{1}{2}}}{8},
\end{aligned}$$

Next, we define the vectors

$$\begin{aligned}
\Psi_l &\equiv \begin{pmatrix} \Psi_{l,0} \\ \vdots \\ \Psi_{l,K} \end{pmatrix} \in \mathbf{R}^{(I+1)(J+1)(K+1)}, \quad \text{with} \\
\Psi_{l,k} &\equiv \begin{pmatrix} \Psi_{l,0k} \\ \vdots \\ \Psi_{l,Jk} \end{pmatrix} \in \mathbf{R}^{(I+1)(J+1)}, \quad \Psi_{l,jk} \equiv \begin{pmatrix} \Psi_{l,0jk} \\ \vdots \\ \Psi_{l,Ijk} \end{pmatrix} \in \mathbf{R}^{(I+1)}; \\
\Phi &\equiv \begin{pmatrix} \Phi_{1-\frac{1}{2}} \\ \vdots \\ \Phi_{K-\frac{1}{2}} \end{pmatrix} \in \mathbf{R}^{IJK}, \quad \text{with} \\
\Phi_{k-\frac{1}{2}} &\equiv \begin{pmatrix} \Phi_{1-\frac{1}{2}k-\frac{1}{2}} \\ \vdots \\ \Phi_{J-\frac{1}{2}k-\frac{1}{2}} \end{pmatrix} \in \mathbf{R}^{IJ}, \quad \Phi_{j-\frac{1}{2}k-\frac{1}{2}} \equiv \begin{pmatrix} \phi_{1-\frac{1}{2}j-\frac{1}{2}k-\frac{1}{2}} \\ \vdots \\ \phi_{I-\frac{1}{2}j-\frac{1}{2}k-\frac{1}{2}} \end{pmatrix} \in \mathbf{R}^I;
\end{aligned}$$

$$Q \equiv \begin{pmatrix} Q_{1-\frac{1}{2}} \\ \vdots \\ Q_{K-\frac{1}{2}} \end{pmatrix} \in \mathbf{R}^{JK}, \quad \text{with}$$

$$Q_{k-\frac{1}{2}} \equiv \begin{pmatrix} Q_{1-\frac{1}{2}k-\frac{1}{2}} \\ \vdots \\ Q_{J-\frac{1}{2}k-\frac{1}{2}} \end{pmatrix} \in \mathbf{R}^{IJ}, \quad Q_{j-\frac{1}{2}k-\frac{1}{2}} \equiv \begin{pmatrix} q_{1-\frac{1}{2}j-\frac{1}{2}k-\frac{1}{2}} \\ \vdots \\ q_{I-\frac{1}{2}j-\frac{1}{2}k-\frac{1}{2}} \end{pmatrix} \in \mathbf{R}^I;$$

In what follows we define the matrix  $H_l$  (known as sweep matrix) for the first sweep case  $\mu_l < 0$ ,  $\eta_l < 0$ ,  $\xi_l < 0$  and the other seven sweep cases can be derived similarly. In order to simplify the notation, we drop hereafter the space grids subscripts from the matrix entries unless otherwise stated. Thus,

$$H_l \equiv \begin{pmatrix} D_l & E_l & & \\ & \ddots & \ddots & \\ & & D_l & E_l \\ & & & D_l & S \\ & & & & S \end{pmatrix} \in \mathbf{R}^{(I+1)(J+1)(K+1) \times (I+1)(J+1)(K+1)}, \quad \text{with}$$

$$D_l \equiv \begin{pmatrix} D_l & U_l & & \\ & \ddots & \ddots & \\ & & D_l & U_l \\ & & & S \end{pmatrix} \in \mathbf{R}^{(I+1)(J+1) \times (I+1)(J+1)}, \quad \text{with}$$

$$D_l \equiv \begin{pmatrix} d & u & & \\ & \ddots & \ddots & \\ & & d & u \\ & & & 1 \end{pmatrix} \in \mathbf{R}^{(I+1) \times (I+1)}, \quad U_l \equiv \begin{pmatrix} \underline{u} & \bar{u} & & \\ & \ddots & \ddots & \\ & & \underline{u} & \bar{u} \\ & & & 1 \end{pmatrix} \in \mathbf{R}^{(I+1) \times (I+1)};$$

$$E_l \equiv \begin{pmatrix} V_l & W_l & & \\ & \ddots & \ddots & \\ & & V_l & W_l \\ & & & S \end{pmatrix} \in \mathbf{R}^{(I+1)(J+1) \times (I+1)(J+1)}, \quad \text{with}$$

$$V_l \equiv \begin{pmatrix} \underline{v} & \bar{v} & & \\ & \ddots & \ddots & \\ & & \underline{v} & \bar{v} \\ & & & 1 \end{pmatrix} \in \mathbf{R}^{(I+1) \times (I+1)}, \quad W_l \equiv \begin{pmatrix} v & \bar{v} & & \\ & \ddots & \ddots & \\ & & v & \bar{v} \\ & & & 1 \end{pmatrix} \in \mathbf{R}^{(I+1) \times (I+1)}.$$

$$\begin{aligned}
S &\equiv \begin{pmatrix} S & S \\ & \ddots & \ddots \\ & & S & S \\ & & & S \end{pmatrix} \in \mathbf{R}^{(I+1)(J+1) \times (I+1)(J+1)}, \quad \text{with} \\
S &\equiv \begin{pmatrix} 1 & 1 \\ & \ddots & \ddots \\ & & 1 & 1 \\ & & & 1 \end{pmatrix} \in \mathbf{R}^{(I+1) \times (J+1)}. \\
\Sigma_l &\equiv \begin{pmatrix} \Sigma_{l,1-\frac{1}{2}} \\ & \ddots \\ & & \Sigma_{l,K-\frac{1}{2}} \\ & & & 0 \end{pmatrix} \in \mathbf{R}^{(I+1)(J+1)(K+1) \times IJK}, \quad \text{with} \\
\Sigma_{l,k-\frac{1}{2}} &\equiv \begin{pmatrix} \Sigma_{l,1-\frac{1}{2}k-\frac{1}{2}} & & \\ & \ddots & \\ & & \Sigma_{l,I-\frac{1}{2}k-\frac{1}{2}} \\ & & & 0 \end{pmatrix} \in \mathbf{R}^{(I+1)(J+1) \times IJ}, \quad \text{and} \\
\Sigma_{l,j-\frac{1}{2}k-\frac{1}{2}} &\equiv \\
&\begin{pmatrix} \frac{\sigma_{1-\frac{1}{2}j-\frac{1}{2}k-\frac{1}{2}} + \kappa_{1-\frac{1}{2}j-\frac{1}{2}k-\frac{1}{2}}}{8} & & \\ & \ddots & \\ & & \frac{\sigma_{I-\frac{1}{2}j-\frac{1}{2}k-\frac{1}{2}} + \kappa_{I-\frac{1}{2}j-\frac{1}{2}k-\frac{1}{2}}}{8} \\ & & & 0 \end{pmatrix} \in \mathbf{R}^{(I+1) \times I}.
\end{aligned}$$

Using these definitions with  $\Psi$  and  $\Phi$  being the unknowns, the fully discrete equation (50) can be written in matrix form as

$$\left( \begin{array}{c|c} H_1 & -\Sigma_1 \\ & \vdots \\ & -\Sigma_N \\ \hline -\frac{w_1}{4\pi}S \dots -\frac{w_N}{4\pi}S & I \end{array} \right) \begin{pmatrix} \Psi_1 \\ \vdots \\ \Psi_N \\ \Phi \end{pmatrix} = \begin{pmatrix} Q_1 \\ \vdots \\ Q_N \\ 0 \end{pmatrix}, \quad (53)$$

where  $I$  is the  $IJK \times IJK$  identity matrix and  $0$  is the  $IJK$  null vector. The linear system (53) can be rewritten in common linear algebra notation as

$$Ax = b \quad (54)$$

with

$$A \equiv \left( \begin{array}{ccc|c} H_1 & & & -\Sigma_1 \\ & \ddots & & \vdots \\ & & H_N & -\Sigma_N \\ \hline -\frac{w_1}{4\pi}S & \dots & -\frac{w_N}{4\pi}S & I \end{array} \right), \quad x \equiv \begin{pmatrix} \Psi_1 \\ \vdots \\ \Psi_N \\ \Phi \end{pmatrix}, \quad \text{and} \quad b \equiv \begin{pmatrix} Q_1 \\ \vdots \\ Q_N \\ 0 \end{pmatrix}.$$

### 3.3 Preconditioning Techniques

In computational radiative transfer the desired quantity is usually the mean intensity  $\Phi$  which is a function only of position  $x$ . Therefore we use the Gaussian elimination to eliminate the intensity  $\Psi_1, \dots, \Psi_N$  from (53) and the reduced equation

$$\left( I - \frac{1}{4\pi} \sum_{l=1}^N w_l S H_l^{-1} \Sigma_l \right) \Phi = \frac{1}{4\pi} \sum_{l=1}^N w_l S H_l^{-1} Q_l, \quad (55)$$

is solved for  $\Phi$ . We rewrite (55) in compact form as

$$(I - \mathcal{A}) \Phi = f, \quad (56)$$

where the Schur matrix  $\mathcal{A}$  and the right hand side  $f$  are given by

$$\mathcal{A} = \frac{1}{4\pi} \sum_{l=1}^N w_l S H_l^{-1} \Sigma_l \quad \text{and} \quad f = \frac{1}{4\pi} \sum_{l=1}^N w_l S H_l^{-1} Q_l.$$

In this section we briefly discuss some numerical methods used in the literature to solve the linear system (56).

#### 3.3.1 Source Iteration

The most popular iterative method to solve (55) is the Richardson iteration known in the radiative transfer community as Source Iteration (SI) method. Given an initial guess  $\Phi^{(0)}$ , the  $(m+1)$ -iterate solution is obtained by

$$\Phi^{(m+1)} = \frac{1}{4\pi} \sum_{l=1}^N w_l S H_l^{-1} \left( Q_l + \Sigma_l \Phi^{(m)} \right), \quad m = 0, 1, \dots \quad (57)$$

It is easy to see that iteration (57) is equivalent to preconditioned block Gauss–Seidel method applied to (54), where the preconditioner is the block lower triangle of the matrix  $A$ . Thus, if  $M$  is the block lower triangle of  $A$ ,

$$M \equiv \begin{pmatrix} H_1 & & & \\ & \ddots & & \\ & & H_N & \\ -\frac{w_1}{4\pi}S & \dots & -\frac{w_N}{4\pi}S & I \end{pmatrix},$$

$x$  and  $b$  are as given in (54), then

$$Mx^{(m+1)} = (M - A)x^{(m)} + b,$$

and

$$x^{(m+1)} = (I - M^{-1}A)x^{(m)} + M^{-1}b. \quad (58)$$

Therefore the  $(m+1)$ -iterate mean intensity satisfy

$$\Phi^{(m+1)} = \frac{1}{4\pi} \sum_{l=1}^N w_l S H_l^{-1} \Psi_l^{(m+1)} = \frac{1}{4\pi} \sum_{l=1}^N w_l S H_l^{-1} (Q_l + \Sigma_l \Phi^{(m)}),$$

which is identical to (57).

Formal results from linear algebra [29, 35] demonstrate that the preconditioned Richardson iteration (58) converges rapidly as long as the norm of the matrix  $(I - M^{-1}A)$  is small. This condition is ensured by taking the scattering ratio  $\gamma$  small, compare [1] for analysis. For  $\gamma \ll 1$  the SI method converges rapidly, but for  $\gamma \approx 1$  (large optical opacity) convergence becomes slow and may restrict the efficiency of the SI algorithm. The SI algorithm can be implemented as follows

Algorithm 1: SI algorithm

```

given the initial guess  $\Phi^{(0)}$ 
do  $m = 0, 1, \dots, itmax$ 
  do  $l = 1, 2, \dots, N$ 
    a. set  $w_l \leftarrow Q_l + \Sigma_l \Phi^{(m)}$ 
    b. solve for  $y_l$ :  $H_l y_l = w_l$ 
    c. set  $w_l \leftarrow S y_l$ 
  end do
  d. compute  $\Phi^{(m+1)} = \frac{1}{4\pi} \sum_{l=1}^N w_l w_l$ 
  e. compute  $r^{(m)} = \Phi^{(m+1)} - \Phi^{(m)}$ 
     if  $\left( \frac{\|r^{(m)}\|_{L^2}}{\|r^{(0)}\|_{L^2}} \leq \tau \right)$  stop
end do
```

Here  $itmax$  is the maximum number of the iterations  $m$ ,  $\tau$  is a given tolerance and  $\|\cdot\|_{L^2}$  is the discrete  $L^2$ -norm. The step (b) can be solved directly using Gaussian elimination known in computational radiative transfer as sweeping procedure. Additionally, for each direction  $\Omega_l$  in  $S_N$  only one of the eight possible sweeps is needed.

### 3.3.2 Diffusion Synthetic Acceleration

Among the methods used to accelerate the SI algorithm are the synthetic acceleration procedures [1, 4]. The procedures consist on splitting the SI in to two-step iterations. Thus, we denote  $\psi^{(m+\frac{1}{2})}$  as first iteration for the SI in the continuous form of the problem (45),

$$\begin{aligned}\Omega \cdot \nabla \psi^{(m+\frac{1}{2})} + (\sigma + \kappa) \psi^{(m+\frac{1}{2})} &= \frac{\sigma}{4\pi} \int_{S^2} \psi^{(m)}(x, \Omega') d\Omega' + \kappa q(x), \\ \psi^{(m+\frac{1}{2})}(\hat{x}, \Omega) &= g(\hat{x}),\end{aligned}\tag{59}$$

and an equation for  $\psi^{(m+1)}$  is required in such a way to be more accurate approximation to  $\psi$  than  $\psi^{(m+\frac{1}{2})}$ . To perform this step with synthetic acceleration method, we subtract (59) from (45),

$$\begin{aligned}\Omega \cdot \nabla (\psi - \psi^{(m+\frac{1}{2})}) + (\sigma + \kappa) (\psi - \psi^{(m+\frac{1}{2})}) &= \frac{\sigma}{4\pi} \int_{S^2} (\psi - \psi^{(m)})(x, \Omega') d\Omega', \\ (\psi - \psi^{(m+\frac{1}{2})})(\hat{x}, \Omega) &= 0,\end{aligned}\tag{60}$$

then (60) are replaced by an approximate problem. The Diffusion Synthetic Acceleration (DSA) method [4] approximates the (60) by the diffusion problem

$$-\nabla \cdot \left( \frac{1}{3(\sigma + \kappa)} \nabla \phi \right) + \kappa \phi = \frac{\sigma}{4\pi} \int_{S^2} (\psi - \psi^{(m)})(x, \Omega') d\Omega', \quad x \in V,$$

Here  $\phi(x)$  is an approximation to the mean intensity

$$\phi(x) \approx \frac{1}{4\pi} \int_{S^2} (\psi^{(m+1)} - \psi^{(m+\frac{1}{2})})(x, \Omega') d\Omega'.$$

Thus the  $(m+1)$ -iterate mean intensity is given by

$$\phi^{(m+1)} = \phi^{(m+\frac{1}{2})} + \phi.$$

Note that (61) does not depend on the angle variable  $\Omega$ , is linear elliptic equation and simple to solve numerically with less computational cost and memory requirement.

In order to build a discretization for the diffusion problem (61) which is consistent to the one used for the radiative transfer equation (45), we consider the same grid structure and the same notations as those used in Sect. 2. Hence a space discretization for the (61) reads as

$$-\mathcal{D}_h^2 \left( \frac{1}{3(\sigma + \kappa)} \phi \right)_{ijk} + \kappa_{i-\frac{1}{2}j-\frac{1}{2}k-\frac{1}{2}} \phi_{i-\frac{1}{2}j-\frac{1}{2}k-\frac{1}{2}} = p_{i-\frac{1}{2}j-\frac{1}{2}k-\frac{1}{2}}, \tag{61}$$

where  $p_{i-\frac{1}{2}j-\frac{1}{2}k-\frac{1}{2}} = \sigma_{i-\frac{1}{2}j-\frac{1}{2}k-\frac{1}{2}}(\phi_{i-\frac{1}{2}j-\frac{1}{2}k-\frac{1}{2}}^{(m+\frac{1}{2})} - \phi_{i-\frac{1}{2}j-\frac{1}{2}k-\frac{1}{2}}^{(m)})$  and the difference operator  $\mathcal{D}_h^2$  is given by  $\mathcal{D}_h^2 = \mathcal{D}_x^2 + \mathcal{D}_y^2 + \mathcal{D}_z^2$ , with

$$\begin{aligned}\mathcal{D}_x^2(\beta\phi)_{ijk} &= \frac{\beta_{ijk} + \beta_{i+1jk}}{2} \frac{\phi_{i+1jk} - \phi_{ijk}}{(\Delta x)^2} - \frac{\beta_{i-1jk} + \beta_{ijk}}{2} \frac{\phi_{ijk} - \phi_{i-1jk}}{(\Delta x)^2}, \\ \mathcal{D}_y^2(\beta\phi)_{ijk} &= \frac{\beta_{ijk} + \beta_{ij+1k}}{2} \frac{\phi_{ij+1k} - \phi_{ijk}}{(\Delta y)^2} - \frac{\beta_{ij-1k} + \beta_{ijk}}{2} \frac{\phi_{ijk} - \phi_{ij-1k}}{(\Delta y)^2}, \\ \mathcal{D}_z^2(\beta\phi)_{ijk} &= \frac{\beta_{ijk} + \beta_{ijk+1}}{2} \frac{\phi_{ijk+1} - \phi_{ijk}}{(\Delta z)^2} - \frac{\beta_{ijk-1} + \beta_{ijk}}{2} \frac{\phi_{ijk} - \phi_{ijk-1}}{(\Delta z)^2}.\end{aligned}$$

The functions  $\kappa_{i-\frac{1}{2}j-\frac{1}{2}k-\frac{1}{2}}$ ,  $\phi_{i-\frac{1}{2}j-\frac{1}{2}k-\frac{1}{2}}$  and  $p_{i-\frac{1}{2}j-\frac{1}{2}k-\frac{1}{2}}$  appeared in (61) are given as in formula (52). The gradient in the boundary conditions is approximated by upwinding without using ghost points. For example, on the boundary surface  $x = a_x$  of the domain  $V$ , the boundary discretization is

$$\phi_{\frac{1}{2}j+\frac{1}{2}k+\frac{1}{2}} - \frac{2}{3(\sigma_{\frac{1}{2}j-\frac{1}{2}k-\frac{1}{2}} + \kappa_{\frac{1}{2}j-\frac{1}{2}k-\frac{1}{2}})} \frac{\phi_{\frac{3}{2}j-\frac{1}{2}k-\frac{1}{2}} - \phi_{\frac{1}{2}j-\frac{1}{2}k-\frac{1}{2}}}{\Delta x} = 0,$$

and similar work has to be done for the other boundaries. All together, the above discretization leads to a linear system of form

$$D\phi = p, \quad (62)$$

where  $D$  is  $IJK \times IJK$  nonsymmetric positive definite matrix obtained from the difference diffusion operator (61) with boundary conditions included, and  $p$  is  $IJK$  vector containing the right hand side term.

Once again the DSA method can be viewed as preconditioned Richardson iteration for the linear system (54) with the diffusion matrix  $D$  like preconditioner,

$$x^{(m+1)} = (I - D^{-1}A)x^{(m)} + D^{-1}b,$$

and  $D^{-1}$  is obtained by solving the diffusion linear system (62). In terms of  $\Phi$  this is equivalent to

$$\Phi^{(k+1)} = \left( I - (I - D^{-1})\mathcal{A} \right) \Phi^{(k)} + (I - D^{-1})b.$$

The implementation of DSA method to approximate the solution of the radiative transfer equation (45) is carried out in the following algorithm

Algorithm 2: DSA algorithm

given the initial guess  $\Phi^{(0)}$

do  $m = 0, 1, \dots, itmax$

(a) – (d) are similar to Algorithm 1 for the intermediate solution  $\Phi^{(m+\frac{1}{2})}$



- (e) compute  $p = \sigma(\Phi^{(m+\frac{1}{2})} - \Phi^{(m)})$
- (f) solve for  $\varphi$ :  $D\varphi = p$
- (g) set  $\Phi^{(m+1)} = \Phi^{(m+\frac{1}{2})} + \varphi$
- (h) compute  $r^{(m)} = \Phi^{(m+1)} - \Phi^{(m)}$
- if  $\left(\frac{\|r^{(m)}\|_{L^2}}{\|r^{(0)}\|_{L^2}} \leq \tau\right)$  stop
- end do

Note that the first lines in Algorithm 2 are similar to the Algorithm 1. However, the source iteration algorithm gives only the intermediate solution  $\Phi^{(m+\frac{1}{2})}$  which has to be corrected by adding the solution  $\varphi$  obtained by the diffusion approach. Furthermore, if iterative methods are used for the diffusion approach, then an inner iteration loop has to be added to the iteration used by the SI algorithm and an outer SI iteration may require less accuracy from the inner iterations.

### 3.3.3 Krylov Subspace Methods

In general the matrices  $A$  and  $\mathcal{A}$  in (54) and (56) respectively are nonsymmetric and not diagonally dominant. Furthermore, since  $\sigma$  and  $\kappa$  are nonnegative functions and  $S_N$  has nonzero directions, the matrix  $A$  has positive diagonal elements and nonpositive off-diagonal elements. In addition, if  $e_{l,i-\frac{1}{2}j-\frac{1}{2}k-\frac{1}{2}} \leq 0$ , for all  $l, i, j, k$ , then the matrix  $A$  is weakly diagonally dominant. This condition is equivalent to

$$h = \max(\Delta x, \Delta y, \Delta z) \leq \max_{ijk} \left( \frac{8|\mu_l|}{\sigma_{i-\frac{1}{2}j-\frac{1}{2}k-\frac{1}{2}} + \kappa_{i-\frac{1}{2}j-\frac{1}{2}k-\frac{1}{2}}}, \frac{8|\eta_l|}{\sigma_{i-\frac{1}{2}j-\frac{1}{2}k-\frac{1}{2}} + \kappa_{i-\frac{1}{2}j-\frac{1}{2}k-\frac{1}{2}}}, \frac{8|\xi_l|}{\sigma_{i-\frac{1}{2}j-\frac{1}{2}k-\frac{1}{2}} + \kappa_{i-\frac{1}{2}j-\frac{1}{2}k-\frac{1}{2}}} \right), \quad \forall l, \quad (63)$$

which means physically that the cell size is no more than eight mean free paths of the particles being simulated. Needless to say that the condition (63) gives the bound of the coarser mesh should be used in the computations.

In this paper we propose two Krylov subspace based methods, namely the BI-Conjugate Gradient Stabilized (Bicgstab) [86] and the Generalized Minimal Residual (Gmres(m)) [71], where  $m$  stands for the number of restarts for Krylov subspace used in the orthogonalization. Bicgstab method has been applied early in [82] to solve (56). The main idea behind these approaches is that the Krylov subspace methods can be interpreted as weighted Richardson iteration

$$x^{(m)} = (I - \alpha P^{-1}A)x^{(m-1)} + \alpha P^{-1}b, \quad 0 < \alpha < 2, \quad m = 1, \dots, \quad (64)$$

applied to the linear system (54), where the relaxation parameters  $\alpha$  and the preconditioner  $P$  are variables within each iteration step. Note that when  $\alpha = 1$  and  $P = M$  the iteration (64) is reduced to the SI method.

The Bicgstab and Gmres(m) algorithms to solve the linear system (56) can be implemented in the conventional way as in [36, 71, 86], with the only difference that the dense matrix  $\mathcal{A}$  can not be explicitly stored. All what is needed, however, is a subroutine that performs a matrix-vector multiplication as shown in the following algorithm

**Algorithm 3: Matrix-vector multiplication**

given a vector  $u$ , to apply the matrix  $\mathcal{A}$  to  $u$  we proceed as  
do  $l = 1, \dots, N$   
a. set  $v_l \leftarrow \Sigma_l u$   
b. solve for  $w_l$ :  $H_l w_l = v_l$   
c. set  $v_l \leftarrow S w_l$   
end do  
d. set  $u \leftarrow u - \frac{1}{4\pi} \sum_{l=1}^N w_l v_l$

Note that only three vectors ( $u$ ,  $v_l$  and  $w_l$ ) are needed to perform the multiplication of the matrix  $\mathcal{A}$  to the vector  $u$ . Moreover, only three calls for the algorithm 3 are required from the Bicgstab or Gmres(m) subroutines.

Preconditioned Bicgstab or Gmres(m) methods can be also used. For instance, in the case when the matrix  $\mathcal{A}$  is diagonally dominant, the Bicgstab or Gmres(m) methods can be accelerated by using the diagonal as a preconditioner. This approach which requires additional computational work can be easily implemented. It is worth to say that incomplete Cholesky or ILU type preconditioners can not be used to solve (56) because the matrix  $\mathcal{A}$  is never formed explicitly.

### 3.4 A Fast Multilevel Preconditioner

We describe in this section multilevel solvers for the linear system (56) using an approximate inverse operator as preconditioner on each level of the multigrid hierarchy. Multilevel methods were first applied to radiative transfer problems in [36]. The author proposes two different type of smoothings to approximate solutions for the one dimensional version of (45) in slab geometry.

To formulate multilevel solvers we first modify our notation slightly. Using the discretizations introduced in Sect. 2 we assume for simplicity, a given sequence of uniform, equidistant nested grids

$$V_1 \subset V_2 \subset \dots \subset V_{L-1} \subset V_L = V_h,$$

on  $V$  with respective mesh sizes  $\Delta x = \Delta y = \Delta z = 2^{-l}$ ,  $l = 1, \dots, L$ . We use the subscripts  $l$  and  $L$  to refer to the coarse and fine level respectively. Therefore the problem statement (56) becomes

$$(I - \mathcal{A}_L) \Phi_L = f_L. \quad (65)$$

With  $M$  being the iteration matrix, multilevel can be written as follows

$$M\Phi_L^{(m+1)} + (I - \mathcal{A}_L - M)\Phi_L^{(m)} = f_L.$$

This formulation is equivalent to,

$$\Phi_L^{(m+1)} = \Phi_L^{(m)} + M^{-1} \left( f_L - (I - \mathcal{A}_L)\Phi_L^{(m)} \right) = \Phi_L^{(m)} + M^{-1}r^{(m)},$$

where  $r$  denotes the residual associated to (65) and is defined by

$$r = f_L - (I - \mathcal{A}_L)\Phi_L.$$

The preconditioner we consider in this section is the Atkinson–Brakhage approximate inverse [8] given as

$$M^{-1} = B_l^L = I + (I - \mathcal{A}_l)^{-1}\mathcal{A}_L. \quad (66)$$

Then the  $(m + 1)$ -iterate solution for (65) is simply

$$\Phi_L^{(m+1)} = \Phi_L^{(m)} + B_l^L r^{(m)}.$$

Analysis of convergence for this kind of multilevel methods has been done in [36]. The central ideas in this analysis are the strong convergence and collective compactness of the operators generated by  $\mathcal{A}_l$ .

Let us first define the two-level (Grid2) algorithm. Applying the multilevel preconditioner (66) to the problem (65) we need the fine-to-coarse grid transfer operator  $\mathcal{R}_L^l$  defined by

$$\mathcal{R}_L^l \Phi_L = \Phi_l,$$

and the coarse-to-fine grid transfer operator  $\mathcal{P}_l^L$  defined by

$$\mathcal{P}_l^L \Phi_l = \Phi_L.$$

A natural way to choose these operators is, bilinear interpolation for  $\mathcal{P}_l^L$  and simple injection for  $\mathcal{R}_L^l$  as in the standard multigrid literature [30]. However, for radiative transfer equation with discontinuous variables these operators have to be changed to those given in [3] which are specially designed for problems with jumping coefficients. Note that to use these operators we require that any discontinuity of  $\kappa$ ,  $\sigma$  or  $q$  in (45) is a spatial mesh point.

The Grid2 algorithm for solving (65) is detailed in the following steps

**Algorithm 4:** Grid2 algorithm

given the fine level  $\{L, \mathcal{A}_L, f_L\}$ , the coarse level  $\{l, \mathcal{A}_l, f_l\}$ , the initial guess  $\Phi_L^{(0)}$  and the tolerance  $\tau$   
do  $m = 0, 1, \dots, itmax$

- a. compute the residual  $r^{(m)} = f_L - (I - \mathcal{A}_L)\Phi_L^{(m)}$
- b. set  $u_L \leftarrow \mathcal{A}_L r^{(m)}$
- c. restriction  $u_l \leftarrow \mathcal{R}_L^l u_L$
- d. solve on the coarse level for  $v_l$ :  $(I - \mathcal{A}_l)v_l = u_l$   
Nyström interpolation
- e. compute  $w_l \leftarrow \mathcal{A}_l v_l$
- f. prolongation  $w_L \leftarrow \mathcal{P}_l^L w_l$
- g. set  $z_L \leftarrow u_L + w_L$
- h. compute the preconditioner  $p \leftarrow r + z_L$
- i. update the solution  $\Phi_L^{(m+1)} = \Phi_L^{(m)} + p$
- j. compute the residual  $r^{(m+1)} = f_L - (I - \mathcal{A}_L)\Phi_L^{(m+1)}$   
if  $\left( \frac{\|r^{(m+1)}\|_{L^2}}{\|r^{(0)}\|_{L^2}} \leq \tau \right)$  stop  
end do

The step (d) usually solves the coarse problem exactly using direct methods. However, since  $\mathcal{A}_l$  is dense matrix which is never explicitly computed nor stored, iterative solvers are required to perform the step (d). In our numerical examples we used Gmres(m) method which has been discussed in Sect. 4. Note that in our context the notation Grid2 for two-level algorithm does not necessarily mean that we consider two levels of mesh refinements. Thus, Algorithm 4 is also applicable in cases where we have two different space discretizations on the same mesh ( $L \neq l + 1$ ).

The fully multilevel algorithm (Gridnest) or nested iteration as referred to in [30] can be implemented recursively as follows

**Algorithm 5: Gridnest algorithm**

- given the finest level  $\{l_{\max}, \mathcal{A}_{l_{\max}}, f_{l_{\max}}\}$ , the coarsest level  $\{l_{\min}, \mathcal{A}_{l_{\min}}, f_{l_{\min}}\}$  and the tolerances  $\{\tau_l\}$ ,  $l = l_{\min}, \dots, l_{\max}$
- a. Solve on the coarsest level for  $\Phi_{l_{\min}}$ :  $(I - \mathcal{A}_{l_{\min}})\Phi_{l_{\min}} = f_{l_{\min}}$   
do  $k = l_{\min} + 1, \dots, l_{\max}$
  - b. set  $l \leftarrow k - 1$
  - c. set  $L \leftarrow k$
  - d. compute the right hand side  $f_L$
  - e. set  $\Phi_L^{(0)} \leftarrow \mathcal{P}_l^L \Phi_l$
  - f. set  $\tau \leftarrow \tau_l$
  - g. call Grid2 to solve for  $\Phi_L$ :  $(I - \mathcal{A}_L)\Phi_L = f_L$   
end do

Some comments are in order. The steps (b)–(f) are needed only to set the inputs, fine level  $\{L, \mathcal{A}_L, f_L\}$ , coarse level  $\{l, \mathcal{A}_l, f_l\}$ , initial guess  $\Phi_L^{(0)}$  and tolerance  $\tau$  to the algorithm Grid2. Recall that Gridnest uses coarse levels to obtain improved initial guesses for fine level problems. The tolerance parameters  $\{\tau_l\}$ , which determine how many iterations of the multilevel algorithm to do on each level, can be considered either fixed or adaptively chosen during the course of computation.

### 3.5 Numerical Results

The methods discussed in the above sections are tested on a PC with AMD-K6 200 processors using Fortran compiler, see [76] for details. In all these methods the iterations are terminated when

$$\frac{\|r^{(m)}\|_{L^2}}{\|r^{(0)}\|_{L^2}} \leq 10^{-5}. \quad (67)$$

To solve the diffusion problem in DSA we used a preconditioned Bicgstab whereas, Gmres(10) is used in Grid2 and Gridnest to solve the coarse problems. These inner iterations are stopped as in (67) but with  $10^{-2}$  instead of  $10^{-5}$ . In all our computations for the two space dimension cases we used a discrete  $S_N$ -direction set with 60 directions from [22].

#### 3.5.1 Radiative Transfer Equation in 1D Slab Geometry

Our first example is the (45) in 1D slab geometry

$$\begin{aligned} \mu \frac{\partial \psi}{\partial x} + (\sigma + \kappa) \psi &= \frac{\sigma}{2} \int_{-1}^1 \psi(x, \mu') d\mu' + \kappa q(x) \\ \psi(0, \mu) &= 1, \quad \mu > 0, \quad \text{and} \quad \psi(1, \mu) = 0, \quad \mu < 0. \end{aligned} \quad (68)$$

We set  $q = 0$ , we used 64 Gauss quadrature nodes in the discrete ordinates and a fine mesh of 512 gridpoints in the space discretization. The convergence results for two different values of  $\sigma$  and  $\kappa$  are shown in Fig. 3. The fast convergence of Grid2 is well demonstrated in both cases. Although the scattering ratio for the two cases is 0.99, Grid2 method shows strong reduction of number of iterations comparing to the other methods. Same observation is shown when the regime is optically thick ( $\sigma = 99$ ,  $\kappa = 1$ ).

Next we want to compare the efficiency of these methods in terms of CPU time and number of iterations when the scattering ratio  $\gamma$  runs in the range  $(0, 1)$ . To this end we set  $\sigma = 10$  and we vary  $\kappa$  keeping the fine gridpoints fixed to 512. In Fig. 4 we plot the scattering ratio versus the number of iterations in the left and versus the CPU time in the right. Grid2 and Gmres(40) preserve roughly the same amount of computational work (referring to number of iterations and CPU time) in the whole interval, while the SI and DSA become costly for values of  $\gamma$  near 1.

#### 3.5.2 Radiative Transfer Equation with Thermal Source

The second example is the (45) in the unit square with a thermal source  $q = B(T)$ , with  $B$  is the frequency-integrated Planckian  $B = a_R T^4$  with  $a_R$  is the radiation constant ( $a_R = 1.8 \times 10^{-8}$ ). We fix the temperature to have the linear profile

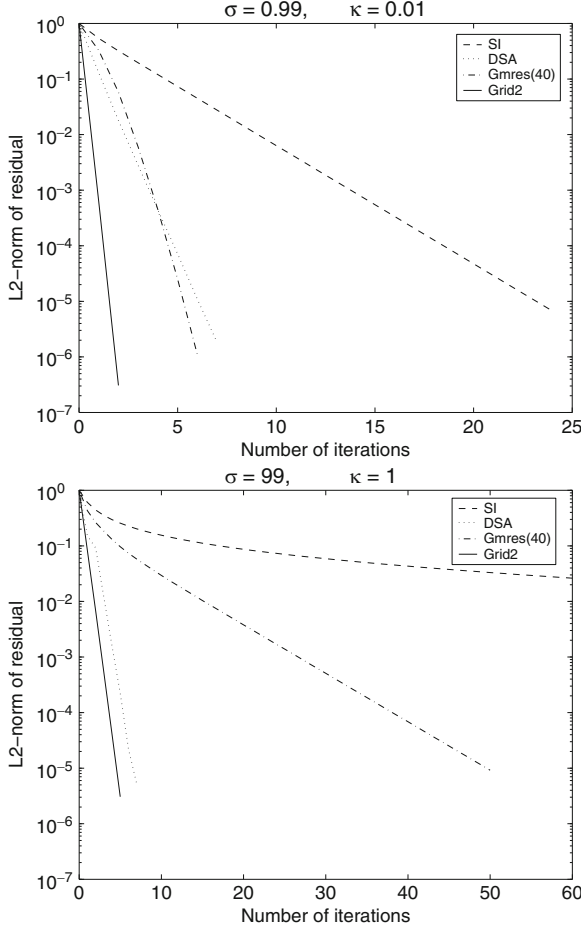


**Fig. 3** Convergence plots for the radiative transfer equation in 1D slab geometry

$T(x, y) = 800x + 1,000$  and the boundary function  $g(\hat{x}, \hat{y}) = B(T(\hat{x}, \hat{y}))$ . In Fig. 5 we show the convergence plots for different values of  $\sigma$  and  $\kappa$  using a fine mesh of  $257 \times 257$  gridpoints. In all cases Grid2 algorithm presents faster convergence behaviour than DSA even in the diffusion regime ( $\sigma = 100$  and  $\kappa = 1$ ).

We summarize in Table 3 the CPU time consumed for each method to perform the computations with the different values of  $\sigma$  and  $\kappa$ . In Table 4 we report, the number of gridpoints  $I \times J$  at each level, the iteration counter  $m$  for that level, the number of iterations in Gmres(10)  $i_{Gmres}$ , the  $L^\infty$ -norm of the residual,  $\|r^{(m)}\|_{L^\infty}$ , and the factor  $\|r^{(m)}\|_{L^\infty} / \|r^{(m-1)}\|_{L^\infty}$ .

The results presented in Table 4 do not include those obtained for  $\sigma = 1$ ,  $\kappa = 1$  or  $\sigma = 100$ ,  $\kappa = 1$  because the number of iterations  $m$  in Grid2 is very large. For instance, for  $\sigma = 100$ ,  $\kappa = 1$  this number surpasses 15 on the coarsest mesh.

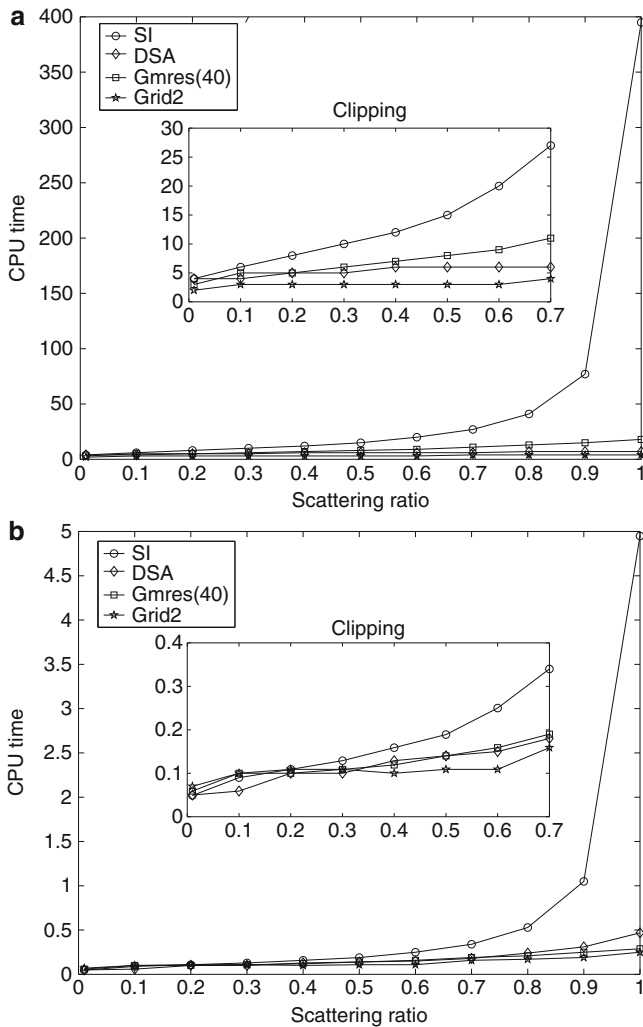


**Fig. 4** Plots of scattering ratio  $\gamma$  versus the number of iterations in (a) and the CPU time (seconds) in (b). In both figures  $\sigma$  is fixed to 10

Nevertheless, in all these test cases we have observed that there is very little variation in the number  $i_{\text{Gmres}}$  and the reduction factor  $\|r^{(m)}\|_{L^\infty} / \|r^{(m-1)}\|_{L^\infty}$  as the meshes are refined.

The results of these tables and Fig. 5 show various interesting features about the behaviours of the preconditioner used by each method. First, where the scattering ratio  $\gamma = 0.99$  ( $\sigma = 100$  and  $\kappa = 1$ ), it is clear that the SI method is unacceptably slow to converge. The convergence rate is improved significantly by Gmres(40), and it is improved even more by DSA method but at the cost of extra work and storage.

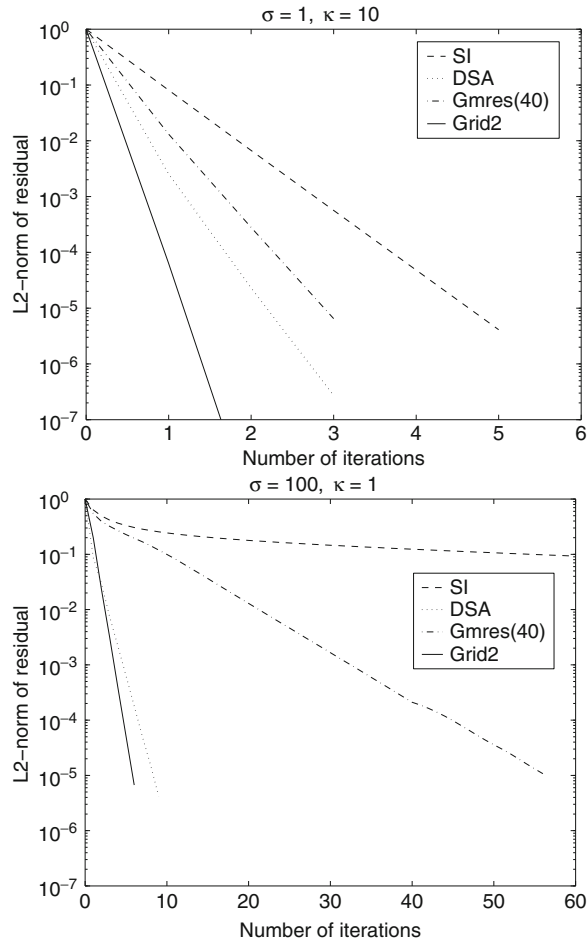


**Fig. 5** Convergence plots for the radiative transfer equation with thermal source

**Table 3** CPU time (in seconds)

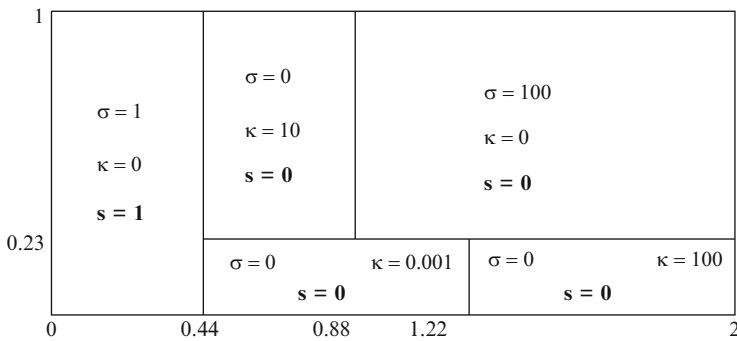
	SI	DSA	Gmres(40)	Grid2
$\sigma = 1, \kappa = 10$	17.8	29.1	15.5	17.1
$\sigma = 1, \kappa = 1$	33.7	77.4	20.8	23.5
$\sigma = 100, \kappa = 1$	2389.8	82.3	174.4	121.7

The most effective method for solving this example, however, is the multilevel Grid2 and Gridnest methods. Second, the number of iterations  $i_{\text{Gmres}}$  in Gridnset remain nearly the same in all levels and is bounded by the number in the coarsest level.



**Table 4** Results obtained by Gridnest for  $\sigma = 1$  and  $\kappa = 10$  at different levels

$I \times J$	$m$	$i_{\text{Gmres}}$	$\ r^{(m)}\ _{L^\infty}$	$\ r^{(m)}\ _{L^\infty} / \ r^{(m-1)}\ _{L^\infty}$
$33 \times 33$	0		0.73E+00	
	1	2	0.32E-01	0.43E-01
	2	2	0.12E-02	0.37E-01
	3	3	0.56E-05	0.46E-04
$65 \times 65$	0		0.11E-01	
	1	2	0.33E-03	0.30E-01
	2	2	0.12E-05	0.36E-04
$129 \times 129$	0		0.83E-02	
	1	2	0.67E-03	0.81E-01
	2	2	0.53E-05	0.79E-04
$257 \times 257$	0		0.22E-02	
	1	2	0.73E-04	0.33E-01
	2	2	0.15E-06	0.20E-04

**Fig. 6** Geometry and values of  $\sigma$ ,  $\kappa$ ,  $s = \kappa q$  for the discontinuous equation

### 3.5.3 Radiative Transfer Equation with Discontinuous Variables

The aim of this example is to test the multilevel algorithm for radiative transfer problem with jumping coefficients. Thus, the problem statement is the (45) augmented by discontinuous scattering, absorption and source term [2]. The space domain geometry and the values of  $\sigma$ ,  $\kappa$  and  $s = \kappa B$  for each subdomain are given in Fig. 6. We take in the first run of this example vacuum boundary conditions whereas, in the second run we use the nonhomogeneous boundary condition  $g$ ,

$$g(\hat{x}, \hat{y}) = \begin{cases} 1 & \text{when } \hat{x} = 0 \text{ and } 0 \leq \hat{y} \leq 1, \\ 1 & \text{when } \hat{y} = 0 \text{ and } 0 < \hat{y} \leq 0.44, \\ 1 & \text{when } \hat{y} = 1 \text{ and } 0 < \hat{y} \leq 0.44, \\ 0 & \text{otherwise.} \end{cases}$$

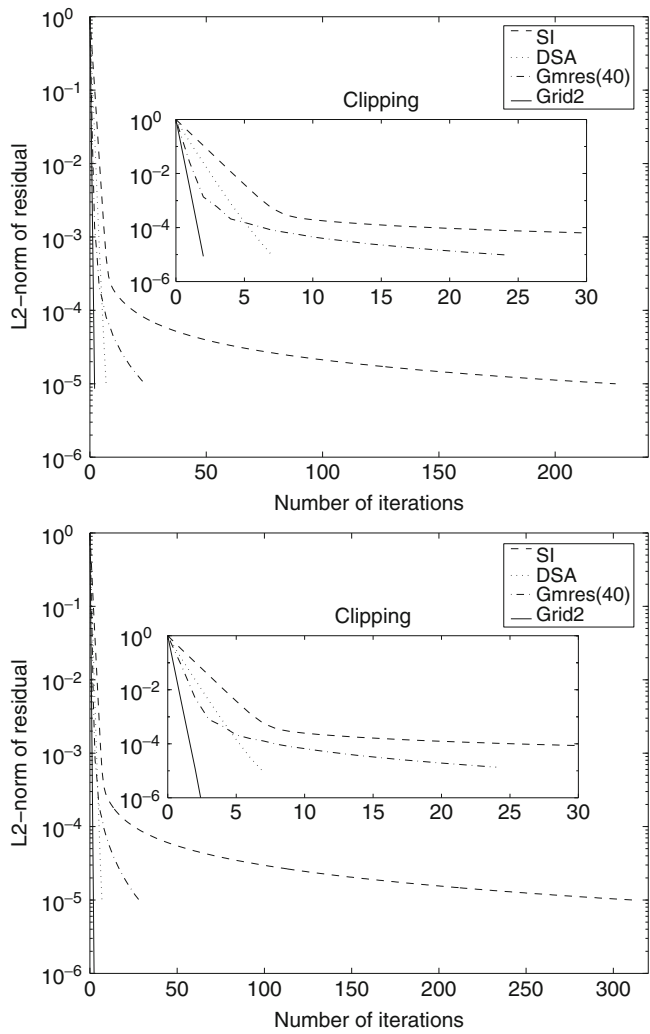


**Fig. 7** Convergence rates for the discontinuous equation subject to vacuum boundary conditions (*top*) and nonhomogeneous boundary conditions (*bottom*)

**Table 5** CPU time (in seconds)

	SI	DSA	Gmres(40)	Grid2
Vacuum boundary condition	794.04	304.42	192.25	205.22
Nonhomogeneous boundary condition	1100.18	397.53	110.07	201.91

The space domain is discretized uniformly into  $400 \times 200$  gridpoints at the finest level. We display in Fig. 7 the convergence rates for the two runs. Table 5 provides the running time used by each method for these computations. A simple inspection

**Table 6** Gridnest results for the discontinuous problem with vacuum boundary

$I \times J$	$m$	$i_{\text{Gmres}}$	$\ r^{(m)}\ _{L^\infty}$	$\ r^{(m)}\ _{L^\infty} / \ r^{(m-1)}\ _{L^\infty}$
$100 \times 50$	0		0.13E+01	
	1	9	0.50E+00	0.39E+00
	2	9	0.13E+00	0.27E+00
	3	8	0.24E-01	0.19E+00
	4	7	0.14E-02	0.57E-01
	5	7	0.45E-05	0.32E-02
$200 \times 100$	0		0.51E-01	
	1	8	0.10E-02	0.21E-01
	2	7	0.78E-05	0.73E-02
	3	7	0.32E-07	0.41E-02
$400 \times 200$	0		0.79E-02	
	1	7	0.40E-04	0.51E-02
	2	7	0.13E-06	0.33E-02
$800 \times 400$	0		0.38E-02	
	1	7	0.24E-04	0.64E-02
	2	7	0.94E-07	0.39E-02

of Fig. 7 shows that Grid2 algorithm solves this problem more effectively than SI or Gmres(40) methods and with less iterations than DSA method.

Furthermore, we note that the Gmres(40) method performs poorly after the seventh iteration in both runs. This may be partly due to the fact that the discontinuous  $\sigma$  and  $\kappa$  coefficients change the matrix structure very badly. While, it is not surprising that the SI algorithm performs very poorly in this case. An examination of the CPU time in Table 5 reveals that Gmres(40) consumes less computational work than the other methods. We have observed that the main part of the CPU time needed in DSA or Grid2 is used by Bicgstab or Gmres(10) to solve the diffusion problem in DSA or the coarse linear system in Grid2, respectively. However, by limiting the number of iterations in Bicgstab and Gmres(10) to 1, or increasing the tolerance from  $10^{-2}$  to  $10^{-1}$ , the results change favourably with significant advantage for Grid2.

Table 6 tabulates the results obtained by Gridnest using four levels. It can be clearly seen that there is very little variation in the number  $i_{\text{Gmres}}$  and the reduction factor  $\|r^{(m)}\|_{L^\infty} / \|r^{(m-1)}\|_{L^\infty}$  as the meshes are refined.

### 3.5.4 Radiative Transfer Equation with Frequency Dependence

Our final example is the frequency-dependent problem

$$\Omega \cdot \nabla \psi(x, \Omega, \nu) + (\sigma + \kappa) \psi(x, \Omega, \nu) = \frac{\sigma}{4\pi} \int_{S^2} \psi(x, \Omega', \nu) d\Omega' + \kappa B(T, \nu), \quad (69)$$

with boundary condition  $\psi = B(T(\hat{x}), \nu)$ . Here  $\psi = \psi(x, \Omega, \nu)$ ,  $T = T(x)$ ,  $\sigma = \sigma(x, \nu)$  and  $\kappa = \kappa(x, \nu)$  denote respectively, the radiation intensity, the temperature, the scattering and the opacity within the frequency  $\nu > 0$ .

In order to discretize the (69) with respect to the frequency variable  $\nu$ , we assume  $N$  frequency bands  $[\nu_l, \nu_{l+1}]$ ,  $l = 1, \dots, N$  with piecewise constant absorption,

$$\kappa = \kappa_l, \quad \forall \nu \in [\nu_l, \nu_{l+1}] \quad l = 1, \dots, N.$$

We define the frequency-averaged intensity in the band  $[\nu_l, \nu_{l+1}]$  by

$$\psi_l = \int_{\nu_l}^{\nu_{l+1}} \psi(x, \Omega, \nu') d\nu'.$$

Then, the (69) are transformed to a system of  $N$  radiative transfer equations of the form

$$\Omega \cdot \nabla \psi_l(x, \Omega) + (\sigma_l + \kappa_l) \psi_l(x, \Omega) = \frac{\sigma_l}{4\pi} \int_{S^2} \psi_l(x, \Omega') d\Omega' + \kappa_l \int_{\nu_l}^{\nu_{l+1}} B(T, \nu') d\nu'. \quad (70)$$

To approximate the frequency integrals we used trapezoidal formula. In our numerical simulations we use eight frequency bands  $[\nu_l, \nu_{l+1}]$ ,  $l = 1, \dots, 8$  from glass manufacturing [47]. These frequencies are given in Table 2 in the introduction.

We compute the solution of the (69) in a unit square, on the refined grid with  $100 \times 100$  gridpoints, and 64 discrete ordinates. Hence the number of unknowns for each frequency band is  $64 \times 10^4$ , and these computations are done for the 8 frequencies such that the overall number of equations amounts  $5.12 \times 10^6$ . The scattering parameter  $\sigma$  is varying in the set  $\{1, 10, 100\}$ . For every frequency band we calculate its corresponding scattering ratio and, we store the number of iterations and the running time obtained by each method. The results are given in Table 7.

All the algorithms iterate the solution in a large iteration numbers for the first frequency bands (with large scattering ratio), then these numbers go decreasing as the frequency bands grow until they reach the minimum for the last frequency band. In this case when the size of scattering ratio is changing dramatically over the frequency bands, only the DSA and Grid2 algorithms lead to satisfying results for all frequencies and also in diffusive limit ( $\sigma = 100$ ). The superiority of Grid2 is clearly demonstrated in Table 7.

## 4 Higher-Order Diffusion Approximations

Approximations that are widely used are the  $P_N$  approximations, cf. Sect. 5.1. A major drawback in higher dimensions and for complicated problems is the large number of equations which have to be solved. We propose the  $SP_N$  approximations as alternatives to the full glass equations. This class of approximations uses diffusion equations instead of the radiative transfer equations. The number of equations is

**Table 7** Number of iterations and CPU time for the eight frequency-bands problem

	Band	Scattering ratio	SI	Gmres(40)	DSA	Grid2
$\sigma = 1$	1	0.71428	13	6	6	3
	2	0.66666	13	6	6	3
	3	0.11494	7	5	4	3
	4	0.06077	6	4	4	3
	5	0.03450	5	4	3	3
	6	0.00371	4	3	3	2
	7	0.00175	3	3	3	2
	8	0.00014	3	2	2	2
CPU(sec) ———			30.45	26.36	39.38	29.29
$\sigma = 10$	1	0.96153	117	17	8	5
	2	0.95238	114	17	8	5
	3	0.56497	21	8	5	4
	4	0.39292	14	7	5	3
	5	0.26329	10	5	5	3
	6	0.03597	5	3	3	3
	7	0.01732	4	3	3	3
	8	0.00173	3	2	2	2
CPU(sec) ———			108.30	36.61	35.13	38.40
$\sigma = 100$	1	0.99601	1577	79	16	15
	2	0.99502	1637	79	17	14
	3	0.92850	151	22	15	10
	4	0.86617	80	16	14	9
	5	0.78137	48	12	15	8
	6	0.27175	10	5	5	4
	7	0.14985	8	4	4	4
	8	0.01381	4	3	3	2
CPU(sec) ———			1190.73	107.80	57.27	122.05

considerably reduced compared to the  $P_N$  equations. The method originates from neutron transport theory in nuclear physics where it was successfully introduced. Nevertheless, it suffered from a lack of theoretical foundation with the result that it was not completely accepted in the field. This has been remedied, however, during the last decade, such that the method has now been substantiated.

We want to study the optically thick regime where the opacity  $\kappa$  is large and the radiation is conveyed in a diffusion-like manner. Therefore, we rewrite the above equations in non-dimensional form introducing reference values which correspond to typical values of the physical quantities. In order to obtain a diffusion scaling we impose the relations

$$t_{ref} = c_m \rho_m \kappa_{ref} x_{ref}^2 \frac{T_{ref}}{I_{ref}}, \quad \text{and} \quad k_{ref} = \frac{I_{ref}}{\kappa_{ref} T_{ref}},$$

on these reference values and define the non-dimensional parameter

$$\varepsilon = \frac{1}{\kappa_{ref} x_{ref}} \quad (71)$$

which is small in the optically thick, diffusive regime. Then the rescaled equations read (without marking the scaled quantities):

$$\varepsilon^2 \frac{\partial T}{\partial t} = \varepsilon^2 \nabla \cdot k \nabla T - \int_{v_1}^{\infty} \int_{S^2} \kappa(B - \psi) d\Omega dv, \quad (72a)$$

$$\forall v > 0, \Omega \in S^2 : \varepsilon \Omega \cdot \nabla \psi = \kappa(B - \psi). \quad (72b)$$

Here, we have neglected scattering. This can be incorporated in a straightforward way, however. The boundary condition for the temperature changes into

$$\varepsilon k n \cdot \nabla T = h(T_b - T) + \alpha \pi \left( \frac{n_2}{n_1} \right)^2 \int_0^{v_1} B(v, T_b) - B(v, T) dv. \quad (72c)$$

It is well known that an *outer* asymptotic expansion of (72a) and (72b) leads to equilibrium diffusion theory, which is, in the cases considered here, expected to be valid in the interior of  $V$ , see e.g. [46, 67, 68]. The diffusion or Rosseland approximation is

$$\frac{\partial T}{\partial t} = \nabla \cdot \left( k + k_r(T) \right) \nabla T, \quad \text{with} \quad k_r(T) = \frac{4\pi}{3} \int_{v_1}^{\infty} \frac{1}{\kappa} \frac{\partial B}{\partial T} dv.$$

However, this diffusion theory is not capable of describing boundary layers and the question arises whether more sophisticated approximations can suitably model the boundary layer effects. In the realm of neutron transport, such higher-order asymptotic corrections to diffusion theory exist, and are reasonably well understood; they are the so-called *simplified*  $P_N$  ( $SP_N$ ) theories, see [9, 80]. These  $SP_N$  theories are, in fact, diffusion in nature i.e. diffusion equations or coupled systems of diffusion equations are employed. They contain boundary layer effects and can be remarkably accurate, much more accurate than the standard Rosseland approximation. In practice, these equations are viewed as an extended form of the classical diffusion theory. No separate boundary layer treatment is necessary because the boundary layers are included in the  $SP_N$  equations. For other approximate theories for the above equations and applications, see for example [17, 49]. The material of this section is taken from [47].

#### 4.1 Asymptotic Analysis and Derivation of the $SP_N$ Approximations

To solve (72a) in the domain  $V$ , we write this equation as

$$\left( 1 + \frac{\varepsilon}{\kappa} \Omega \cdot \nabla \right) \psi(x, t, \Omega, v) = B(v, T).$$

and apply Neumann's series to formally invert the operator

$$\begin{aligned}\psi &= \left(1 + \frac{\varepsilon}{\kappa} \Omega \cdot \nabla\right)^{-1} B \\ &\cong \left[1 - \frac{\varepsilon}{\kappa} \Omega \cdot \nabla + \frac{\varepsilon^2}{\kappa^2} (\Omega \cdot \nabla)^2 - \frac{\varepsilon^3}{\kappa^3} (\Omega \cdot \nabla)^3 + \frac{\varepsilon^4}{\kappa^4} (\Omega \cdot \nabla)^4 \dots\right] B.\end{aligned}\quad (73)$$

Integrating with respect to  $\Omega$  and using the result

$$\int_{S^2} (\Omega \cdot \nabla)^n d\Omega = [1 + (-1)^n] : \frac{2\pi}{n+1} \nabla^n,$$

where  $\nabla^2 = \nabla \cdot \nabla = \Delta$  is the Laplacian, we get

$$\varphi = \int_{S^2} \psi d\Omega = 4\pi \left[1 + \frac{\varepsilon^2}{3\kappa^2} \nabla^2 + \frac{\varepsilon^4}{5\kappa^4} \nabla^4 + \frac{\varepsilon^6}{7\kappa^6} \nabla^6 \dots\right] B + \mathcal{O}(\varepsilon^8).$$

Hence,

$$\begin{aligned}4\pi B &= \left[1 + \frac{\varepsilon^2}{3\kappa^2} \nabla^2 + \frac{\varepsilon^4}{5\kappa^4} \nabla^4 + \frac{\varepsilon^6}{7\kappa^6} \nabla^6\right]^{-1} \varphi + \mathcal{O}(\varepsilon^8) \\ &= \left\{1 - \left[\frac{\varepsilon^2}{3\kappa^2} \nabla^2 + \frac{\varepsilon^4}{5\kappa^4} \nabla^4 + \frac{\varepsilon^6}{7\kappa^6} \nabla^6\right] \right. \\ &\quad \left. + \left[\frac{\varepsilon^2}{3\kappa^2} \nabla^2 + \frac{\varepsilon^4}{5\kappa^4} \nabla^4 + \frac{\varepsilon^6}{7\kappa^6} \nabla^6\right]^2 \right. \\ &\quad \left. - \left[\frac{\varepsilon^2}{3\kappa^2} \nabla^2 + \frac{\varepsilon^4}{5\kappa^4} \nabla^4 + \frac{\varepsilon^6}{7\kappa^6} \nabla^6\right]^3 \dots\right\} \varphi + \mathcal{O}(\varepsilon^8),\end{aligned}$$

so we have the asymptotic expansion

$$\forall \nu > 0: \quad 4\pi B = \left[1 - \frac{\varepsilon^2}{3\kappa^2} \nabla^2 - \frac{4\varepsilon^4}{45\kappa^4} \nabla^4 - \frac{44\varepsilon^6}{945\kappa^6} \nabla^6\right] \varphi + \mathcal{O}(\varepsilon^8). \quad (74)$$

If we discard terms of  $\mathcal{O}(\varepsilon^4)$ ,  $\mathcal{O}(\varepsilon^6)$  or  $\mathcal{O}(\varepsilon^8)$  we obtain the  $SP_1$ ,  $SP_2$  and  $SP_3$  approximations, respectively. All these equations contain the frequency  $\nu$  as a parameter.

#### 4.1.1 $SP_1$ and Diffusion Approximations

From (74), we obtain

$$4\pi B = \varphi - \frac{\varepsilon^2}{3\kappa^2} \nabla^2 \varphi + \mathcal{O}(\varepsilon^4)$$

and up to  $\mathcal{O}(\varepsilon^4)$  we may write the equation in the form

$$\forall v > 0: \quad -\varepsilon^2 \nabla \cdot \frac{1}{3\kappa} \nabla \varphi + \kappa \varphi = \kappa(4\pi B). \quad (75a)$$

In this equation,  $v$  is simply a parameter. Thus, in practice, these equations would be solved independently for each frequency or frequency group and subsequently coupled via (72a). By (75a),

$$\int_{v_1}^{\infty} \int_{S^2} \kappa(B - I) d\Omega dv = \int_{v_1}^{\infty} \kappa(4\pi B - \varphi) dv = -\varepsilon^2 \int_{v_1}^{\infty} \nabla \cdot \frac{1}{3\kappa} \nabla \varphi dv + \mathcal{O}(\varepsilon^4).$$

Thus, the energy equation (72a) becomes up to  $\mathcal{O}(\varepsilon^2)$ :

$$\frac{\partial T}{\partial t} = \nabla \cdot k \nabla T + \int_{v_1}^{\infty} \nabla \cdot \frac{1}{3\kappa} \nabla \varphi dv. \quad (75b)$$

Equations (75b) and (75a) are the  $SP_1$  approximation to (72a) and (72b). Since (75b) is only of order  $\mathcal{O}(\varepsilon^2)$  the approximation is  $\mathcal{O}(\varepsilon^2)$ . Using  $\varphi = 4\pi B + \mathcal{O}(\varepsilon^2)$  in (75b) one obtains up to  $\mathcal{O}(\varepsilon^2)$

$$\begin{aligned} \frac{\partial T}{\partial t} &= \nabla \cdot k \nabla T + \int_{v_1}^{\infty} \nabla \cdot \frac{1}{3\kappa} \nabla (4\pi B) dv \\ &= \nabla \cdot k \nabla T + \nabla \cdot \left( \frac{4\pi}{3} \int_{v_1}^{\infty} \frac{1}{\kappa} \frac{\partial B}{\partial T} dv \right) \nabla T, \end{aligned} \quad (76)$$

i.e. we have obtained the conventional equilibrium *diffusion* or *Rosseland approximation* (73). However, (75a) permits a boundary layer behaviour near the boundary  $\partial V$  that is not present in (76).

#### 4.1.2 $SP_2$ Approximation

From (74), we get for  $\varepsilon$  going to 0

$$4\pi B = \varphi - \frac{\varepsilon^2}{3\kappa^2} \nabla^2 \varphi - \frac{4\varepsilon^2}{15\kappa^2} \nabla^2 \left( \frac{\varepsilon^2}{3\kappa^2} \nabla^2 \varphi \right) + \mathcal{O}(\varepsilon^6).$$

This implies

$$\frac{\varepsilon^2}{3\kappa^2} \nabla^2 B = \varphi - 4\pi B + \mathcal{O}(\varepsilon^4).$$

Hence, with  $\mathcal{O}(\varepsilon^6)$  error, the expansion above gives

$$4\pi B = \varphi - \frac{\varepsilon^2}{3\kappa^2} \nabla^2 \varphi - \frac{4\varepsilon^2}{15\kappa^2} \nabla^2 [\varphi - 4\pi B] = \varphi - \frac{\varepsilon^2}{3\kappa^2} \nabla^2 \left[ \varphi + \frac{4}{5} (\varphi - 4\pi B) \right],$$



or equivalently,

$$-\varepsilon^2 \nabla \cdot \frac{1}{3\kappa} \nabla \left[ \varphi + \frac{4}{5}(\varphi - 4\pi B) \right] + \kappa \varphi = \kappa(4\pi B). \quad (77)$$

Equation (77) implies

$$\int_{v_1}^{\infty} \int_{S^2} \kappa(B - I) d\Omega dv = -\varepsilon^2 \int_{v_1}^{\infty} \nabla \cdot \frac{1}{3\kappa} \nabla \left[ \varphi + \frac{4}{5}(\varphi - 4\pi B) \right] dv + \mathcal{O}(\varepsilon^4).$$

Thus, the energy equation (72b) becomes up to  $\mathcal{O}(\varepsilon^4)$

$$\frac{\partial T}{\partial t} = \nabla \cdot k \nabla T + \int_{v_1}^{\infty} \nabla \cdot \frac{1}{3\kappa} \nabla \left[ \varphi + \frac{4}{5}(\varphi - 4\pi B) \right] dv. \quad (78)$$

These two equations can be written in a more advantageous way if we define

$$\xi = \varphi + \frac{4}{5}(\varphi - 4\pi B). \quad (79)$$

Introducing the new variable  $\xi$  into (77) and (78) we obtain the  $SP_2$  equations:

$$\frac{\partial T}{\partial t} = \nabla \cdot k \nabla T + \int_{v_1}^{\infty} \nabla \cdot \frac{1}{3\kappa} \nabla \xi dv, \quad \text{and} \quad (80a)$$

$$-\varepsilon^2 \nabla \cdot \frac{3}{5\kappa} \nabla \xi + \kappa \xi = \kappa(4\pi B). \quad (80b)$$

There is a remarkable similarity between the  $SP_2$  (80) and the  $SP_1$  (75). This is because the  $SP_1$  equations contain some, but not all, of the  $\mathcal{O}(\varepsilon^4)$  correction terms. In the realm of neutron transport, the  $SP_2$  approximation has not found favour because, in the presence of material inhomogeneities, it yields discontinuous solutions. However, it is obvious that (80b) and (80a) can not produce a discontinuous solution.

Also, in the realm of neutron transport, the  $SP_1$  and  $SP_2$  solutions are not capable of exhibiting boundary layer behaviour, while the more complicated  $SP_3$  solution described below does incorporate this in a remarkably accurate way. However, the radiative transfer  $SP_1$  and  $SP_2$  equations stated here can contain boundary layer behaviour. The  $SP_3$  approximation derived in the following should capture significant radiative transfer boundary effects that are not captured by the  $SP_1$  and  $SP_2$  approximations.

### 4.1.3 $SP_3$ Approximation

Ignoring terms of  $\mathcal{O}(\varepsilon^8)$  in (74), we get

$$\begin{aligned}
4\pi B &= \varphi - \frac{\varepsilon^2}{3\kappa^2} \nabla^2 \left[ \varphi + \frac{4\varepsilon^2}{15\kappa^2} \nabla^2 \varphi + \frac{44\varepsilon^4}{315\kappa^4} \nabla^4 \varphi \right] + \mathcal{O}(\varepsilon^8) \\
&= \varphi - \frac{\varepsilon^2}{3\kappa^2} \nabla^2 \left[ \varphi + \left( 1 + \frac{11\varepsilon^2}{21\kappa^2} \nabla^2 \right) \left( \frac{4\varepsilon^2}{15\kappa^2} \varphi \right) \right] + \mathcal{O}(\varepsilon^8) \\
&= \varphi - \frac{\varepsilon^2}{3\kappa^2} \nabla^2 \left[ \varphi + \left( 1 - \frac{11\varepsilon^2}{21\kappa^2} \nabla^2 \right)^{-1} \left( \frac{4\varepsilon^2}{15\kappa^2} \varphi \right) \right] + \mathcal{O}(\varepsilon^8) \quad (81)
\end{aligned}$$

Hence, if we define

$$\varphi_2 \equiv \left( 1 - \frac{11}{21} \frac{\varepsilon^2}{\kappa^2} \nabla^2 \right)^{-1} \left( \frac{2\varepsilon^2}{15\kappa^2} \varphi \right), \quad (82)$$

then (81) becomes up to  $\mathcal{O}(\varepsilon^8)$ :

$$4\pi B = \varphi - \frac{\varepsilon^2}{3\kappa^2} \nabla^2 (\varphi + 2\varphi_2)$$

or

$$\forall v > 0: \quad -\varepsilon^2 \nabla \cdot \frac{1}{3\kappa} \nabla (\varphi + 2\varphi_2) + \kappa \varphi = \kappa (4\pi B), \quad (83a)$$

while (82) becomes

$$\begin{aligned}
-\frac{11\varepsilon^2}{21\kappa^2} \nabla^2 \varphi_2 + \varphi_2 &= \frac{2}{15} \frac{\varepsilon^2}{\kappa^2} \nabla^2 \varphi = \frac{2}{5} \left( \frac{\varepsilon^2}{3\kappa^2} \nabla^2 \varphi \right) \\
&= \frac{2}{5} \left[ -4\pi B + \varphi - \frac{2\varepsilon^2}{3\kappa^2} \nabla^2 \varphi_2 \right]
\end{aligned}$$

or

$$\left( \frac{4}{15} - \frac{11}{21} \right) \frac{\varepsilon^2}{\kappa^2} \nabla^2 \varphi_2 + \varphi_2 = \frac{2}{5} (\varphi - 4\pi B)$$

or eventually

$$\forall v > 0: \quad -\varepsilon^2 \nabla \cdot \frac{9}{35\kappa} \nabla \varphi_2 + \kappa \varphi_2 - \frac{2}{5} \kappa \varphi = -\frac{2}{5} \kappa (4\pi B). \quad (83b)$$

By (83a) we get up to  $\mathcal{O}(\varepsilon^6)$

$$\int_{v_1}^{\infty} \int_{S^2} \kappa (B - I) \, d\Omega \, dv = -\varepsilon^2 \int_{v_1}^{\infty} \nabla \cdot \frac{1}{3\kappa} \nabla (\varphi + 2\varphi_2) \, dv.$$

Thus, the energy equation (72b) becomes

$$\frac{\partial T}{\partial t} = \nabla \cdot k \nabla T + \int_{v_1}^{\infty} \nabla \cdot \frac{1}{3\kappa} \nabla (\varphi + 2\varphi_2) \, dv. \quad (83c)$$

Equation (83c) together with the two approximate (83a, 83b) form the  $SP_3$  approximation to the system (72a) and (72b).

These equations can be rewritten in a computationally more advantageous way. Let us calculate  $\theta\{(83a)\} + \{(83b)\}$  :

$$-\varepsilon^2 \nabla \cdot \frac{1}{\kappa} \nabla \left\{ \frac{\theta}{3} (\varphi + 2\varphi_2) + \frac{9}{35} \varphi_2 \right\} + \kappa \left\{ \theta \varphi + \varphi_2 - \frac{2}{5} \varphi \right\} = \kappa \left( \theta - \frac{2}{5} \right) (4\pi B).$$

We seek linear combinations of both equations such that the two functions in the brackets on the left are scalar multiples. More explicitly, we look for  $\theta$  that fulfills the condition

$$\frac{\theta}{3} (\varphi + 2\varphi_2) + \frac{9}{35} \varphi_2 = \mu^2 \left( \theta \varphi + \varphi_2 - \frac{2}{5} \varphi \right), \quad (84)$$

where  $\mu^2 > 0$  is a constant to be determined later. Equation (84) holds for arbitrary  $\varphi$  and  $\varphi_2$  iff

$$\frac{\theta}{3} = \mu^2 \left( \theta - \frac{2}{5} \right) \quad \text{and} \quad \frac{2\theta}{3} + \frac{9}{35} = \mu^2.$$

The second of these equations may be solved for  $\theta$  and we get a quadratic equation in  $\mu^2$ :

$$\frac{1}{2} \mu^2 - \frac{9}{70} = \mu^2 \left( \frac{2}{3} \mu^2 - \frac{11}{14} \right).$$

Its discriminant is positive and thus we obtain two positive real solutions

$$\mu_1^2 = \frac{3}{7} - \frac{2}{7} \sqrt{\frac{6}{5}}, \quad \text{and} \quad \mu_2^2 = \frac{3}{7} + \frac{2}{7} \sqrt{\frac{6}{5}},$$

and the corresponding values of the scalar  $\theta$  are

$$\theta_1 = \frac{9}{35} - \frac{3}{7} \sqrt{\frac{6}{5}}, \quad \text{and} \quad \theta_2 = \frac{9}{35} + \frac{3}{7} \sqrt{\frac{6}{5}}.$$

Now relation (84) implies, for  $n = 1, 2$ ,

$$\left( -\varepsilon^2 \nabla \cdot \frac{1}{\kappa} \nabla \mu_n^2 + \kappa \right) \left[ \theta_n \varphi + \varphi_2 - \frac{2}{5} \varphi \right] = \left( \theta_n - \frac{2}{5} \right) \kappa (4\pi B). \quad (85)$$

This suggests that we define two new independent variables for  $n = 1, 2$

$$I_n = \frac{\theta_n \varphi + \varphi_2 - 2/5 \varphi}{\theta_n - 2/5} = \varphi + \frac{1}{\theta_n - 2/5} \varphi_2 = \varphi + \gamma_n \varphi_2 \quad (86)$$

where

$$\gamma_n = \frac{1}{\theta_n - 2/5} = \frac{5}{7} \left[ 1 + (-1)^n 3 \sqrt{\frac{6}{5}} \right].$$

The two equations in (85) are now

$$-\varepsilon^2 \mu_1^2 \nabla \cdot \frac{1}{\kappa} \nabla I_1 + \kappa I_1 = \kappa(4\pi B), \quad (87a)$$

$$-\varepsilon^2 \mu_2^2 \nabla \cdot \frac{1}{\kappa} \nabla I_2 + \kappa I_2 = \kappa(4\pi B). \quad (87b)$$

The advantage of this form of the  $SP_3$  equations is that the diffusion equations are uncoupled. It will be seen below that there remains, however, a weak coupling in the boundary conditions.

The linear transformation of variables above is inverted according to the formulae

$$\varphi = \frac{\gamma_2 I_1 - \gamma_1 I_2}{\gamma_2 - \gamma_1}, \quad \text{and} \quad \varphi_2 = \frac{I_2 - I_1}{\gamma_2 - \gamma_1}. \quad (88)$$

Defining three constants

$$w_0 = \frac{1}{\gamma_2 - \gamma_1} = \frac{7}{30} \sqrt{\frac{5}{6}} = \frac{7}{36} \sqrt{\frac{6}{5}}, \quad \text{and} \quad (89a)$$

$$w_1 = \frac{\gamma_2}{\gamma_2 - \gamma_1} = \frac{1}{6} \left( 3 + \sqrt{\frac{5}{6}} \right), \quad w_2 = \frac{-\gamma_1}{\gamma_2 - \gamma_1} = \frac{1}{6} \left( 3 - \sqrt{\frac{5}{6}} \right) \quad (89b)$$

we can write  $\varphi = w_1 I_1 + w_2 I_2$  and  $\varphi_2 = w_0(I_2 - I_1)$  and we have furthermore

$$\frac{1}{3}(\varphi + 2\varphi_2) = \frac{1}{3}(w_1 - 2w_0)I_1 + \frac{1}{3}(w_2 + 2w_0)I_2 = a_1 I_1 + a_2 I_2.$$

Here again we introduced constants

$$a_1 = \frac{w_1 - 2w_0}{3} = \frac{1}{30} \left( 5 - 3\sqrt{\frac{5}{6}} \right), \quad \text{and} \quad a_2 = \frac{w_2 + 2w_0}{3} = \frac{1}{30} \left( 5 + 3\sqrt{\frac{5}{6}} \right).$$

In this way, the  $SP_3$  energy equation (83c) above becomes:

$$\frac{\partial T}{\partial t} = \nabla \cdot k \nabla T + \int_{v_1}^{\infty} \nabla \cdot \frac{1}{\kappa} \nabla (a_1 I_1 + a_2 I_2) dv. \quad (90)$$

## 4.2 Boundary Conditions for $SP_N$ Approximations

The boundary conditions for the  $SP_N$  equations in neutron transport come from a variational principle, see [9, 80]. Here, we use the boundary conditions developed for the transport case to state (and rewrite in a more suitable form) the boundary conditions for  $SP_1$ ,  $SP_2$  and  $SP_3$  approximations to the transport problem (72b) with the boundary condition (44c).

We consider the transport equation (72b)

$$\forall v > 0 : \quad \varepsilon \Omega \cdot \nabla \psi(x, \Omega) + \kappa I(x, \Omega) = \kappa B, \quad x \in V,$$

with semi-transparent boundary conditions on  $\partial V$

$$\psi(x, \Omega) = \rho(n \cdot \Omega) \psi(x, \Omega') + (1 - \rho(n \cdot \Omega)) \psi_b(x, \Omega), \quad n \cdot \Omega < 0.$$

Let us define the scalar flux as before

$$\varphi(x) = \int_{S^2} \psi(x, \Omega) d\Omega,$$

and define two integrals of the influx into the domain for  $m = 1, 3$

$$\psi_m(x) = \int_{n \cdot \Omega < 0} (1 - \rho(n \cdot \Omega)) P_m(|\Omega \cdot n|) I_b(x, \Omega) d\Omega, \quad x \in \partial V. \quad (91)$$

Here, the Legendre polynomials of order 1 and 3 are used:

$$P_1(\mu) = \mu, \quad \text{and} \quad P_3(\mu) = \frac{5}{2}\mu^3 - \frac{3}{2}\mu.$$

Furthermore, it is convenient in the sequel to have the following integrals at hand:

$$\begin{aligned} r_1 &= 2\pi \int_0^1 \mu \rho(\mu) d\mu, & r_5 &= 2\pi \int_0^1 P_3(\mu) \rho(\mu) d\mu, \\ r_2 &= 2\pi \int_0^1 \mu^2 \rho(\mu) d\mu, & r_6 &= 2\pi \int_0^1 P_2(\mu) P_3(\mu) \rho(\mu) d\mu, \\ r_3 &= 2\pi \int_0^1 \mu^2 \rho(\mu) d\mu, & r_7 &= 2\pi \int_0^1 P_3(\mu) P_3(\mu) \rho(\mu) d\mu, \\ r_4 &= 2\pi \int_0^1 \mu P_3(\mu) \rho(\mu) d\mu, \end{aligned}$$

The boundary conditions in [9, 80] were derived for the case  $\rho = 0 = \text{const}$ . For semi-transparent boundary conditions the same arguments apply and the calculations can be analogously carried out, the only difference being modifications in the coefficients. We therefore content ourselves with stating the resulting equations. In the  $SP_1$  approximation (75a), the boundary condition for  $\varphi$  is:

$$\forall v > 0 : \quad (1 - 2r_1) \varphi(x) + (1 + 3r_2) \frac{2\varepsilon}{3\kappa} n \cdot \nabla \varphi(x) = 4\psi_1(x). \quad (92)$$

The boundary condition for  $\varphi$  in the  $SP_2$  approximation (80b) is, see [80]:

$$\begin{aligned} (1 - 2r_1) \varphi + (1 + 3r_2) \frac{2\varepsilon}{3\kappa} n \cdot \nabla \left[ \varphi + \frac{4}{5} (\varphi - 4\pi B) \right] \\ + (1 - 4(3r_3 - r_1)) \frac{1}{2} (\varphi - 4\pi B) = 4\psi_1. \end{aligned} \quad (93)$$

These equations reduce to (92) if one deletes the  $(\varphi - 4\pi B)$  terms in them. They can be written in a more advantageous way if we define  $\xi$  as in Sect. 2 which is equivalent to

$$\varphi = \frac{5}{9}\xi + \frac{4}{9}(4\pi B).$$

One obtains

$$\begin{aligned} (1 - 2r_1)\left(\frac{5}{9}\xi + \frac{4}{9}(4\pi B)\right) + (1 + 3r_2)\frac{2\varepsilon}{3\kappa}n \cdot \nabla \xi \\ + (1 - 4(3r_3 - r_1))\frac{1}{2}\left(\frac{5}{9}\xi + \frac{4}{9}(4\pi B) - 4\pi B\right) = 4\psi_1, \end{aligned}$$

or, using the abbreviations

$$\alpha_1 = \frac{5}{6}(1 - 4r_3) \quad \alpha_2 = \frac{1}{6}(-1 + 12r_1 - 20r_3)$$

the  $SP_2$  boundary conditions for  $\xi$  in (80b) can be written:

$$\forall v > 0: \quad \alpha_1 \xi(r) + (1 + 3r_2)\frac{2\varepsilon}{3\kappa}n \cdot \nabla \xi(r) = \alpha_2 4\pi B(T(x)) + 4\psi_1(x). \quad (94)$$

The boundary conditions (92) and (93) were derived variationally, not from a boundary layer analysis. They should be accurate if  $I_b(x, \Omega)$  is a reasonably smooth function of  $\Omega$ , but they could be inaccurate if  $I_b$  is not smooth.

Finally, the  $SP_3$  boundary conditions for  $\varphi$  and  $\varphi_2$  in (83a) and (83b) are, see [9]: for all frequencies  $v > 0$  and  $x \in \partial V$  there must hold

$$\begin{aligned} (1 - 2r_1)\frac{1}{4}\varphi(x) + (1 - 8r_3)\frac{5}{16}\varphi_2(x) + (1 + 3r_2)\frac{\varepsilon}{6\kappa}n \cdot \nabla \varphi(x) \\ + \left(\frac{1 + 3r_2}{3} + \frac{3r_4}{2}\right)\frac{2\varepsilon}{3\kappa}n \cdot \nabla \varphi_2(x) = \psi_1(x), \end{aligned} \quad (95a)$$

$$\begin{aligned} -(1 + 8r_5)\frac{1}{16}\varphi(x) + (1 - 8r_6)\frac{5}{16}\varphi_2(x) + 3r_4\frac{\varepsilon}{6\kappa}n \cdot \nabla \varphi(x) \\ + \left(r_4 + \frac{3}{14}(1 + 7r_7)\right)\frac{\varepsilon}{\kappa}n \cdot \nabla \varphi_2(x) = \psi_3(x). \end{aligned} \quad (95b)$$

or formally

$$\begin{aligned} A_1 \varphi(x) + A_2 \varphi_2(x) + A_3 \frac{\varepsilon}{\kappa}n \cdot \nabla \varphi(x) + A_4 \frac{\varepsilon}{\kappa}n \cdot \nabla \varphi_2(x) = \psi_1(x) \\ B_1 \varphi(x) + B_2 \varphi_2(x) + B_3 \frac{\varepsilon}{\kappa}n \cdot \nabla \varphi(x) + B_4 \frac{\varepsilon}{\kappa}n \cdot \nabla \varphi_2(x) = \psi_3(x). \end{aligned}$$

We still have to derive boundary conditions for  $I_1$  and  $I_2$ . Using the formulae in (88), we can transform the boundary conditions for  $\varphi$  and  $\varphi_2$  into boundary conditions for  $I_1$  and  $I_2$ . The equations above then become

$$\begin{aligned}
 & (A_1 \gamma_2 w_0 - A_2 w_0) I_1 + (-A_1 \gamma_1 w_0 + A_2 w_0) I_2 \\
 & \quad + (A_3 \gamma_2 w_0 - A_4 w_0) \frac{\varepsilon}{\kappa} n \cdot \nabla I_1 \\
 & \quad + (-A_3 \gamma_2 w_0 + A_2 w_0) \frac{\varepsilon}{\kappa} n \cdot \nabla I_2 = \psi_1 \\
 & (B_1 \gamma_2 w_0 - B_2 w_0) I_1 + (-B_1 \gamma_1 w_0 + B_2 w_0) I_2 \\
 & \quad + (B_3 \gamma_2 w_0 - B_4 w_0) \frac{\varepsilon}{\kappa} n \cdot \nabla I_1 \\
 & \quad + (-B_3 \gamma_2 w_0 + B_2 w_0) \frac{\varepsilon}{\kappa} n \cdot \nabla I_2 = \psi_3
 \end{aligned}$$

or, again formally rewritten for writing convenience,

$$\begin{aligned}
 C_1 I_1 + C_2 I_2 + C_3 \frac{\varepsilon}{\kappa} n \cdot \nabla I_1 + C_4 \frac{\varepsilon}{\kappa} n \cdot \nabla I_2 &= \psi_1 \\
 D_1 I_1 + D_2 I_2 + D_3 \frac{\varepsilon}{\kappa} n \cdot \nabla I_1 + D_4 \frac{\varepsilon}{\kappa} n \cdot \nabla I_2 &= \psi_3.
 \end{aligned}$$

We eliminate the gradient term  $n \cdot \nabla I_2$  in the first equation and  $n \cdot \nabla I_1$  in the second in order to get boundary conditions for the  $I_1$  and  $I_2$  equations, respectively. We find

$$\begin{aligned}
 & (C_1 D_4 - D_1 C_4) I_1 + (C_3 D_4 - D_3 C_4) \frac{\varepsilon}{\kappa} n \cdot \nabla I_1 \\
 & \quad = -(C_2 D_4 - D_2 C_4) I_2 + (D_4 \psi_1 - C_4 \psi_3) \\
 & \quad - (C_2 D_3 - D_2 C_3) I_2 + (C_3 D_4 - D_3 C_4) \frac{\varepsilon}{\kappa} n \cdot \nabla I_2 \\
 & \quad = (C_1 D_3 - D_1 C_3) I_1 - (D_3 \psi_1 - C_3 \psi_3)
 \end{aligned}$$

so, if we set  $D = C_3 D_4 - D_3 C_4$  and define constants

$$\begin{aligned}
 \alpha_1 &= (C_1 D_4 - D_1 C_4)/D, & \alpha_2 &= -(C_2 D_3 - D_2 C_3)/D, \\
 \beta_1 &= -(C_1 D_3 - D_1 C_3)/D, & \beta_2 &= (C_2 D_4 - D_2 C_4)/D,
 \end{aligned}$$

then we end up with  $SP_3$  boundary conditions in the following form:

$$\alpha_1 I_1(x) + \frac{\varepsilon}{\kappa} n \cdot \nabla I_1(x) = -\beta_2 I_2(x) + (D_4 \psi_1(x) - C_4 \psi_3(x))/D, \quad (96a)$$

$$\alpha_2 I_2(x) + \frac{\varepsilon}{\kappa} n \cdot \nabla I_2(x) = -\beta_1 I_1(x) - (D_3 \psi_1(x) - C_3 \psi_3(x))/D. \quad (96b)$$

Equations (96a) and (96a) are the boundary conditions to go with the diffusion equations (87a) and (87b), respectively. The coupling of  $I_1$  and  $I_2$  in the boundary conditions is very weak.

Consider, for example, the simple case when there is no reflection  $\rho = 0$  and  $\psi_b(x, \Omega) = \psi_b(x)$  is isotropic. Then by (91),

$$\psi_m(x) = 2\pi\psi_b(x) \int_0^1 P_m(\mu) d\mu = \pi\psi_b(x) \begin{cases} 1, & \text{for } m = 1, \\ \frac{1}{4}, & \text{for } m = 3. \end{cases}$$

The constants  $r_1, \dots, r_7$  are all zero such that we find after some calculations  $D = \frac{1}{144}\sqrt{6/5}$  and the constants in the boundary conditions are

$$\begin{aligned} \alpha_1 &= \frac{5}{96} \left( 34 + 11\sqrt{6/5} \right), & \alpha_2 &= \frac{5}{96} \left( 34 + 11\sqrt{6/5} \right), \\ \beta_1 &= \frac{5}{96} \left( 2 - \sqrt{6/5} \right), & \beta_2 &= \frac{5}{96} \left( 2 + \sqrt{6/5} \right). \end{aligned}$$

Finally, the source terms in (96a) and (96b) become in this case

$$\begin{aligned} \left[ 6\psi_1(x) - 2 \left( 3 \pm 5\sqrt{\frac{6}{5}} \right) \psi_3(x) \right] &= \pi\psi_b(x) \left[ 6 + 2 \left( 3 \pm 5\sqrt{\frac{6}{5}} \right) \frac{1}{4} \right] \\ &= \frac{5}{2} \pi\psi_b(x) \left[ 3 \pm \sqrt{\frac{6}{5}} \right]. \end{aligned}$$

The approximate  $SP_N$ -theories stated above are simpler than transport theory because they do not contain the angular variable  $\Omega$ . However, they do contain the frequency variable  $\nu$ . It is formally possible to derive simpler theories in which the frequency is eliminated. We refer to [48].

## 5 Moment Models

First we briefly review the basics of the moment approach. Consider again the transport equation (32) for the radiation. We will assume isotropic scattering here. This equation is in fact a system of infinitely many coupled integro-differential equations that describes the distribution  $\psi$  of all photons in time, space and velocity space. On the one hand this system is computationally very expensive and on the other hand we are not interested in the photon distribution itself but in macroscopic quantities like the mean energy or mean flux of the radiation field. For instance, only the gradient of the radiative flux enters into the energy balance. The macroscopic quantities are moments of the distribution function. Let

$$\langle \cdot \rangle := \int_{S^2} \cdot d\Omega \quad (97)$$



denote the average over all directions. The energy, flux vector and pressure tensor of the radiation field are defined, respectively, as

$$E := \langle \psi \rangle, \quad F := \langle \Omega \psi \rangle, \quad P := \langle (\Omega \otimes \Omega) \psi \rangle. \quad (98)$$

To derive equations for the macroscopic quantities we multiply the transport equation by 1 and  $\Omega$  and average over all directions. We obtain the conservation laws

$$\nabla F = \kappa(\langle B \rangle - E) \quad (99)$$

$$\nabla P = -(\kappa + \sigma)F. \quad (100)$$

These are four equations (the first is a scalar equation, the second has three components) for 10 unknowns ( $E$  scalar,  $F$  3-component vector,  $P$  symmetric  $3 \times 3$ -matrix). Hence we have to pose an additional condition. Usually this condition is a constitutive equation for the highest moment  $P$ , expressed in terms of the lower moments  $E$  and  $F$ . This is referred to as the closure problem. The simplest approximation, the so-called  $P_1$  approximation, is obtained if we assume that the underlying distribution is isotropic. Thus, we obtain  $P = \frac{1}{3}E$  and therefore

$$\nabla F = \kappa(\langle B \rangle - E) \quad (101)$$

$$\nabla \frac{1}{3}E = -(\kappa + \sigma)F. \quad (102)$$

The general  $P_N$  closure is usually derived in a different way.

## 5.1 Spherical Harmonics

The Spherical Harmonics approach is one of the oldest approximate methods for radiative transfer [20, 33]. For the sake simplicity, we restrict our explanation to the case of slab geometry. The derivation for three-dimensional case can be found for example in [12] and also in standard textbooks [14, 41, 62]. The idea of the spherical harmonics approach is to express the angular dependence of the distribution function in terms of a Fourier series,

$$\psi(\mu) = \sum_{l=0}^{\infty} \psi_l^{SH} \frac{2l+1}{2} P_l(\mu), \quad (103)$$

where  $P_l$  are the Legendre polynomials. These form an orthogonal basis of the space of polynomials with respect to the standard scalar product on  $[-1, 1]$ ,

$$\int_{-1}^1 P_l(\mu) P_k(\mu) d\mu = \frac{2}{2l+1} \delta_{lk}. \quad (104)$$

In more space dimensions, one uses spherical harmonics, which are an orthogonal system on the unit sphere.

If we truncate the Fourier series at  $l = N$  we have

$$\psi^{SH}(\mu) = \sum_{l=0}^N \psi_l^{SH} \frac{2l+1}{2} P_l(\mu). \quad (105)$$

One can obtain equations for the Fourier coefficients

$$\psi_l^{SH} = \int_{-1}^1 \psi^{SH}(\mu) P_l(\mu) d\mu \quad (106)$$

by testing (32) with  $P_l(\mu)$  and then integrating. Thus we get

$$\nabla \int_{-1}^1 \mu P_l(\mu) \psi^{SH}(\mu) d\mu = \kappa(2\langle B \rangle \delta_{l0} - \psi_l^{SH}) + \sigma(\psi_0 \delta_{l0} - \psi_l^{SH}) \quad (107)$$

for the moments  $\psi_l^{SH}$  of the distribution function. Using the recursion relation

$$(l+1)P_{l+1}(\mu) + lP_{l-1}(\mu) = (2l+1)\mu P_l(\mu) \quad (108)$$

we obtain

$$\nabla \left( \frac{l+1}{2l+1} \psi_{l+1}^{SH} + \frac{l}{2l+1} \psi_{l-1}^{SH} \right) = \kappa(2\langle B \rangle \delta_{l0} - \psi_l^{SH}) + \sigma(\psi_0 \delta_{l0} - \psi_l^{SH}). \quad (109)$$

This is a linear system of first order partial differential equations. For a criterion on how many moments are sufficient for a given problem see [78].

The two most widely used boundary conditions are Mark [54, 55] and Marshak [56] boundary conditions. The idea of the Mark boundary conditions is to assign the values of the distribution at certain directions  $\mu_i$  which are the zeros of the Legendre polynomial of order  $N+1$ . That this is in fact a natural boundary condition becomes clear in the next section.

Marshak's boundary conditions, on the other hand, demand that the ingoing half moments of the distribution are prescribed, i.e. for the left boundary

$$\int_0^1 P_l(\mu) \psi(\mu) d\mu. \quad (110)$$

This, in some sense, reflects the boundary conditions for the full equations.

## 5.2 Minimum Entropy Closure

The approximations based on the expansion of the distribution function into a polynomial or the equivalent diffusion approximations suffer from serious drawbacks. First, anisotropic situations are not correctly described. This becomes apparent most drastically for a ray of light, where  $|P| = E$ . Also, the distribution function can become negative and thus the moments computed from the distribution can become unphysical. Second, boundary conditions cannot be incorporated exactly. At a boundary we usually prescribe the ingoing flux only. Here we have to prescribe values for the full moments. These moments contain the unknown outgoing radiation. Moreover, a polynomial expansion cannot capture discontinuities in the angular photon distribution. Krook [42] remarks that at the boundary there is usually a discontinuity in the distribution between in- and outgoing particles.

In this section, we want to describe one idea which resolves the first problem. The idea is to use an Entropy Minimization Principle to obtain the constitutive equation for  $P$ . This principle has become the main concept of Rational Extended Thermodynamics [61].

We want to explain the Entropy Minimization Principle and its practical application by means of our simple moment system (99–100). To close the system we determine a distribution function  $\psi_{ME}$  that minimizes the radiative entropy

$$H_R^*(\psi) = \int_{\mathcal{S}^2} \int_0^\infty h_R^*(\psi) dv d\Omega \quad (111)$$

with

$$h_R^*(\psi) = \frac{2kv^2}{c^3} (n \log n - (n+1) \log(n+1)) \quad \text{where} \quad n = \frac{c^2}{2hv^3} \psi \quad (112)$$

under the constraint that it reproduces the lower order moments,

$$\langle \psi_{ME} \rangle = E \quad \text{and} \quad \langle \Omega \psi_{ME} \rangle = F. \quad (113)$$

The entropy is the the well-known entropy for bosons adapted to radiation fields [63, 70]. At first sight, it is not clear why the distribution should minimize the entropy when all that is known for non-equilibrium processes is that there exists an entropy inequality. But it can be shown [15] that the minimization of the entropy for given moments and the entropy inequality are equivalent.

The above minimization problem can be solved explicitly and the pressure can be written as [16]

$$P = D(f)E. \quad (114)$$

Here,  $f = \frac{F}{E}$  is the relative flux,

$$D(f) = \frac{1 - \chi(f)}{2} I + \frac{3\chi(f) - 1}{2} \frac{f \otimes f}{|f|^2} \quad (115)$$

is the Eddington tensor and

$$\chi(f) = \frac{5 - 2\sqrt{4 - 3|f|^2}}{3} \quad (116)$$

is the Eddington factor. The Eddington tensor can always be written in the form (115) under the assumption that the intensity is symmetric about a preferred direction [50]. The minimum entropy Eddington factor satisfies the natural constraints

$$\text{tr}(D) = 1 \quad (117)$$

$$D(f) - f \otimes f \geq 0 \quad (118)$$

$$f^2 \leq \chi(f) \leq 1 \quad (119)$$

In the literature, the Eddington factor (116) has been derived based on many, apparently not connected, ideas. Levermore [50] assumed that there existed a reference frame in which the distribution was exactly isotropic and used the covariance of the radiation stress tensor. Anile et al. [7] derived it by collecting physical constraints on the Eddington factor and supposing the existence of an additional conservation law, where the conserved quantity behaves like the physical entropy near radiative equilibrium. The minimum entropy system was thoroughly investigated in [16, 84]. Further variable Eddington factors have been proposed, cf. [50, 59] and references therein.

The closed system has several desirable properties. The flux is limited in a natural way, i.e.  $|f| < 1$ . Physically, this corresponds to the fact that information cannot travel faster than the speed of light. Furthermore, the underlying distribution function is always positive. Also, the system can be transformed to a symmetric hyperbolic system [7], which makes it accessible to a general mathematical theory [21]. Again, Marshak type boundary conditions can be derived.

### 5.3 Flux-Limited Diffusion and Entropy Minimization

The classical diffusion approximation is a linear parabolic partial differential equation. In this equation, information is propagated at infinite speed. This can also be seen from the fact that the flux  $|F|$  is not bounded by the energy  $E$  (relative flux  $f < 1$ ). But this should hold, due to the definition of the moments. Thus the classical diffusion approximation contradicts fundamental physical concepts.

Therefore the concept of flux-limited diffusion has been introduced. A diffusion equation is called flux-limited if

$$|F| \leq E. \quad (120)$$

The following is a summary of [50]. We begin by writing the moment equations in the form

$$\nabla F = \kappa(\langle B \rangle - E) \quad (121)$$

$$\nabla(DE) = -(\sigma + \kappa)F, \quad (122)$$

with the Eddington tensor  $D$ . Two assumptions in the derivation of the classical diffusion equation will be modified. First, the Eddington tensor is only identically equal to  $\frac{1}{3}$  for isotropic radiation. For a ray of light (“free-streaming”), on the other hand, we should have  $|DE| = E$ . Second, one should not neglect  $\partial_t F$ . Instead, we note that in the diffusive as well as in the free-streaming regime, the spatial and temporal derivatives of the relative flux  $f = \frac{F}{E}$  and the Eddington tensor  $D$  can be neglected.

Rewriting the equations in terms of  $f$  and  $E$  we get

$$\nabla(fE) = \kappa(\langle B \rangle - E) \quad (123)$$

$$\nabla(DE) = -(\sigma + \kappa)fE. \quad (124)$$

The second equation becomes

$$\nabla(DE) = -(\sigma + \kappa)fE. \quad (125)$$

Inserting (123) into (125), we obtain

$$f\nabla f + \nabla((D - f \otimes f)E) + \bar{\sigma}fE = 0 \quad (126)$$

with  $\bar{\sigma} = \frac{\kappa\langle B \rangle + \sigma E}{E}$ . If we drop the derivatives of  $f$  and  $D$ , we arrive at

$$(D - f \otimes f)\nabla E + \bar{\sigma}fE = 0, \quad (127)$$

or

$$(D - f \otimes f)R = f \quad \text{with} \quad R = -\frac{1}{\bar{\sigma}} \frac{\nabla E}{E}. \quad (128)$$

The idea is now to

1. Choose  $D$  as a function of  $f$
2. Solve  $(D - f \otimes f)R = f$  for  $f$
3. Insert  $f(R)$  into the first moment equation to obtain a diffusion approximation

The first step shows how the concept of flux-limited diffusion is related to a (non-linear) moment closure. If

$$D = \frac{1 - \chi}{2} I + \frac{3\chi - 1}{2} \frac{f \otimes f}{|f|} \quad (129)$$

then  $f$  is an eigenvector of  $D$  and also of  $(D - f \otimes f)$  with

$$(D - f \otimes f)f = (\chi - |f|^2)f. \quad (130)$$

Hence the equation  $(D - f \otimes f)R = f$  has the solution

$$R = \frac{f}{\chi - f^2}. \quad (131)$$

Solving this equation for  $f$  and writing the result as

$$f = \lambda(R)R \quad (132)$$

we arrive at the closure

$$F = -\frac{1}{\bar{\sigma}}\lambda\left(\frac{1}{\bar{\sigma}}\frac{\nabla E}{E}\right)\nabla E. \quad (133)$$

If one chooses for  $D$  the minimum entropy Eddington factor then [50]

$$\lambda = \frac{3(1 - \beta^2)^2}{(3 + \beta^2)^2} \quad (134)$$

where  $\beta$  is implicitly given by

$$R = \frac{4\beta(3 + \beta^2)}{(1 - \beta^2)^2}. \quad (135)$$

The same boundary conditions as for the diffusion approximation can be used.

## 5.4 Partial Moments

In spite of its advantages the minimum entropy system still suffers from a major drawback. In Fig. 8 we show a numerical test case [11] with two colliding beams. The parameters are  $\kappa = 2.5$ ,  $\sigma = 0$ . The temperature inside the medium is zero.

At both sides, beams with a radiative temperature  $T_R := \left(\frac{E}{\sigma_{SB}}\right)^{1/4}$ , where  $\sigma_{SB}$  is Stefan–Boltzmann’s constant, of 1000 and relative fluxes of  $f = \pm 0.99$ , respectively, enter. Figure 8 shows the radiative energy. The full moment model has a qualitatively wrong solution with two shocks. This is not surprising since this Eddington factor, as stated above, is related to radiation which is isotropic in a certain frame [50]. This assumption is violated in the test case above. The unphysical behavior can be remedied by combining Minimum Entropy with the partial moment idea described in the following.

The partial moment idea is somehow intermediate between the Discrete Ordinates approach and Moment Models. In Discrete Ordinates models the integral over all directions is discretized with a numerical quadrature rule. This yields a coupled system of finitely many transport equations, each describing transport into one direction.

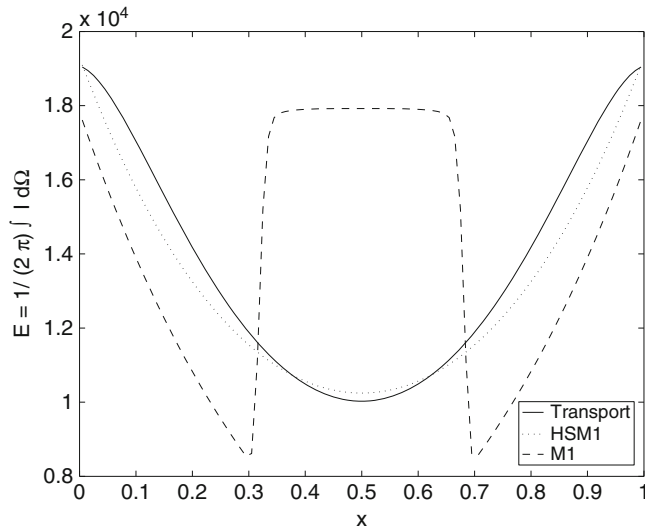


**Fig. 8** Radiative energy. Artificial radiative shock wave in the full moment entropy ( $M_1$ ) model

Let  $\mathcal{A}$  be a partition of the unit sphere  $S^2$ , where  $A \in \mathcal{A}$  denotes the set of the angular integration. Instead of integrating over all directions we average over each  $A \in \mathcal{A}$  separately. Thus we define the average

$$\langle \cdot \rangle_A := \int_A \cdot d\Omega. \quad (136)$$

Again, we multiply the transport equation by 1 and  $\Omega$  and average over each  $A \in \mathcal{A}$  to obtain

$$\nabla F_A = \langle S \rangle_A \quad (137)$$

$$\nabla P_A = \langle \Omega S \rangle_A. \quad (138)$$

We define the corresponding partial moments by

$$E_A = \langle I \rangle_A \quad (139)$$

$$F_A = \langle \Omega I \rangle_A \quad (140)$$

$$P_A = \langle (\Omega \otimes \Omega) I \rangle_A. \quad (141)$$

To close this system we have to find an equation for the partial pressures  $P_A$  as functions of the partial energies  $E_A$  and partial fluxes  $F_A$ .

Examples for the choice of  $\mathcal{A}$ , which are used later, are

- For the full moment model we have  $A = S^2$ , i.e. the integral is over the full sphere.

- For the half moment model we have  $A \in \{S^2_+, S^2_-\}$ . Here,  $S^2_+ = \{\Omega \in S^2 : \Omega_x > 0\}$  is the positive half sphere, where the  $x$ -component of  $\Omega$  is positive, and  $S^2_- = \{\Omega \in S^2 : \Omega_x < 0\}$  analogously is the negative half sphere.
- For the quarter moment model we have  $A \in \{S^2_{++}, S^2_{+-}, S^2_{--}, S^2_{-+}\}$ . Here,  $S^2_{++} = \{\Omega \in S^2 : \Omega_x > 0, \Omega_y > 0\}$  is the quarter sphere in the first quadrant. Analogously,  $S^2_{+-} = \{\Omega \in S^2 : \Omega_x > 0, \Omega_y < 0\}$  etc.

One could also choose other sets for the angular integration.

## 5.5 Partial Moment $P_N$ Closure

The basic idea of the  $P_N$  closure is to expand the photon distribution into a polynomial. Here we use the same idea, but separately for both half ranges. This approach has been investigated in the literature in different forms and contexts and mostly in connection with boundary conditions, for example recently in [11]. Schuster and Schwarzschild [73, 74] introduce two constant distributions for left- and rightgoing photons ( $P_0$  approximation). Krook [42], based on ideas of Sykes [79], considers half moment in one space dimension with a  $P_N$  closure. Sherman [77] compares full- $P_N$  and half- $P_N$  numerically in 1D. Özisik et al. [64] derive a half moment  $P_1$  closure in spherical geometry. Further references can be found in [57], where also an octuple  $P_1$  closure in cylindrical geometry is introduced. Similar ideas appear in related subjects, like gas dynamics, cf. [13] and references therein.

For the half moment  $P_1$  system in one space-dimension, for instance, we assume that in each half range the distribution can be represented by a polynomial of degree one. The coefficients of the polynomial are determined by the constraint that the lower order half moments should be reproduced. The half moment  $P_1$  system reads,

$$\partial_x F_+ = \kappa \left( \frac{1}{2} \langle B \rangle - E_+ \right) + \sigma \left( \frac{1}{2} (E_+ + E_+) - E_+ \right) \quad (142)$$

$$\partial_x (\chi_+ (f_+) E_+) = \kappa \left( \frac{1}{4} \langle B \rangle - F_+ \right) + \sigma \left( \frac{1}{4} (E_+ + E_+) - F_+ \right) \quad (143)$$

$$\partial_x F_- = \kappa \left( \frac{1}{2} \langle B \rangle - E_- \right) + \sigma \left( \frac{1}{2} (E_- + E_-) - E_- \right) \quad (144)$$

$$\partial_x (\chi_- (f_-) E_-) = \kappa \left( -\frac{1}{4} \langle B \rangle - F_- \right) + \sigma \left( -\frac{1}{4} (E_- + E_-) - F_- \right). \quad (145)$$

The partial Eddington factors are

$$\chi_{\pm}(f_{\pm}) = -\frac{1}{6} \pm f_{\pm} \quad \text{with} \quad f_{\pm} = \frac{F_{\pm}}{E_{\pm}}. \quad (146)$$

We note that this is a hyperbolic system. The eigenvalues associated to the “+” moments are positive, while the eigenvalues associated to the “-” moments are



negative, in accordance with physical intuition. This structure makes the formulation of accurate boundary conditions easy. We simply prescribe the ingoing half moments, in accordance with the conditions for the full equations. For more discussions, including existence and uniqueness results, and the explicit quarter moment  $P_1$  closure in two space-dimensions we refer the reader to [72].

## 5.6 Partial Moment Entropy Closure

The partial moment entropy closure was introduced for radiative heat transfer in [19] and developed in [18, 25, 85]. For the sake of completeness we recall the procedure explained earlier. We have to find a distribution function  $\psi_{ME}$  that minimizes the radiative entropy  $H_R^*$  given by (111–112), under the constraint that it reproduces the lower order partial moments,

$$\langle \psi_{ME} \rangle_A = E_A \quad \text{and} \quad \langle \Omega \psi_{ME} \rangle_A = F_A \quad (147)$$

for all  $A \in \mathcal{A}$ . The minimizer is given by

$$\psi_{ME} = \sum_{A \in \mathcal{A}} \frac{1}{\alpha_A^4 (1 + \beta_A \cdot \Omega)^4} \mathbf{1}_A, \quad (148)$$

where  $\alpha_A$  and  $\beta_A$  are Lagrange multipliers corresponding to the constraints. This formula differs from the one given in [19] since we consider frequency-averaged quantities here. It can be obtained from the minimizer in [19] by integration over  $\mathbf{v}$ .

In the case of  $\mathcal{A} = \{S_+^2, S_-^2\}$ , the half moments over this distribution can be computed explicitly.

Note that  $E_{\pm} \geq 0, F_{+} \geq 0, F_{-} \leq 0$ . Multiplying the transfer equation with  $m(\mu) = 1^+, 1^-, \mu^+, \mu^-$  and integrating with respect to  $\mathbf{v}$  and  $\mu$  we get

$$\varepsilon \partial_x F_{+} = \kappa \left( \frac{1}{2} \langle B \rangle - E_{+} \right) + \sigma \left( \frac{1}{2} (E_{+} + E_{+}) - E_{+} \right) \quad (149)$$

$$\varepsilon \partial_x \langle (\mu^+)^2 \psi \rangle = \kappa \left( \frac{1}{4} \langle B \rangle - F_{+} \right) + \sigma \left( \frac{1}{4} (E_{+} + E_{+}) - F_{+} \right) \quad (150)$$

$$\varepsilon \partial_x F_{-} = \kappa \left( \frac{1}{2} \langle B \rangle - E_{-} \right) + \sigma \left( \frac{1}{2} (E_{+} + E_{+}) - E_{+} \right) \quad (151)$$

$$\varepsilon \partial_x \langle (\mu^-)^2 \psi \rangle = \kappa \left( -\frac{1}{4} \langle B \rangle - F_{-} \right) + \sigma \left( -\frac{1}{4} (E_{+} + E_{+}) - F_{-} \right). \quad (152)$$

This system is closed by an entropy minimization principle. Then, the minimizer  $\psi_{ME}$  is determined by

$$H_R^*(\psi_{ME}) = \min_{\psi} \{ H_R^*(\psi) : \langle m(\mu) \psi \rangle = (E_{+}, E_{-}, F_{+}, F_{-}) \},$$

i.e.  $\psi_{ME}$  minimizes the entropy under the constraint of a reproduction of the half space moments with  $E_+ \geq 0, E_- \geq 0, F_+ \geq 0, F_- \leq 0$  as above.

Solutions of similar minimization problems are discussed in [16]. A straightforward computation shows that in the present case the unique solution  $\psi_{ME} = \psi_{ME}(T, \mu) = \psi_{ME}(T, \mu, \nu)$  is given by

$$\psi_{ME}(T, \mu) = \frac{2h\nu^3}{c^2} \frac{1}{\exp(\frac{h\nu}{kT}(\alpha_-(1^- + \beta_-\mu^-) + \alpha_+(1^+ + \beta_+\mu^+))) - 1},$$

where  $\alpha_+ > 0, \alpha_- > 0$  and  $\beta_+ > -1, \beta_- < 1$  are determined by the constraints

$$\begin{aligned} \langle 1^\pm \psi_{ME} \rangle &= \frac{\sigma_{SB}}{\pi} T^4 \frac{\beta_\pm^2 \pm 3\beta_\pm + 3}{3\alpha_\pm^4 (1 \pm \beta_\pm)^3} = E^\pm \\ \langle \mu^\pm \psi_{ME} \rangle &= \frac{\sigma_{SB}}{\pi} T^4 \frac{\beta_\pm \pm 3}{6\alpha_\pm^4 (1 \pm \beta_\pm)^3} = F^\pm. \end{aligned}$$

The temprature  $T$  is introduced here as a normalization parameter to measure the deviation from the usual Planckian. We mention in passing that in general maximization of entropy is a touchy business, see for example [34].

Having solved the minimization problem, one obtains

$$\frac{1}{c} \langle (\mu^\pm)^2 \psi_{ME} \rangle = \frac{\sigma}{c\pi} T^4 \frac{1}{3\alpha_\pm^4 (1 \pm \beta_\pm)^3} = \chi_\pm(f_\pm) E_\pm,$$

if we define the relative fluxes  $f_\pm = \frac{F_\pm}{cE_\pm}$  and the Eddington factors

$$\chi_\pm(f_\pm) = \frac{8f_\pm^2}{1 \pm 6f_\pm + \sqrt{1 \pm 12f_\pm - 12f_\pm^2}}.$$

Approximating  $\langle (\mu^\pm)^2 \psi \rangle \sim \langle (\mu^\pm)^2 \psi_{ME} \rangle$  in (149)–(152) and using the above computation we arrive at

$$\partial_x F_+ = \kappa \left( \frac{1}{2} \langle B \rangle - E_+ \right) + \sigma \left( \frac{1}{2} (E_+ + E_+) - E_+ \right) \quad (153)$$

$$\partial_x (\chi_+(f_+) E_+) = \kappa \left( \frac{1}{4} \langle B \rangle - F_+ \right) + \sigma \left( \frac{1}{4} (E_+ + E_+) - F_+ \right) \quad (154)$$

$$\partial_x F_- = \kappa \left( \frac{1}{2} \langle B \rangle - E_- \right) + \sigma \left( \frac{1}{2} (E_- + E_-) - E_- \right) \quad (155)$$

$$\partial_x (\chi_-(f_-) E_-) = \kappa \left( -\frac{1}{4} \langle B \rangle - F_- \right) + \sigma \left( -\frac{1}{4} (E_- + E_-) - F_- \right). \quad (156)$$

The system (153–156) is a stationary hyperbolic equation with relaxation terms. An analysis of the equations has been performed in [26].

The eigenvalues associated to  $E_+$  and  $F_+$  are always positive while the eigenvalues associated to  $E_-$  and  $F_-$  are always negative. This result agrees with intuition since  $E_+$  and  $F_+$  describe transport to the right, while  $E_-$  and  $F_-$  describe transport to the left. Therefore we have to prescribe two boundary conditions on the left and right hand side, respectively. We use at  $x = 0$ :

$$F_+ = \langle \mu^+ [\rho(\mu)\psi_{ME}(T, -\mu) + (1 - \rho(\mu))B(T_{\text{out}})] \rangle \quad (157)$$

$$\chi_+ E_+ = \langle (\mu^+)^2 [\rho(\mu)\psi_{ME}(T, -\mu) + (1 - \rho(\mu))B(T_{\text{out}})] \rangle \quad (158)$$

and the analogous conditions at  $x = 1$ . Equations (153)–(158) are solved together with the temperature equation in the form

$$\varepsilon^2 \partial_t T = \varepsilon^2 k \partial_{xx} T - 2\pi\kappa \left( \frac{2\sigma_{SB}}{\pi} T^4 - (E_+ + E_-) \right) \quad (159)$$

and corresponding boundary conditions.

The Partial Moment Entropy approximation has a lot of desirable physical and mathematical properties. The underlying distribution function is always positive. Hence the relative flux and the speed of propagation are limited. The system is symmetrizable hyperbolic. This makes it accessible to a powerful mathematical theory guaranteeing well-posedness locally in time. Like the full moment entropy approximation [16], the system correctly approaches the diffusive limit and the free-streaming limit. The eigenvalues of the half moment and quarter moment entropy approximation have a special structure. For the half moment case, the eigenvalues of the “+” direction are always positive, the eigenvalues of the “−” direction are always negative. Both are bounded in modulus by the speed of light  $c$ . This property makes very simple and accurate numerical schemes possible, for example kinetic schemes or upwind schemes. The formulation of accurate boundary conditions is again straight-forward.

## 6 Frequency-Averaged Moment Equations

Moment models are obtained by testing (32) with functions depending on direction, in our case  $(1, \mu)^T$ , then integrating the result over all the directions and frequencies. Then, the system does only depend on time and space variables, and is hence far cheaper to solve. However, this has a cost since we are not always able to reproduce neither frequency dependent problems nor very stiff directional configurations such as the collision of two opposite beams [11, 19].

In order to solve this difficulty, we do not average over all directions and all frequencies but distinguish photons going to the left and to the right and different frequency bands.

Let

$$\langle g \rangle_m^+ = \int_{v_{m-\frac{1}{2}}}^{v_{m+\frac{1}{2}}} \int_0^1 g d\mu dv \quad \text{and} \quad \langle g \rangle_m^- = \int_{v_{m-\frac{1}{2}}}^{v_{m+\frac{1}{2}}} \int_{-1}^0 g d\mu dv \quad (160)$$

denote the average over all right/left-going photons in the  $m^{\text{th}}$  frequency band  $[v_{m-\frac{1}{2}}, v_{m+\frac{1}{2}}]$ . We denote the bands as half-open intervals to have mathematically disjoint sets. However, since only integrals over the bands matter, one could also use closed intervals. The moments  $E_{R,m}^+ = \langle \psi \rangle_m^+$ ,  $F_{R,m}^+ = \langle \Omega \psi \rangle_m^+$  and  $P_{R,m}^+ = \langle (\Omega \otimes \Omega) \psi \rangle_m^+$  are respectively the radiative energy, the radiative flux and the radiative pressure inside the  $m^{\text{th}}$  group and the positive half-space. The quantities for the negative half space are defined in analogy.

Testing (32) with  $(1, \mu)^T$  and averaging with the above defined averages we get

$$\partial_x F_{R,m}^+ = \hat{\kappa}_m^+ a \theta_{m,+}^4 - \tilde{\kappa}_m^+ E_{R,m}^+ + \tilde{\sigma}_m^+ \left( \frac{E_{R,m}^+ + E_{R,m}^-}{2} - E_{R,m}^+ \right) \quad (161)$$

$$\partial_x P_{R,m}^+ = \hat{\kappa}_m^+ \frac{a}{2} \theta_{m,+}^4 - \check{\kappa}_m^+ F_{R,m}^+ - \tilde{\sigma}_m^+ \left( \frac{E_{R,m}^+ + E_{R,m}^-}{4} - F_{R,m}^+ \right) \quad (162)$$

and

$$\partial_x F_{R,m}^- = \hat{\kappa}_m^- a \theta_{m,-}^4 - \tilde{\kappa}_m^- E_{R,m}^- + \tilde{\sigma}_m^- \left( \frac{E_{R,m}^+ + E_{R,m}^-}{2} - E_{R,m}^- \right) \quad (163)$$

$$\partial_x P_{R,m}^- = -\hat{\kappa}_m^- \frac{a}{2} \theta_{m,-}^4 - \check{\kappa}_m^- F_{R,m}^- - \tilde{\sigma}_m^- \left( -\frac{E_{R,m}^+ + E_{R,m}^-}{4} - F_{R,m}^- \right), \quad (164)$$

where we have used the following frequency averages of the frequency dependent quantities  $\kappa$  and  $\sigma$ :

$$\hat{\kappa}_m^+ = \frac{\langle \kappa B \rangle_m^+}{\langle B \rangle_m^+}, \quad \tilde{\kappa}_m^+ = \frac{\langle \kappa \psi \rangle_m^+}{\langle \psi \rangle_m^+}, \quad \check{\kappa}_m^+ = \frac{\langle \kappa \mu \psi \rangle_m^+}{\langle \mu \psi \rangle_m^+} \quad \text{and} \quad \tilde{\sigma}_m^+ = \frac{\langle \sigma \psi \rangle_m^+}{\langle \psi \rangle_m^+}. \quad (165)$$

## 6.1 Entropy Minimization

For each  $m$  (161)–(164) is a system of 4 equations for 6 unknown moments. To obtain a well-posed system one usually expresses the highest moment, here  $P_{R,m}^\pm$ , as a function of the lower order moments, here  $E_{R,m}^\pm$  and  $F_{R,m}^\pm$ . This is referred to as “closure” of the system.

To close the system here, we use entropy minimization, see [7, 16, 51, 61]. Compare [19] for the grey half space model and [83] for the multigroup full space model.

Let us first recall the definition of the radiative entropy,

$$h_R(I) = \frac{2k\nu^2}{c^3} \left[ n_I \ln n_I - (n_I + 1) \ln(n_I + 1) \right] \quad (166)$$

where

$$n_I = \frac{c^2}{2h\nu^3} \psi. \quad (167)$$

According to the entropy minimization principle, we determine a distribution function that minimizes the radiative entropy under the constraint that it reproduces the lower order moments,

$$H_R(\psi_{ME}) = \min_{\psi} \left\{ H(\psi) = \sum_m (\langle h_R(\psi) \rangle_m^+ + \langle h_R(\psi) \rangle_m^-) : : \right. \\ \left. \forall m : \langle \psi \rangle_m^{\pm} = E_m^{\pm} \text{ and } c \langle \mu \psi \rangle_m^{\pm} = F_m^{\pm} \right\}. \quad (168)$$

This gives the closure function,

$$\psi_{ME}(\Omega, \nu) = \sum_m 1_{[\nu_{m-\frac{1}{2}}; \nu_{m+\frac{1}{2}}]} \left[ \frac{2h\nu^3}{c^2} \left[ \exp\left(\frac{h\nu}{k} (\alpha_m^+ (1 + \beta_m^+ \mu^+) + \alpha_m^- (1 + \beta_m^- \mu^-))\right) - 1 \right]^{-1} \right] \quad (169)$$

where  $\alpha_m^{\pm}, \beta_m^{\pm}$  are Lagrange multipliers, that are defined to reproduce the moments.

## 6.2 Inversion of the System

The next step is to express the Lagrange multipliers  $\alpha_m^{\pm}, \beta_m^{\pm}$  as functions of  $E_{R,m}^{\pm}, F_{R,m}^{\pm}$  and to substitute

$$P_{R,m}^{\pm} \approx \langle \psi_{ME}(\alpha_m^{\pm}, \beta_m^{\pm}) \rangle_m^{\pm} = \langle \psi_{ME}(E_{R,m}^{\pm}, F_{R,m}^{\pm}) \rangle_m^{\pm}. \quad (170)$$

Hence we obtain a system for  $E_{R,m}^{\pm}$  and  $F_{R,m}^{\pm}$ .

For the grey half space model [19], the Lagrange multipliers as functions of the moments can be computed explicitly. However, with the introduction of multigroup variables this is not the case anymore. Integrations require the knowledge of the following function,

$$\Xi(\eta) = \int_0^{\eta} \xi^3 [\exp(\xi) - 1]^{-1} d\xi. \quad (171)$$

For example,

$$E_m^+ = \frac{1}{c} \int_0^1 \int_{\nu_{m-\frac{1}{2}}}^{\nu_{m+\frac{1}{2}}} \psi_{ME} d\nu d\mu \\ = \int_0^1 \frac{2k^4}{h^3 c^3} (\alpha_m^+ (1 + \beta_m^+ \mu^+))^{-1} (\Xi(\nu'_{m+\frac{1}{2}}) - \Xi(\nu'_{m-\frac{1}{2}})) d\mu \quad (172)$$

with  $v' = \frac{h\nu}{k} \alpha^+ (1 + \beta^+ \mu^+)$ . Unfortunately, except for  $\eta = 0$  and  $\eta = +\infty$  there is no analytic expression of  $\Xi$ . A numerical calculation would be too expensive since we have to be very accurate. Therefore, in [83] an approximation was introduced, which we can also be used here,

$$\Xi(\eta) \simeq C_\infty + \exp(-C_* \eta) \sum_{i=0}^{imax} C_i \eta^i \quad (173)$$

The constants  $C_i$  are chosen so that the approximation has a very good behaviour in the vicinity of  $\eta = 0$ . For our applications, taking  $imax = 5$  is sufficient.

Once this approximation is made, it is possible to integrate and hence to compute the Lagrange multipliers of the minimization problem as functions of the moments. Then, we are able to compute the radiative pressures as functions of the radiative energies and fluxes. Moreover, we can show that we can write the pressures in Eddington form,  $P_R^\pm = D_R^\pm E_R^\pm$ , where

$$D_m^\pm = \frac{(1 - \chi_m^\pm)}{2} : I_d + \frac{(3\chi_m^\pm - 1)}{2} : \frac{F_m^\pm \otimes F_m^\pm}{\|F_m^\pm\|^2}. \quad (174)$$

The scalars  $\chi_m^\pm$  are called Eddington factors.

### 6.3 Properties

The multigroup half space model keeps the interesting properties of the other moment models closed by entropy minimization, that is to say

- The main physical properties remain: conservation of the total energy and dissipation of the total entropy. Moreover, the addition of multigroup allows to have a better balanced-energy in the case of strongly frequency-dependant problems.
- The model naturally limits the flux. This property can be expressed as follows:

$$\forall m, : \frac{F_m^\pm}{E_m^\pm} < 1 \quad (175)$$

This means that the photons cannot travel faster than the speed of the light. We note that this important property is often not satisfied by macroscopic models.

- For 1D problems, it is very easy to make a simple numerical scheme that can efficiently solve every possible angular configuration. This is done only by using upwind schemes (see [19]). We chose to develop only a four-moments model to obtain a simple and very competitive model. However, in some situations one might need more moments to capture the physical solution [78].
- The cost of the method is low and can be lowered to be less than the number of groups times the cost of the half space model by doing a pressure precalculation.

These properties are the most important ones but it is to note that the multigroup half space model keeps all the properties (and limitations) of both the half space [19] and multigroup full space [83] models.

## 7 Numerical Comparisons

### 7.1 Numerical Results

The approximations presented above have different mathematical structures. The Discrete Ordinates, Spherical Harmonics and partial  $P_N$  equations are linear first order partial differential equations. The minimum entropy and the partial moment entropy system are nonlinear hyperbolic first order partial differential equations. On the other hand the diffusion and flux-limited diffusion equations are parabolic equations, whereas the  $SP_N$  equations are elliptic/parabolic. We remark that, although they are closely related, the minimum entropy moment model and flux-limited diffusion with the same Eddington factor are not completely equivalent, but can in fact have very different solutions. For example, the solutions for the minimum entropy system can have shocks whereas this is impossible for flux-limited diffusion.

In the following Figures we show some numerical comparisons of the different models. The abbreviations in the legends mean

- *S40/Transport*: Discrete Ordinates Solution with 40 directions
- *P1*:  $P_1$  approximation with Marshak boundary conditions
- *SP1*:  $SP_1$ /Diffusion approximation with Marshak boundary condition
- *FLD*: flux-limited diffusion with minimum entropy Eddington factor and Marshak boundary conditions
- *HSP1*: half  $P_1$  approximation
- *HSM1*: half moment entropy approximation
- *Quarter Space*: quarter moment entropy approximation

The *transport* solution has been obtained with a direct discretization as described above. The parabolic equations *SP1* and *FLD* have been discretized with a standard finite difference scheme. For the balance laws *P1*, *HSP1*, *HSM1* and *Quarter Space* we used kinetic schemes based on the distribution function from the moment closure. All of the latter systems have eigenvalues in modulus less than the speed of light. Thus, similar CFL conditions hold. To be valid in the diffusive limit, the kinetic schemes can be modified to become asymptotic preserving, cf. [19] for a simple analysis in 1D.

### 7.2 Grey Transport

First, we investigate the transport equation (with fixed temperature) without frequency dependence. In Fig. 9 we consider a given temperature profile in the unit

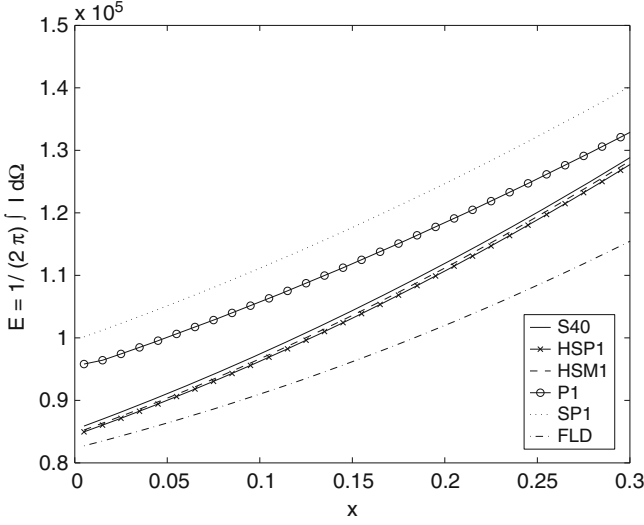


**Fig. 9** Steady radiative energy for a fixed temperature profile  $T(x) = 1000 + 800x$  in the interval  $[0, 1]$ ,  $\kappa = 1$ ,  $\sigma = 0.1$

interval  $[0, 1]$ ,  $T(x) = 1000 + 800x$ . This temperature enters into the Planck source term  $\langle B \rangle$  via Stefan–Boltzmann’s law

$$\langle B \rangle(T) = \sigma_{SB} T^4. \quad (176)$$

At the boundary we prescribe black body radiation at the corresponding temperature as ingoing radiation. In Fig. 9 we see that the high order Discrete Ordinates solution (considered as benchmark result) and the half moment approximations agree very well, whereas  $P_1$ ,  $SP_1$  and flux-limited diffusion differ significantly.

This becomes more striking in the 2D example in Fig. 10. The  $P_1$  and  $SP_1$  approximations are unable to capture the simple anisotropy in this test case, whereas the quarter moment model and the solution of the full equations agree very well.

### 7.3 Grey Cooling

Here we apply the above methods to a cooling problem. We use an initial temperature of 1,000 K and an outside temperature of 300 K. The parameters  $a$ ,  $\varepsilon$ ,  $\kappa$  are set equal to 1.  $\alpha$  and the reflectivity are chosen equal to 0.  $k$  is chosen equal to 1 and 0.1, i.e. we consider two situations where heat conduction and radiation are dominating, respectively.  $u$  is chosen equal to zero. The gridsize is  $\Delta x = 0.01$ ,  $\Delta t = 10^{-4}$ . For the radiative transfer solution a Gaussian quadrature with 64 points is used for the angular discretization. We use the above first order finite difference discretization



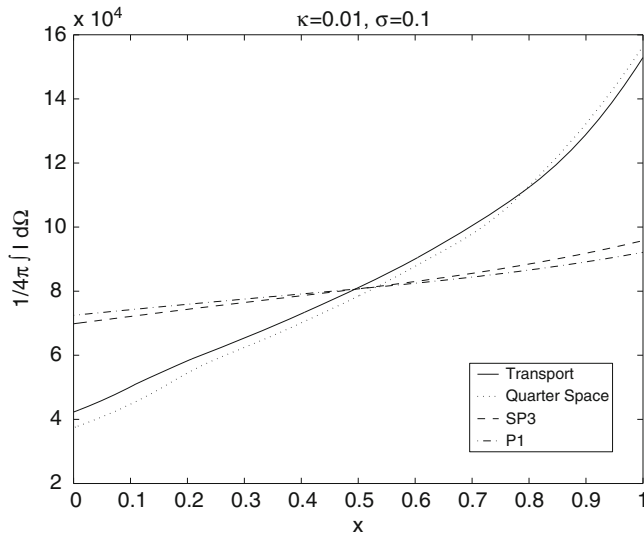


**Fig. 10** Steady radiative energy for a fixed temperature profile  $T(x) = 1000 + 400(x+y)$  in  $[0, 1]^2$ ,  $\kappa = 0.01$ ,  $\sigma = 0.1$ . Cut along the diagonal

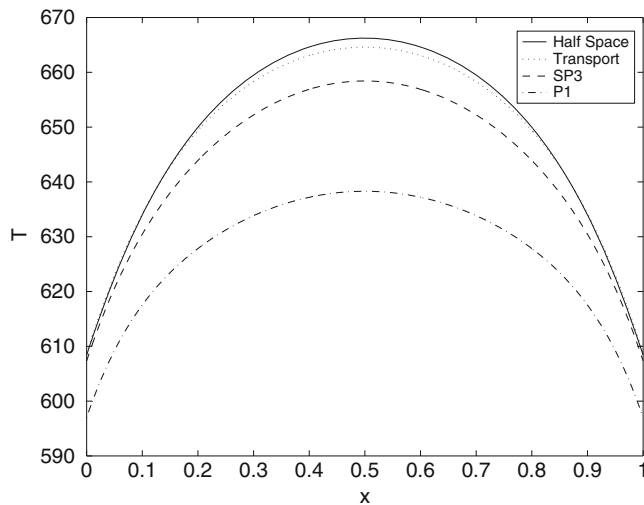


**Fig. 11** Temperatures at time  $t = 0.01$  with  $k = 1$

in space and a Newton iteration to obtain an approximate solution of the nonlinear equations (153–156). The calculated temperatures are shown in Figs. 11 and 13. The mean intensities, i.e.  $E_+ + E_-$  in the half moment case and  $\langle \mu I \rangle$  for the radiative transfer solutions, are shown in Figs. 12 and 14. The results obtained with the half space moment method, the  $P_1$  approximation, the  $SP_3$  approximation [47]

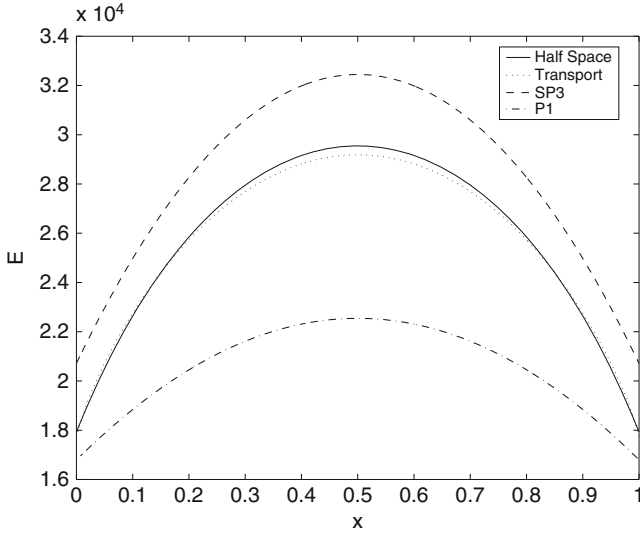


**Fig. 12** Mean intensity at time  $t = 0.01$  with  $k = 1$

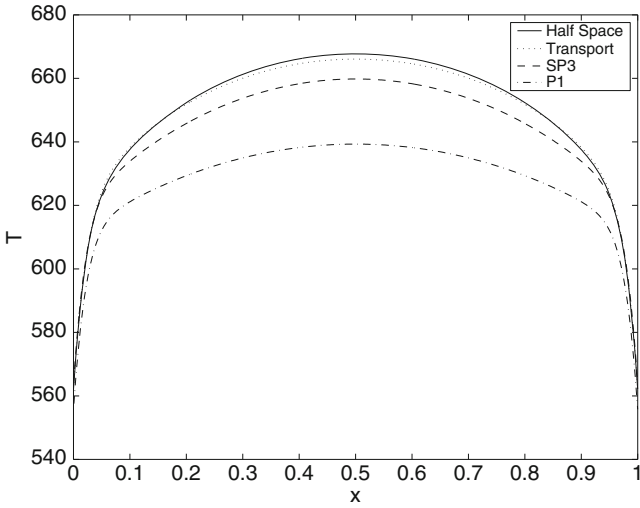


**Fig. 13** Temperatures at time  $t = 0.01$  with  $k = 0.1$

and the solution of the full transport equation are compared. We note that the usual Rosseland or diffusion approximation [45] gives in all cases results which are far less accurate than the solutions considered here. As can be seen in the figures the half moment method outperforms the other methods in both cases.

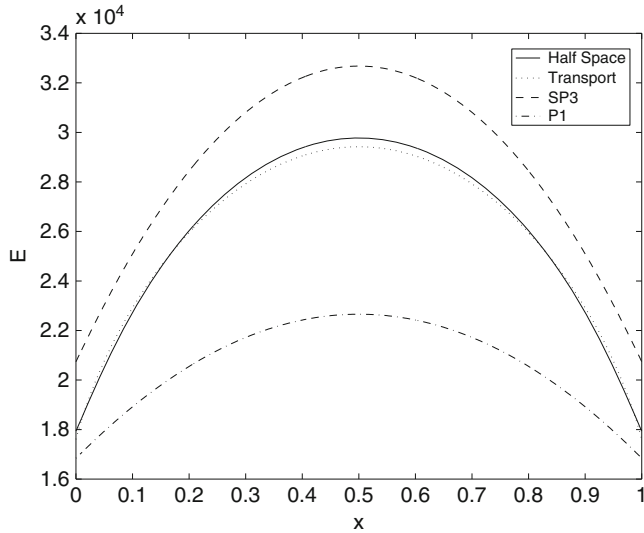


Fig. 14 Mean intensity at time  $t = 0.01$  with  $k = 0.1$

## 7.4 Multigroup Transport

First we consider only the equation for the radiative intensity with a fixed matter temperature profile. We divide the spectrum into four bands  $[\lambda_{i-\frac{1}{2}}, \lambda_{i+\frac{1}{2}}[$  ( $]v_{i+\frac{1}{2}}, v_{i-\frac{1}{2}}]$  respectively) with piecewise constant  $\kappa_i$  on  $[\lambda_{i-\frac{1}{2}}, \lambda_{i+\frac{1}{2}}[$ . We used  $\lambda_{\frac{1}{2}} = 0 \mu m$ ,  $\lambda_{\frac{3}{2}} = 1.035 \mu m$ ,  $\lambda_{\frac{5}{2}} = 2.07 \mu m$ ,  $\lambda_{\frac{7}{2}} = 7 \mu m$  and  $\lambda_{\frac{9}{2}} = \infty$  and  $\sigma = 0$ .

In Figs. 15–17 we compare the results obtained with the half space moment model to the solution of the full RHT equations using a source iteration as well as diffusive  $P_1$  and  $SP_3$  approximations. For details on these equations we refer the reader to [47]. The classical Rosseland approximation gives in all cases considered here far less accurate results.

For the radiative energy

$$E_R = \int_0^\infty \int_{-1}^1 \psi d\mu dv = \sum_m (E_{R,m}^+ + E_{R,m}^-) \quad (177)$$

we define, in analogy to Stefan's law, the radiative temperature

$$T_R := \left( \frac{2\pi E_R}{a} \right)^{1/4}. \quad (178)$$

The parameters corresponding to Fig. 15 are  $\kappa_1 = 100 m^{-1}$ ,  $\kappa_2 = 1 m^{-1}$ ,  $\kappa_3 = 10 m^{-1}$ ,  $\kappa_4 = \infty$  and represent a rather diffusive, optically thick physical regime.

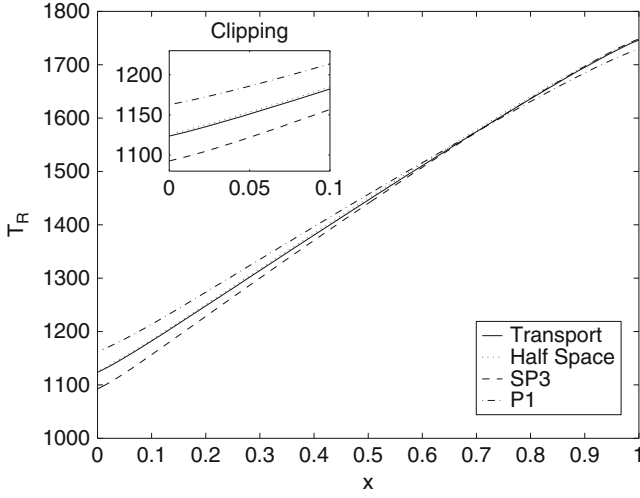


**Fig. 15** Steady radiative temperature for a fixed matter temperature profile,  $T(x) = 1000 + 800x$ ,  $T_b(0) = 1000$ ,  $T_b(1) = 1800$ . Diffusive regime. Four frequency bands

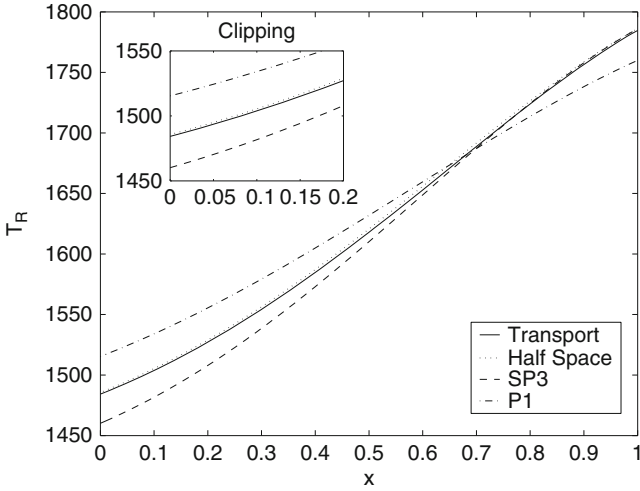


**Fig. 16** Steady radiative temperature for a fixed matter temperature profile,  $T(x) = 500 + 1500x$ ,  $T_b(0) = 500$ ,  $T_b(1) = 2000$ . Transport regime. Four frequency bands

The half space model performs better than the diffusive approximations which are designed for this physical situation. The differences become more striking in Fig. 16 where we chose a rather opposite physical regime with large photon mean free path,  $\kappa_1 = 0.1 \text{ m}^{-1}$ ,  $\kappa_2 = 0.01 \text{ m}^{-1}$ ,  $\kappa_3 = 1 \text{ m}^{-1}$ ,  $\kappa_4 = \infty$ . We chose the same absorption coefficients in Fig. 17. However, while in the first two cases the boundary

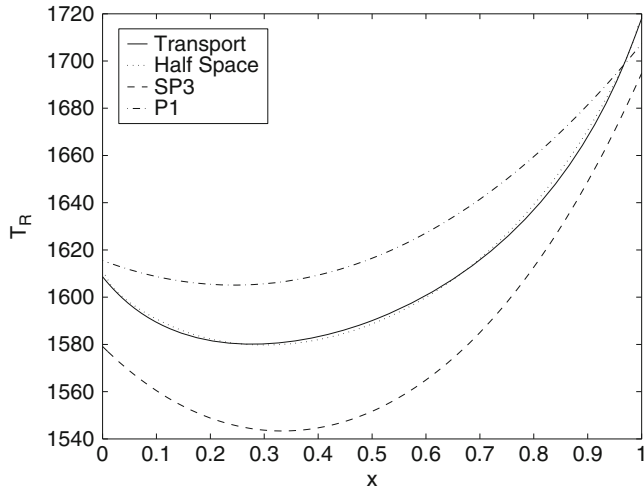


**Fig. 17** Steady radiative temperature for a fixed matter temperature profile,  $T(x) = 500$ ,  $T_b(0) = 1500$ ,  $T_b(1) = 2000$ . Transport regime. Four frequency bands

temperature agreed with the interior matter temperature we chose here a much higher boundary temperature which corresponds to heat flux entering the medium. The half space model is far more accurate than the diffusive approximations.

## 7.5 Multigroup Cooling

In our next test case we consider the transport equation coupled to the heat equation. We use  $k = h = 1$ ,  $\alpha = 0$  and  $\rho = 0$ . The outside temperature is  $T_b = 1,000$  at the left and  $T_b = 1,800$  at the right boundary. The scattering and absorption coefficients are chosen as in our second and third uncoupled test cases. In Fig. 18 we show the steady radiative temperature. Again, the new half space model agrees best with the full transport solution.

## 7.6 Adaptive methods for the Simulation of 2-d and 3-d Cooling Processes

The application that we study here is the cooling of a glass cube representing a typical fabrication step in glass manufacturing. We consider clean glass, which means that the treatment of scattering can be omitted. The frequencies are approximated by an eight-band model. The values used are given in Table 2. Furthermore, we set

$$k = 1, \quad h = 0.001, \quad T_b = 300$$

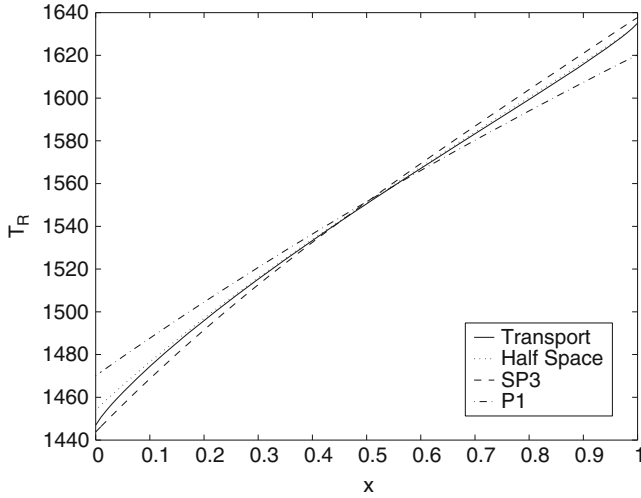


**Fig. 18** Steady radiative temperature for the coupled equations,  $T_b(0) = 1,000$ ,  $T_b(1) = 1,800$ . Transport regime. Four frequency bands

and start with a uniform temperature distribution  $T_0(x) = 1,000$ . The time integration is stopped at  $t = 0.001$ .

We use a space-time adaptive method described in detail in [38]. We validate the  $SP_N$ -solutions with numerical solutions to the full RHTE. The full RHTE is solved by a diamond differencing discretization coupled with a discrete ordinate method which uses 60 directions [10, 76]. This is for the present situation sufficient to obtain an accurate solution for the transport problem provided the spatial grid is chosen fine enough.

### 7.6.1 Two-Dimensional Glass Cooling

We consider an infinitely long square glass block which allows us to use a two-dimensional approximation on the scaled square domain  $\Omega = [0, 1]^2$ .

In Fig. 19, we show temperature distributions at the final time  $t_e = 0.001$  obtained for the  $SP_3$ -approximation. As expected, the strongest cooling takes place in the corners of the computational domain. The meshes automatically chosen by our adaptive approach are highly refined at the boundary caused by the steep temperature gradients there. In this case, a stable uniform discretization of the two-dimensional RHTE requires the solution of a linear system with more than 4.8 million unknowns in each time step, whereas the dimension of the linear algebraic systems for the adaptive  $SP_3$ -approximation is not greater than 272,000.

In Fig. 20 the  $SP_N$ -solutions are compared to the full RHTE- and Rosseland approximation. In particular, they reconstruct the temperature near the boundary much more accurately than the Rosseland approximation which is often used in engineering practice.

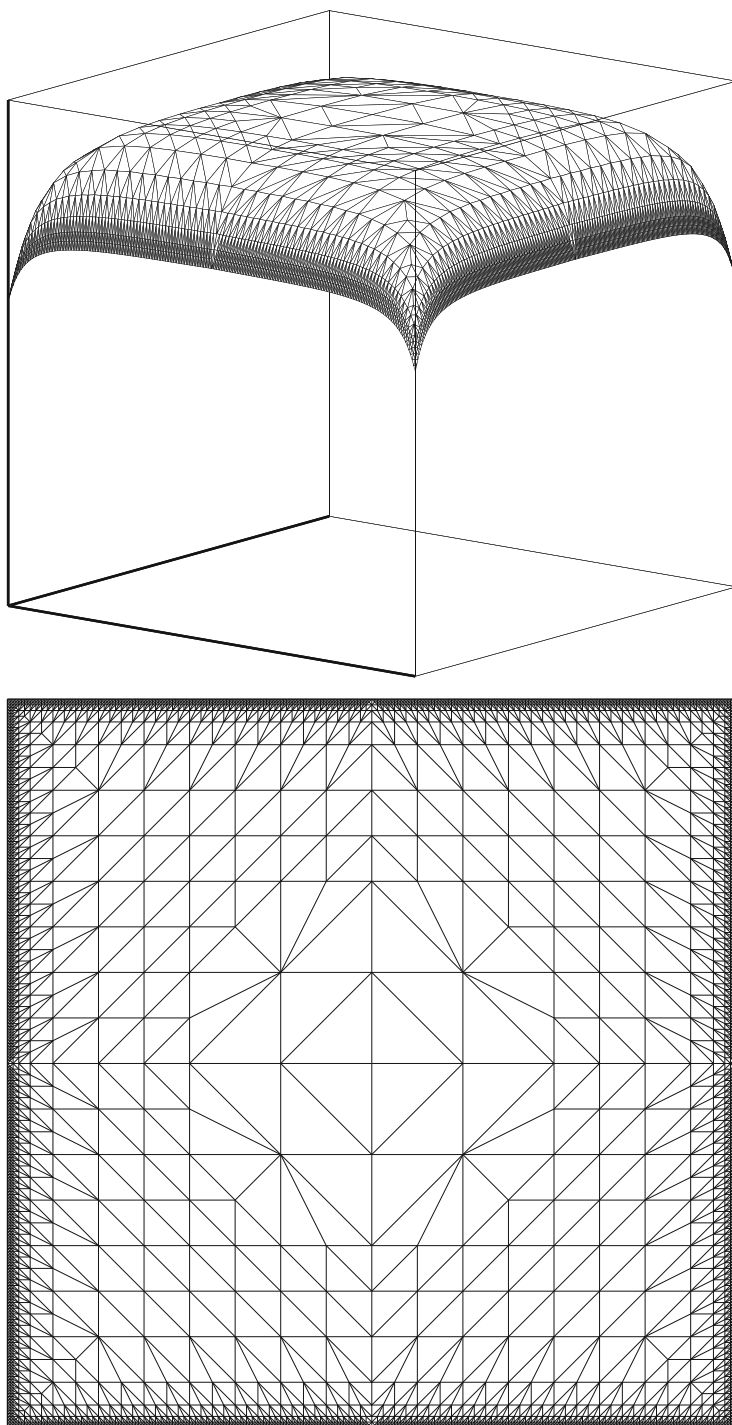


**Fig. 19** Two-dimensional temperature distributions and spatial meshes on  $\Omega = [0, 1]^2$  resulting from  $SP_3$ -approximations at  $t_e = 0.001$ . The temperature axis ranges from 300 to 1,000. Strong refinement takes place in the boundary layer due to the large temperature gradients there

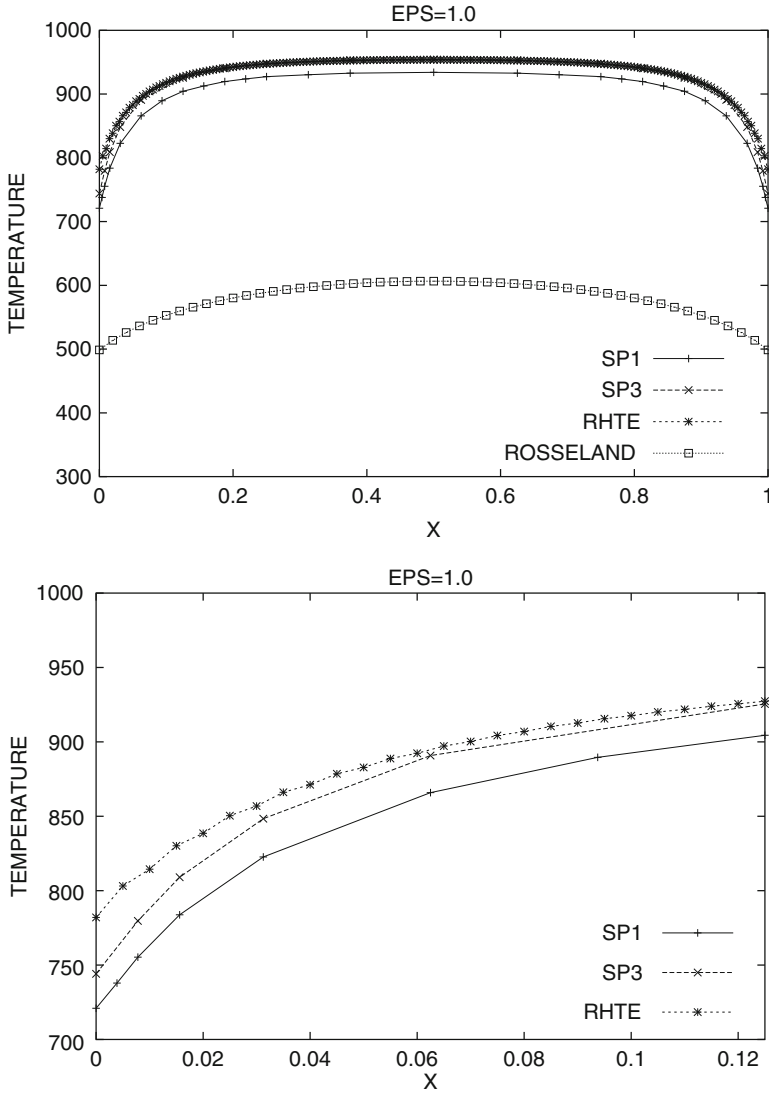


**Fig. 20** Comparison of two-dimensional temperature distributions at  $t_e = 0.001$  along the line  $y = 0.5$  obtained from different radiation models. The  $SP_3$ -solution matches very well with the RHTE solution inside the glass cube. Some differences are visible in the boundary region. Both  $SP_N$ -approximations give much more accurate results than the Rosseland approximation

The time steps in the adaptive procedure increase rapidly by two orders of magnitude reflecting the ongoing diffusive smoothing in the boundary layer. Altogether 9 and 24 time steps are needed. In contrast, a uniform time discretization yielding the same accuracy, requires 100 steps.



Concerning the computation times the parameters discussed above lead to the following results: Using the method described above without adaptivity in space and time for Rosseland,  $SP_1$  and  $SP_3$  the computational effort is approximately doubled

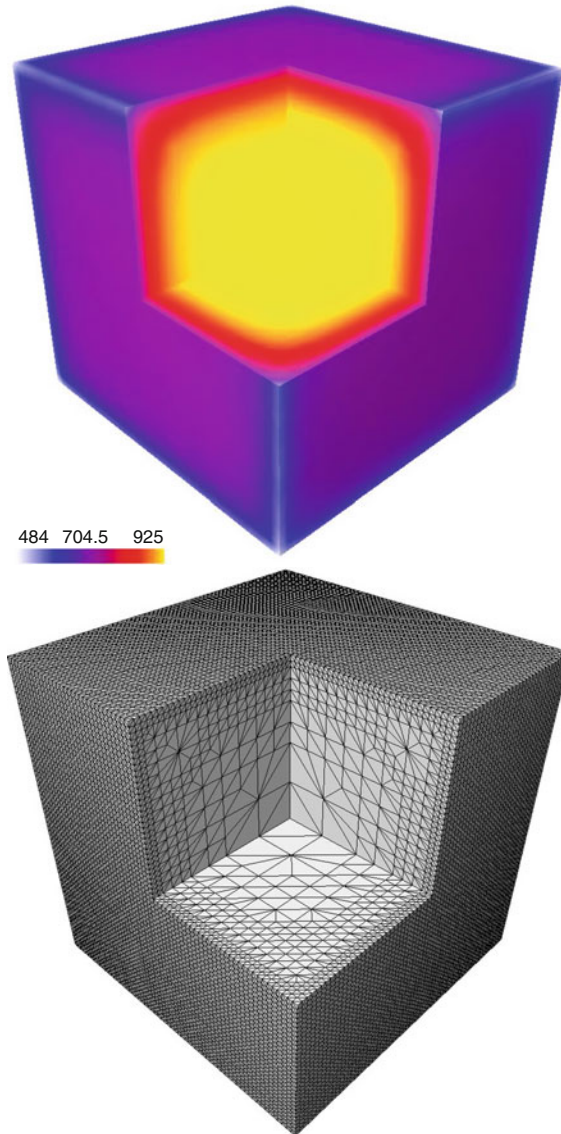


**Fig. 21** Three-dimensional temperature distribution and adaptive spatial mesh on  $\Omega = [0, 1]^3$  resulting from the  $SP_3$ -approximation at  $t_e = 0.001$ . We removed one small cube to present details from inside the glass cube. Refinement takes place in the boundary layer due to the large temperature gradients there. The adaptive mesh consists of 82,705 grid points

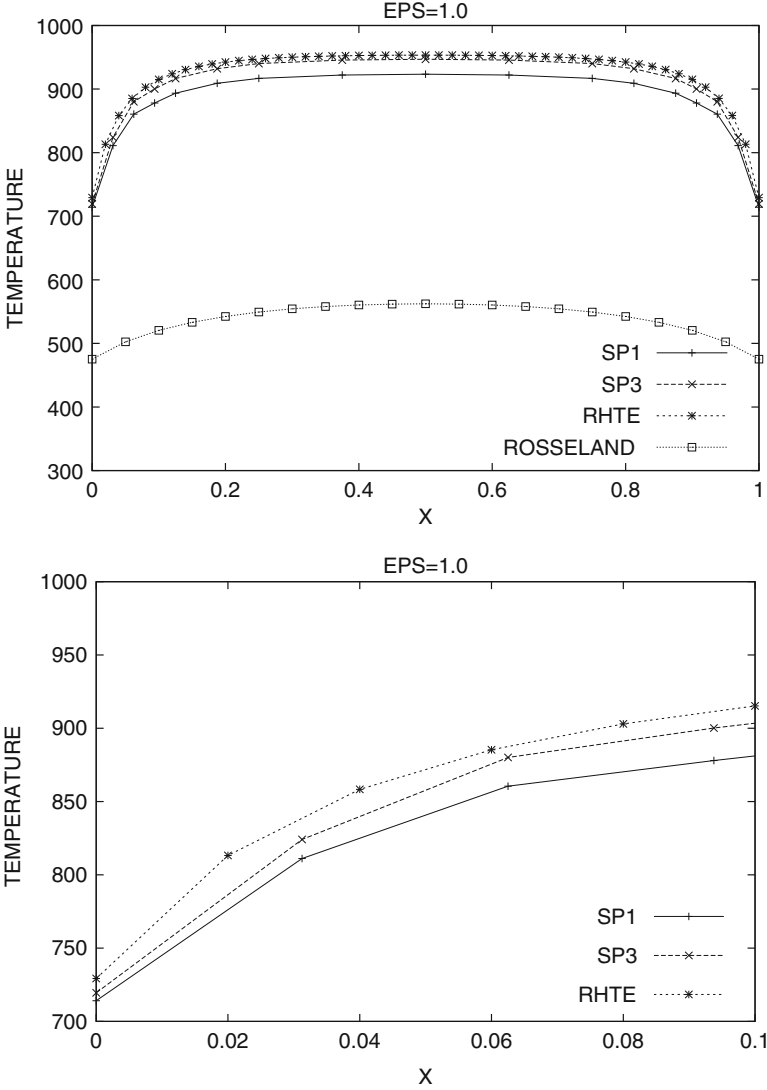


**Fig. 22** Comparison of three-dimensional temperature distributions at  $t_e = 0.001$  along the line  $y = z = 0.5$  obtained from different radiation models. The  $SP_3$ -solution matches very well with the RHTE solution, whereas the Rosseland approximation gives quite poor results

from Rosseland to  $SP_1$  and from  $SP_1$  to  $SP_3$ . The solution of the RHT problem using the multigrid method described in [76] takes again approximately twice as much time as the  $SP_3$  solution for the same accuracy. Adaptivity in space yields a factor of 3–5 in computation time for the present situation and adaptivity in time yields a factor of 10–50.

### 7.6.2 Three-Dimensional Glass Cooling

We consider a glass block which is represented by a scaled cube  $\Omega = [0, 1]^3$ .

Figure 21 displays the  $SP_3$ -solution and the adaptive three-dimensional grid chosen by our method for  $TOL_x = 0.01$ . As already observed in the two-dimensional case, the  $SP_N$ -solutions approximate the temperature computed from the full RHTE very well. In contrast to the Rosseland approximation, they exhibit physically correct boundary layers as can be seen from Fig. 22. To accurately capture these boundary layers, the use of local refinement is essential.

The mesh shown in Fig. 21 consists of 82,705 nodes, leading to a linear system of order 1,405,985. A uniform method requires approximately 250,000 grid points to reach a comparable solution quality. The solution of the full RHTE is done on a  $100 \times 100 \times 100$ -grid, yielding a linear system with 480 million unknowns which has to be solved in each time step. The comparison of the computation times yields similar results as in 2-D.

To conclude, these investigations show that the  $SP_N$ -equations and moment methods described above are a relatively inexpensive way to improve the accuracy of classical diffusion models. Compared to the solution of full radiative heat transfer equations, the complexity and computer time are considerably reduced. Further reduction can be achieved by fully adaptive discretization methods steered by robust a posteriori error estimators.

**Acknowledgements** We wish to thank all our collaborators and co-authors, in particular B. Dubroca, T. Götz, J. Lang, E.W. Larsen, M. Seaïd, G. Thömmes, R. Turpault and R. Pinnau. Parts of this work have been taken from the articles [18, 23–25, 27, 38, 47, 48, 76, 85]. This work was supported by German Research Foundation DFG under grants KL 1105/7 and 1105/14.

## References

1. Adams, M.L., Larsen, E.W.: Fast iterative methods for deterministic particle transport computations. *Prog. Nucl. Energy* **40**, 3–159 (2002)
2. Adams, M.L.: Subcell balance formulations for radiative transfer on arbitrary grids. *Transp. Theory and Stat. Phys.* **26**, 385–431 (1997)
3. Alcouffe, R., Brandt, A., Dendy, J., Painter, J.: The multigrid method for diffusion equations with strongly discontinuous coefficients. *SIAM J. Sci. Stat. Comp.* **2**, 430–454 (1981)
4. Alcouffe, R.: Diffusion synthetic acceleration methods for the diamond-differenced discrete-ordinates equations. *Nucl. Sci. Eng.* **64**, 344–355 (1977)
5. Agoshkov, V.: On the existence of traces of functions in spaces used in transport theory problems. *Sov. Math. Dokl.* **33**, 628–632 (1986)
6. Agoshkov, V.: Boundary value problems for transport equations. Birkhäuser, Boston (1998)
7. Anile, A.M., Pennisi, S., Sammartino, M.: A thermodynamical approach to Eddington factors. *J. Math. Phys.* **32**, 544–550 (1991)
8. Atkinson, K.E.: Iterative variants of the Nyström method for the numerical solution of integral equations. *Numer. Math.* **22**, 17–31 (1973)
9. Brantley, P.S., Larsen, E.W.: The simplified  $P_3$  approximation. *Nucl. Sci. Eng.* **134**, 1–21 (2000)

10. Brown, P.N.: A linear algebraic development of diffusion synthetic acceleration for three-dimensional transport equations. *SIAM. J. Numer. Anal.* **32**, 179–214 (1995)
11. Brunner, T.A., Holloway, J.P.: One-dimensional Riemann solvers and the maximum entropy closure. *J. Quant. Spectrosc. Radiat. Transfer* **69**, 543–566 (2001)
12. Cheng, P.: Dynamics of a radiating gas with applications to flow over a wavy wall. *AIAA J.* **4**, 238–245 (1966)
13. Clause, P.-J., Mareschal, M.: Heat transfer in a gas between parallel plates: Moment method and molecular dynamics. *Phys. Rev. A* **38**, 4241–4252 (1988)
14. Davison, B.: Neutron transport theory. Oxford University Press, Oxford (1958)
15. Dreyer, W.: Maximisation of the entropy in non-equilibrium. *J. Phys. A* **20**, 6505–6517 (1987)
16. Dubroca, B., Feugeas, J.L.: Entropic moment closure hierarchy for the radiative transfer equation. *C. R. Acad. Sci. Paris Ser. I* **329**, 915–920 (1999)
17. Dubroca, B.: Thèse d'Etat, Dept. of Mathematics, University of Bordeaux (2000)
18. Dubroca, B., Frank, M., Klar, A., Thömmes, G.: Half space moment approximation to the radiative heat transfer equations. *Z. Angew. Math. Mech.* **83**, 853–858 (2003)
19. Dubroca, B., Klar, A.: Half moment closure for radiative transfer equations. *J. Comput. Phys.* **180**, 584–596 (2002)
20. Eddington, A.: The Internal Constitution of the Stars. Dover, New York (1926)
21. Fischer, A.E., Marsden, J.E.: The Einstein evolution equations as a first-order quasi-linear hyperbolic system I. *Commun. Math. Phys.* **26**, 1–38 (1972)
22. Fiveland, W.A.: The selection of discrete ordinate quadrature sets for anisotropic scattering. *ASME HTD. Fundam. Radiat. Heat Transf.* **160**, 89–96 (1991)
23. Frank, M.: Partial Moment Models for Radiative Transfer. PhD thesis, TU Kaiserslautern (2005)
24. Frank, M.: Approximate models for radiative transfer. *Bull. Inst. Math. Acad. Sinica (New Series)* **2**, 409–432 (2007)
25. Frank, M., Dubroca, B., Klar, A.: Partial moment entropy approximation to radiative transfer. *J. Comput. Phys.* **218**, 1–18 (2006)
26. Frank, M., Pinnau, R.: Analysis of a half moment model for radiative heat transfer equations. *Appl. Math. Lett.* **20**, 189–193 (2007)
27. Frank, M., Seaid, M., Janicka, J., Klar, A., Pinnau, R.: A comparison of approximate models for radiation in gas turbines. *Prog. Comput. Fluid Dyn.* **4**, 191–197 (2004)
28. Golse, F., Perthame, B.: Generalized solution of the radiative transfer equations in a singular case. *Commun. Math. Phys.* **106**, 211–239 (1986)
29. Greenbaum, A.: Iterative Methods for Solving Linear Systems. SIAM, Philadelphia (1997)
30. Hackbusch, W.: Multi-Grid Methods and Applications. Springer Series in Computational Mathematics, vol. 4. Springer, New York (1985)
31. Howell, R., Siegel, J.R.: Thermal Radiation Heat Transfer, 3rd edn. Taylor & Francis, New York (1992)
32. Huang, K.: Introduction to Statistical Physics. Taylor and Francis, New York (2001)
33. Jeans, J.H.: The equations of radiative transfer of energy. *Mon. Not. R. Astron. Soc.* **78**, 28–36 (1917)
34. Junk, M.: Domain of definition of levermore's five-moment system. *J. Stat. Phys.* **93**, 1143–1167 (1998)
35. Kelley, C.T.: Iterative Methods for Linear and Nonlinear Equations. SIAM, Philadelphia (1995)
36. Kelley, C.T.: Multilevel Source Iteration Accelerators for the Linear Transport Equation in Slab Geometry. *Transp. Theory Stat. Phys.* **24**, 679–707 (1995)
37. Kelley, C.T.: Existence and uniqueness of solutions of nonlinear systems of conductive radiative heat transfer equations. *Transp. Theory Stat. Phys.* **25**, 249–260 (1996)
38. Klar, A., Lang, J., Seaid, M.: Adaptive solutions of SPN-Approximations to radiative heat transfer in glass. *Int. J. Therm. Sci.* **44**, 1013–1023 (2005)
39. Klar, A., Schmeiser, C.: Numerical passage from radiative heat transfer to nonlinear diffusion models. *Math. Mod. Meth. Appl. Sci.* **11**, 749–767 (2001)

40. Klar, A., Siedow, N.: Boundary layers and domain decomposition for radiative heat transfer and diffusion equations: Applications to glass manufacturing processes. *Eur. J. Appl. Math.* **9–4**, 351–372 (1998)
41. Korganoff, V.: *Basic Methods in Transfer Problems*. Dover, New York (1963)
42. Krook, M.: On the solution of equations of transfer. *Astrophys. J.* **122**, 488 (1955)
43. Laitinen, M.T., Tiihonen, T.: Integro-differential equation modelling heat transfer in conducting, radiating and semitransparent materials. *Math. Meth. Appl. Sci.* **21**, 375–392 (1998)
44. Laitinen, M.T., Tiihonen, T.: Conductive-radiative heat transfer in grey materials. *Quart. Appl. Math.* **59** 737–768 (2001)
45. Larsen, E.W., Keller, J.B.: Asymptotic solution of neutron transport problems for small mean free path. *J. Math. Phys.* **15**, 75 (1974)
46. Larsen, E.W., Pomraning, G., Badham, V.C.: Asymptotic analysis of radiative transfer problems. *J. Quant. Spectr. Radiat. Transf.* **29**, 285–310 (1983)
47. Larsen, E.W., Thömmes, G., Klar, A., Seaïd, M., Götz, T.: Simplified  $P_N$  approximations to the equations of radiative heat transfer in glass. *J. Comput. Phys.* **183**, 652–675 (2002)
48. Larsen, E.W., Thömmes, G., Klar, A.: New frequency-averaged approximations to the equations of radiative heat transfer. *SIAM Appl. Math.* **64** 565–582 (2003)
49. Lentès, F.T., Siedow, N.: Three-dimensional radiative heat transfer in glass cooling processes. *Glastech. Ber. Glass Sci. Technol.* **72**, 188–196 (1999)
50. Levermore, C.D.: Relating Eddington factors to flux limiters. *J. Quant. Spectroscop. Radiat. Transf.* **31**, 149–160 (1984)
51. Levermore, C.D.: Moment closure hierarchies for kinetic theories. *J. Stat. Phys.* **83** (1996)
52. Lewis, E.E., Miller, W.F. Jr., *Computational Methods of Neutron Transport*. Wiley, New York (1984)
53. Lopez-Pouso, O.: Trace theorem and existence in radiation. *Adv. Math. Sci. Appl.* **10**, 757–773 (2000)
54. Mark, J.C.: The spherical harmonics method, part I. Tech. Report MT 92, National Research Council of Canada (1944)
55. Mark, J.C.: The spherical harmonics method, part II. Tech. Report MT 97, National Research Council of Canada (1945)
56. Marshak, R.E.: Note on the spherical harmonic method as applied to the milne problem for a sphere. *Phys. Rev.* **71**, 443–446 (1947)
57. Mengüç, M.P., Iyer, R.K.: Modeling of radiative transfer using multiple spherical harmonics approximations. *J. Quant. Spectrosc. Radiat. Transf.* **39** (1988), 445–461.
58. Mercier, B.: Application of accretive operators theory to the radiative transfer equations. *SIAM J. Math. Anal.* **18**, 393–408 (1987)
59. Minerbo, G.N.: Maximum entropy Eddington factors. *J. Quant. Spectrosc. Radiat. Transf.* **20**, 541–545 (1978)
60. Modest, M.F.: *Radiative Heat Transfer*, 2nd edn. Academic, San Diego (1993)
61. Müller, I., Ruggeri, T.: *Rational extended thermodynamics*. Springer, New York (1998)
62. Murray, R.L.: *Nuclear reactor physics*. Prentice Hall, New Jersey (1957)
63. Ore, A.: Entropy of radiation. *Phys. Rev.* **98**, 887 (1955)
64. Özisik, M.N., Menning, J., Hälg, W.: Half-range moment method for solution of the transport equation in a spherical symmetric geometry. *J. Quant. Spectrosc. Radiat. Transf.* **15**, 1101–1106 (1975)
65. Planck, M.: Distribution of energy in the spectrum. *Ann. Phys.* **4**, 553–563 (1901)
66. Pomraning, G.C.: *The equations of radiation hydrodynamics*. Pergamon, New York (1973)
67. Pomraning, G.C.: Initial and boundary conditions for equilibrium diffusion theory. *J. Quant. Spectrosc. Radiat. Transf.* **36**, 69 (1986)
68. Pomraning, G.C.: Asymptotic and variational derivations of the simplified  $P_N$  equations. *Ann. Nucl. Energy* **20**, 623 (1993)
69. Porzio, M.M., Lopez-Pouso, O.: Application of accretive operators theory to evolutive combined conduction, convection and radiation. *Rev. Mat. Iberoam.* **20**, 257–275 (2004)

70. Rosen, P.: Entropy of radiation. *Phys. Rev.* **96**, 555 (1954)
71. Saad, Y., Schultz, M.H.: GMRES: A generalized minimal residual algorithm for solving non-symmetric linear systems. *SIAM. J. Sci. Statist. Comput.* **7**, 856–869 (1986)
72. Schäfer, M., Frank, M., Pinnau, R.: A hierarchy of approximations to the radiative heat transfer equations: Modelling, analysis and simulation. *Math. Meth. Mod. Appl. Sci.* **15**, 643–665 (2005)
73. Schuster, A.: Radiation through a foggy atmosphere. *Astrophys. J.* **21**, 1–22 (1905)
74. Schwarzschild, K.: Über das Gleichgewicht von Sonnenatmosphären, *Akad. Wiss. Göttingen. Math. Phys. Kl. Nachr.* **195**, 41–53 (1906)
75. Seaid, M.: Notes on Numerical Methods for Two-Dimensional Neutron Transport Equation, Technical Report Nr. **2232**, TU Darmstadt (2002)
76. Seaid, M., Klar, A.: Efficient Preconditioning of Linear Systems Arising from the Discretization of Radiative Transfer Equation, *Challenges in Scientific Computing*. Springer, Berlin (2003)
77. Sherman, M.P.: Moment methods in radiative transfer problems. *J. Quant. Spectrosc. Radiat. Transf.* **7**, 89–109 (1967)
78. Struchtrup, H.: On the number of moments in radiative transfer problems. *Ann. Phys.* **266**, 1–26 (1998)
79. Sykes, J.B.: Approximate integration of the equation of transfer. *Mon. Not. R. Astron. Soc.* **111**, 377 (1951)
80. Tomašević, D.I., Larsen, E.W.: The Simplified  $P_2$  Approximation. *Nucl. Sci. Eng.* **122**, 309–325 (1996)
81. Turek, S.: An efficient solution technique for the radiative transfer equation. *IMPACT, Comput. Sci. Eng.* **5**, 201–214 (1993)
82. Turek, S.: A generalized mean intensity approach for the numerical solution of the radiative transfer equation. *Computing* **54**, 27–38 (1995)
83. Turpault, R.: Construction d'une modèle M1-multigroupe pour les équations du transfert radiatif. *C. R. Acad. Sci. Paris Ser. I* **334**, 1–6 (2002)
84. Turpault, R.: A consistent multigroup model for radiative transfer and its underlying mean opacities. *J. Quant. Spectrosc. Radiat. Transf.* **94**, 357–371 (2005)
85. Turpault, R., Frank, M., Dubroca, B., Klar, A.: Multigroup half space moment approximations to the radiative heat transfer equations. *J. Comput. Phys.* **198**, 363–371 (2004)
86. Van der Vorst, H.A.: BI-CGSTAB: A fast and smoothly converging variant of BI-CG for the solution of nonsymmetric linear systems. *SIAM. J. Sci. Statist. Comput.* **13**, 631–644 (1992)
87. Viskanta, R., Anderson, E.E.: Heat transfer in semitransparent solids. *Adv. Heat Transf.* **11**, 318 (1975)
88. Viskanta, R., Mengüç, M.P.: Radiation heat transfer in combustion systems. *Prog. Energy Combust. Sci.* **13**, 97–160 (1987)

Mathematical Models in the Manufacturing of Glass

C.I.M.E. Summer School, Montecatini Terme, Italy 2008

Farina, A.; Klar, A.; Mattheij, R.M.M.; Mikelić, A.; Siedow,

N. - Fasano, A. (Ed.)

2011, XI, 227 p., Softcover

ISBN: 978-3-642-15966-4